Spectrally Efficient Non-Orthogonal Multiple Access (NOMA) Techniques for Future Generation Mobile Systems

By

Ibrahim Bukar

Submitted for the degree of Doctor of Philosophy

School of Engineering and Informatics

University of Sussex

2016

Declaration

I hereby declare that this thesis has not been and will not be submitted in whole or in part to another University for the award of any other degree.

Signature:

Ibrahim Bukar

Date :

UNIVERSITY OF SUSSEX

Thesis submitted in fulfilment of the requirements for the degree of Doctor of Philosophy

Spectrally Efficient Non-Orthogonal Multiple Access (NOMA) Techniques for Future Generation Mobile Systems

By: Ibrahim Bukar

Summary

With the expectation of over a 1000-fold increase in the number of connected devices by 2020, efficient utilization of the limited bandwidth has become ever more important in the design of mobile wireless systems. Furthermore, the ever-increasing demand for higher data rates has made it necessary for a new waveform design that satisfies not only throughput demands, but network capacity as well. One such technique recently proposed is the non-orthogonal multiple access (NOMA) which utilizes the distance-dependent power domain multiplexing, based on the principles of signal superposition.

In this thesis, new spectrally efficient non-orthogonal signal techniques are proposed. The goal of the schemes is to allow simultaneous utilization of the same time-frequency network resources. This is achieved by designing component signals in both power and phase domain such that users are precoded or preformed to form a single and uniquely decodable composite signal. The design criteria are based on maximizing either the sum rate or spectral efficiency, minimizing multi-user interference and detection ambiguity, and maximizing the minimum Euclidean distance between the composite constellation points. The design principles are applied in uplink, downlink and coordinated multipoint (CoMP) scenarios. We assume ideal channel state with perfect estimation, low mobility and synchronization scenarios so as to prove the concept and serve as a bound for any future work in non-ideal conditions. Extensive simulations and numerical analysis are carried to show the superiority and compatibility of the schemes.

First, a new NOMA signal design called uplink NOMA with constellation precoding is proposed. The precoding weights are generated at the eNB based on the number of users to be superposed. The eNB signals the precoding weights to be employed by the users to adjust their transmission. The adjustments utilize the channel state information estimated from common periodic pilots broadcasted by the eNB. The weights ensure the composite received signal at the eNB belongs to the pre-known constellation. Furthermore, the users precode to the eNB antenna that requires the least total transmit power

from all the users. At the eNB, joint maximum likelihood (JML) detection is employed to recover the component signals. As the composite constellation is as that of a single user transmitting that same constellation, multiple access interference can be viewed as absent, which allows multiple users to transmit at their full rates. Furthermore, the power gain achieved by the sum of the component signals maximizes the sum rate.

Secondly, the constellation design principle is employed in the downlink scenario. In the scheme, called downlink NOMA with constellation preforming, the eNB preforms the users signal with power and phase weights prior to transmission. The preforming ensures multi-user interference is eliminated and the spectral efficiency maximized. The preformed composite constellation is broadcasted by the eNB which is received by all users. Subsequently, the users perform JML detection with the designed constellation to extract their individual component signals. Furthermore, improved signal reliability is achieved in transmit and receive diversity scenarios in the schemes called distributed transmit and receive diversity combining, respectively.

Thirdly, the constellation preforming on the downlink is extended to MIMO spatial multiplexing scenarios. The first MIMO scheme, called downlink NOMA with constellation preforming, each eNB antenna transmits a preformed composite signal composed of a set of multiple users' streams. This achieves spatial multiplexing with diversity with less transmit antennas, reducing costs associated with multiple RF chains, while still maximizing the sum rate. In the second MIMO scheme, a highly spectrally efficient MIMO preforming scheme is proposed. The scheme, called group layer MIMO with constellation preforming, the eNB preforms to a specific group of users on each transmit antenna. In all the schemes, the users perform JML detection to recover their signals.

Finally, the adaptability of the constellation design is shown in CoMP. The scheme, called CoMP with joint constellation processing, the additional degrees of freedom, in form of interfering eNBs, are utilized to enable spatial multiplexing to a user with a single receive antenna. This is achieved by precoding each stream from the coordinating eNB with weights signalled by a central eNB. Consequently, the inter-cell interference is eliminated and the sum-rate maximized. To reduce the total power spent on precoding, an active cell selection scheme is proposed where the precoding is employed on the highest interferers to the user. Furthermore, a power control scheme is applied the design principle, where the objective is to reduce cross-layer interference by adapting the transmission power to the mean channel gain.

Acknowledgements

First, I would like to express my sincere appreciation and everlasting gratitude to my beloved parents Mustapha and Rakiya Bukar, my beloved wife Maryam, and the entirety of our family. Their love, support and huge sacrifices will never be forgotten. I dedicate this thesis for you and hope it will make you proud.

My sincerest gratitude to my supervisor Dr Falah Ali. I thank him for his unlimited patience, time, honest criticism, and encouragement throughout the duration of my studies. His thorough understanding of wireless communications, creativity, and work ethics has been a source of inspiration to me and has helped me throughout my studies.

Finally, I would also like to think my colleagues at the communication research lab: Murtala Aminu, Tom Hayes, Fei, Andreas, and Victor. Their help, support, and friendship have made the past four years an enjoyable experience.

List of Publications

- I. Bukar and F. Ali, "Subcarrier Multiplexing in LTE-COMP OFDMA", in *2015 IEEE 81st Vehicular Technology Conference (VTC Spring)*, 2015, pp. 1-5.
- I. Bukar and F. Ali, "Highly Spectrally Efficient NOMA Constellation Designs", *To be Submitted to: IEEE Communication Letters.*
- I. Bukar and F. Ali, "Downlink NOMA with Constellation Preforming", *To be Submitted to: IET Journal on Communication.*
- I. Bukar and F. Ali, "Spectrally Efficient MIMO NOMA with Constellation Preforming", *To be Submitted to: IET Journal on Communication.*

List of Abbreviations

Abbreviation	Definition
3G	3rd Generation
3GPP	3rd Generation Partnership Project
4G	4th Generation
5G	5th Generation
5GNOW	5th Generation Non-Orthogonal Waveforms
ACS	Active Cell Selection
AWGN	Additive White Gaussian Noise
BD	Block Diagonalization
BER	Bit Error Rate
BS	Base Station
CCI	Co-Channel Interference
CDMA	Coding Division Multiple Access
CeNB	Coordinating eNB
CI	Channel Inversion
CN	Core Network
CoMP	Coordinated Multipoint
CP	Cyclic Prefix
CPP	Common Periodic Pilot
CRS	Cell-Specific Reference Signals
CS/CB	Coordinated Scheduling/Beamforming
CSI	Channel State Information
CSIR	Channel State Information at the Receiver
CSIT&R	Channel State Information at Transmitter and Receiver
d_{min}	Minimum Euclidean Distance
DoF	Degrees-of-Freedom

DL-SCH	Downlink Shared Channels
DPC	Dirty Paper Coding
eNB	EUTRAN-NodeB
EP	Equal Power
EPC	Enhanced packet Core
FDD	Frequency Domain Duplex
FDMA	Frequency Division Multiple Access
FFT	Fast Fourier Transform
Gbps	Gigabits per Second
GMAC	Gaussian Multiple Access Channel
H-ARQ	Hybrid Automatic Requests
i.i.d	independently identically distributed
ICI	Inter-Channel-Interference
IFFT	Inverse Fast Fourier Transform
IP	Internet Protocol
ISI	Inter-Symbol Interference
JCP	Joint Constellation Processing
JML	Joint Maximum Likelihood
JP	Joint Processing
LDS	Low-Density Spreading
LTE	Long Term Evolution
LTE/A	Long Term Evolution/Advanced
LUT	Look Up Table
M2M	Machine-to-Machine
MAC	Multiple Access Channel
M-AC	Medium-Access Control
MAI	Multiple Access Interference
MAS	Multiple Access Schemes
Mbps	Megabits per Second
MCA	Mean Channel Adaptation
MCG	Mean Channel Gain
METIS	The Mobile and wireless communication Enablers for the Twenty-twenty Information Society
MIMO	Multiple-Input Multiple Output

MISO	Multi-Input Single-Output
MMSE	Minimum Square Error
MPA	Message-Passing Algorithm
MRC	Maximum Ratio Combing
MUD	Multi-User Detection
MUI	Multiple User Interference
MU-MIMO	Multiuser MIMO
MUSA	Multi-User Shared Access
NCPf	NOMA with Constellation Preforming
DTAD	Distributed Transmit Antenna Diversity
RD	Receive Diversity
NOMA	Non-Orthogonal Multiple Access
OFDM	Orthogonal Frequency Division Multiplexing
OFDMA	Orthogonal Frequency Division Multiple Access
OMA	Orthogonal Multiple Access
PAPR	Peak-to-Average Power Ratio
PBCH	Physical Broadcast Channel
PDCCH	Physical Downlink Control Channel
PDCP	Packet Data Convergence Protocol
PDF	Probability Density Function
PDMA	Pattern Division Multiple Access
PD	Power Domain
PDSCH	Physical Downlink Shared Channel
PHY	Physical Layer
PMCH	Physical Multicast Channel
PMI	Precoder-Matrix Indication
PRACH	Physical Random-Access Channel
PUCCH	Physical Uplink Control Channel
PUSCH	Physical Uplink Shared Channel
QoS	Quality of Service
RAN	Radio-Access Network
RB	Resource Blocks
RE	Resource Element
RF	Radio Frequency

RI	Rank Indication
RLC	Radio-Link Control
RRM	Radio Resource Management
SC-FDMA	Single Carrier Frequency Division Multiple Access
SCMA	Sparse-Code Multiple Access
SER	Symbol Error Rates
SIC	Successive Interference Cancellation
SIMO	Single-Input Multi-Output
SINR	Signal-to-Interference-Plus-Noise Ratios
SM	Spatial Multiplexing
SMD	Spatial Multiplexing and Diversity
SNR	Signal-to-Noise Ratio
SPC	Superposition Coding
SRS	Sounding Reference Signals
STBC	Space-Time Block Coding
SU-MIMO	Sinlge User MIMO
SVD	Singular Value Decomposition
TCI	Truncated Channel Inversion
TDD	Time Domain Duplex
TDMA	Time Division Multiple Access
THP	Tomlinson-Harashima Precoding
TTI	Transmission Time Interval
UHD	Ultra High Definition
NCPr	NOMA with Constellation Precoding
UL-SCH	Uplink Shared Channels
UP	Unequal Power
WiMAX	Worldwide Interoperability for Microwave Access
ZF	Zero Forcing

List of Notations

$\|\mathbf{h}\|$	Magnitude of complex value $\mathbf{h}$
$\|\|\mathbf{h}\|\|$	Vector Euclidean norm
$(\cdot)^*$	Conjugate transposition
$(\cdot)^T$	Transposition
$\mathbb{C}^{m \times n}$	Complex $m \times u$ matrix
$\mathbb{E}$	Expectation value
$\aleph(m, n)$	Mean m with variance n
$\mathbf{H}^\dagger$	Moore-Penrose inverse of matrix $\mathbf{H}$
$H(x)$	Entropy of x
$\mathbf{I}_m$	$m \times n$ Identity matrix
$\min(m, n)$	Minimum elements
$tr(\cdot)$	Matrix trace
$\mathbf{U}[\mathbf{A}\|\mathbf{B}]$	$\mathbf{U}$ as a function of $\mathbf{A}$ and $\mathbf{B}$

Contents

List of Tables

List of Figures

Chapter 1

Introduction

1.1 Motivation

Wireless mobile communication systems have become evermore crucial in everyday life and a key factor in human and economic development. Nowadays, most aspects of human activities are tied to mobile internet services such as video streaming, socializing, business related activities and other modern life dependent services. Furthermore, the emergence of new technologies such as Machine-to-Machine (M2M) systems, ultra high definition (UHD) 4K videos, real-time interactive services and cloud computing has transformed mobile devices from voice-data-telephony circuit switched devices to an all IP dependent devices. As a result, the growth of global mobile data traffic is expected to keep increasing aggressively. Therefore, efficient use of the limited available spectrum is a crucial and challenging task to meet the increasing number of connected devices and their demands. Furthermore, power and complexity constraints add more difficulties on the development of next generation mobile systems.

To meet these demands, a number of requirements need to be satisfied. First, the

number of users that can be accommodated within a cell needs to be significantly increased without necessarily increasing the number of Base Stations (BS). Secondly, future generation data and multimedia traffic require a high data rate in order of hundreds of Mb/s for high mobility users and up to Gb/s for low mobility or fixed users with the end-to-end latencies not exceeding 5 ms. Thirdly, the expected increase in data traffic should not have a significant cost on battery life. Finally the cost of delivering high quality services and high data rate should be kept affordable. Therefore, fulfilling these requirements requires maximising bandwidth efficiency, exploiting all available degrees of freedom (time, frequency, power and space), minimising power consumption and utilization of fading and interference which would lead to improved performance and capacity.

To address these challenges, the latest and evolving wireless networking standards such as the Worldwide Interoperability for Microwave Access (WiMAX), Third Generation Partnership Project (3GPP), represented by Long Term Evolution advanced (LTE)-Advanced and the ITU's IMT-Advanced, all envisage the concurrent deployment of a number of compatible technologies in the physical and multiple access layers.

One of these key technologies is multi-carrier Multiple Access Schemes (MAS) which are based on Orthogonal Frequency Division Multiplexing (OFDM) such as Orthogonal Frequency Division Multiple Access (OFDMA) and Single Carrier OFDMA (SC-OFDMA). These schemes enable efficient as well as robust performance against fading by converting the channel bandwidth into many parallel, overlapping and orthogonal flat fading sub channels.

To further improve the spectral efficiency, Non-Orthogonal Multiple Access (NOMA) has recently been proposed for the future 5th Generation (5G) mobile systems to comple-

ment the existing orthogonal MAS [1] [2]. NOMA utilizes the principles of superposition coding where multiple users are scheduled in the power domain such that they share the same time/frequency resource simultaneously. The combined received signals are detected by employing Successive Interference Cancellation (SIC), which inherently, requires large power separation between users for successful detection. This increases the overall system capacity, however, as the users transmit at different power levels, throughput fairness is poor for the weaker power users.

Another technology that is envisioned to be used concurrently with OFDMA and NOMA is Multiple-Input-Multiple-Output (MIMO) communication which exploits the rich scattering environment and the availability of multiple antennas at both the transmitter and receiver to allow many users to access the network, simultaneously achieving linear increase in system capacity without consuming extra bandwidth or power. In addition to its capacity gain, MIMO can provide spatial diversity to improve the Bit Error Rate (BER) performance. However MIMO is limited by the number of receive antennas, the amount of feedback required for scheduling and precoding, and by channel correlations due to insufficient antenna separation at the terminals and/or poor scattering environment. As a result, the sum rate capacity and BER performance are significantly degraded. Moreover the cost of employing multiple Radio Frequency RF chains remains high.

1.2 Research Aims and Objectives

- To design low-feedback and spectrally efficient non-orthogonal multiple access schemes based on the principle of signal superposition.
- To design low-complexity and low-overhead spatial diversity schemes for non-

orthogonal multiuser based on superposition coding.

- Design high-rate spatial multiplexing and diversity schemes that utilize less transmit antennas without comprising their transmission rate.

1.3 Contributions of the Thesis

A number of contributions have been made in this work; below is a summary of main findings and contributions:

1. A novel NOMA signal design called Uplink NOMA With Constellation Precoding (UL-NCPr) is proposed. The goal of the scheme is to allow simultaneous utilization of the same time/frequency network resources. This is achieved by designing component signals in both power and phase domain such that as many users form a single and uniquely decodable composite signal. As the composite constellation is as that of a single user transmitting that same constellation, multiple access interference can be viewed as absent, which allows multiple users to transmit at their full rates. This relaxes the large power separation required for NOMA based on power domain superposition. Furthermore, this departs from user-specific power control and successive interference cancellation receivers, to a new approach that optimises power and phase domain precoding utilizing only a small common pilot and without the need for Channel State Information (CSI) to decode the users signals. Furthermore, the power gain achieved by the sum of the component signals maximizes the sum rate.

2. A novel downlink NOMA constellation design scheme called NOMA with Constellation Preforming (NCPf) where the power and phase domain are utilized to

improve link capacity in the distant-dependant based signal superposition. The objective is based on maximizing the minimum Euclidean distance of composite received signals to resolve the detection ambiguity. The simplicity and compatibility of these methods enable integration into various existing and future wireless communication systems. The key contributions of the proposed technique are:

- Efficient utilization of a single transmitter to transmit multi-user signals on the same time/frequency resource. This is in comparison to spatial multiplexing schemes where each stream requires separate RF chains.
- Interference elimination by multi-user signal superposition. The users see the received signal as a single composite signal without interference from other users' signals. Consequently, increased capacity without significant loss in error performance is achieved.
- Improved signal reliability from spatial diversity without incurring the substantial increase in both complexity and overheads.
- A novel Spatial Multiplexing (SM) and Diversity (SMD) preforming scheme called NCPf-SMD, where the total number of independent multi-user streams are more than the number of available transmit antennas, compared to the required one-to-one antenna-stream relationship in traditional MIMO SM.
- Significant reduction in the cost of Radio Frequency (RF) chains associated with transmit antennas, while still achieving spatial multiplexing and diversity gains.
- Reduction in signalling overheads, maximize system capacity without employing channel precoding.

- A high link capacity scheme called Group Layered NCPf (GL-NCPr), were less transmit antennas are utilized to serve a high number of users without the effect of co-channel interference. This results in a highly spectrally efficient scheme reducing the number of transmit antenna used for communication and at the same time, increase the number of users served.

3. A novel Coordinated Multipoint (CoMP) spatial multiplexing scheme is proposed, where inter-cell interference is utilized to improve spectral efficiency to a user with a single receive antenna. The aim of the scheme is to eliminate inter-cell interference by coordinating then interferers with useful signals such that they combine and serve a user even with a single antenna. Maximum likelihood detection is employed at the receiver to provide optimum signal reliability and performance. Furthermore, we propose two power control schemes as follows:

   - Coordination to eliminate inter-cell interference and improve spectral efficiency by actively selecting the strongest interferers to the user.
   - Reduction in cross-layer interference by adapting the transmission power to the average channel gains. Thereby allowing increased network capacity without the consequence of co-channel interferences.

1.4 Outline of the Thesis

The thesis is organized as follows. Introduction to LTE, technical background theory and literature review of the related work are presented in Chapter 2. The principles and features of the traditional wireless multiple access techniques are presented. Next, an overview and review of MIMO communication system is carried. We end the chapter

with the requirements and challenges of the proposed future 5G.

In Chapter 3, a novel NOMA UL-NCPr is proposed. First, the related work and motivation is presented before introducing the constellation design principles of UL-NCPr. Next a detailed description of UL-NCPr system model is given. This includes signal model, the constellation design, antenna selection and Joint Maximum Likelihood (JML) detection. In the constellation design, the design objectives and considerations, requirements and search algorithm are presented. Next is the signalling and synchronization which include the common periodic pilot and synchronization acquisition. A detailed performance analysis is carried out before ending the chapter with simulation modelling and results to evaluate the performance of the scheme.

Chapter 4, the constellation design principle is proposed in a downlink broadcast scheme. We introduce and present the design principle. Next, a detailed system model were the constellation design, search algorithm and JML detection are presented. A detailed performance analysis is carried out. Finally, the system model and simulation results are presented.

Chapter 5 presents four downlink multi-antenna constellation schemes. First, two spatial diversity schemes in two sections (Receive and transmit diversity) are described. Next, our novel NOMA MIMO with spatial multiplexing and diversity scheme is introduced. The system model along with two detection methods are presented . Next, performance analysis on all the four schemes are carried out. Finally, the simulation models results are presented and discussed

Chapter 6 introduces our novel CoMP spatial multiplexing scheme. First, the scheme is introduced followed by the motivation and related works. The principles of joint constellation processing is presented. Next, the joint constellation precessing system model,

maximum like hood detection are transmission procedures are presented. To reduce the total power spent on precoding, an active cell selection scheme is presented. The system model and procedures are described. Next, a cross-layer interference minimization scheme is presented where the transmission power is adapted to the mean channel gain. The system model and procedures are described. Next, the simulation model of the schemes are described followed by the presentation and discussions of the simulation results.

Finally, Chapter 7 concludes the thesis, with a summary of main findings and contributions and some discussion on future work.

Chapter 2

Technical Background

2.1 LTE and LTE-Advanced

2.1.1 Introduction

The evolution of 3rd Generation (3G) into 4th Generation (4G) LTE mobile systems is driven by the emergence and enhancements of new technologies in mobile communication systems. These were developed due to the need for more efficient utilization of the limited available spectrum, increased throughput, the competition between mobile operators and challenges from other mobile technologies [3, 4, 5].

One of the key drivers of 4G is the rapid increase in the number of users and devices accessing the internet. This required future mobile systems to support Internet Protocol (IP) based services. As earlier generation mobile systems were built for circuit switched services, primarily voice, the need for more efficient and back-compatible end-to-end IP networks became the core operational principle for 4G systems. The mobility and roaming capabilities of mobile devices also allows mobile network operators create targeted services to end users.

IP technology enables a range of services with different requirements. The main design requirements for a radio interface supporting a variety of services are:

- Data rate: Many services with lower data rates such as voice are important and still occupy a large part of a mobile networks overall capacity. However, the ever increasing demand for higher data rates for web browsing, video streaming and file transfer pushes the peak data rates for mobile systems from Mbit/s for 3G to Gbit/s for 4G.

- Capacity: Not only the peak data rates provided to the end-user that are of importance, but also the total data rate that can be provided on average from each deployed base station site and per hertz of licensed spectrum.

- Delay: Real-time and interactive services such as conference calls, gaming, healthcare related applications e.t.c have requirements for very low latency, thus making it a primary design target.

- Cost/Energy: As the number of connected devices and data consumption increases, so does the network energy footprint. Therefore, minimizing cost-per-bit and joule-per-bit is essential to improve operational efficiency and consumer satisfaction.

2.1.2 LTE Architecture

The LTE architecture of both the Radio-Access Network (RAN) and the Core Network (CN) together are referred to as the LTE RAN and the Enhanced packet Core (EPC), respectively, as illustrated in Figure 2.1. The RAN is responsible for all radio-related functionality including, scheduling, radio-resource handling, multi-antenna schemes,

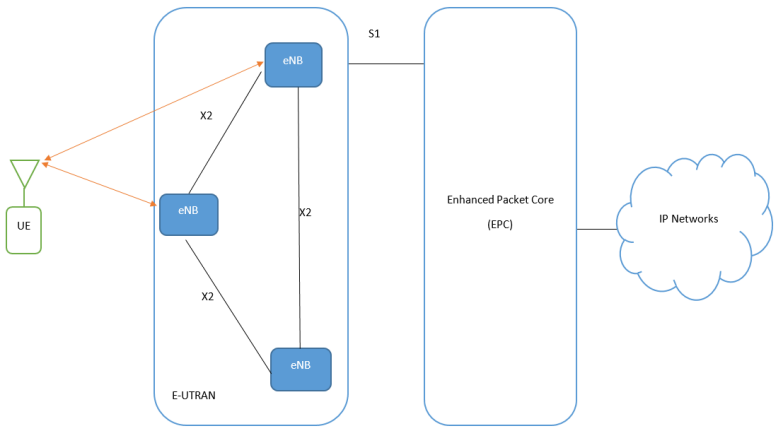

Figure 2.1: LTE high level network architecture

retransmissions and coding. The EPC is responsible for back-end network functions such as authentication, charging functionality, and the setup of end-to-end connections. The separation of RAN with EPC allows for several radio-access technologies to be served by the same core network, making it back compatible with earlier generation mobile systems [6, 7].

The LTE RAN provides one or more radio bearers to which IP packets are mapped according to their Quality-of-Service requirements. These include the Packet Data Convergence Protocol (PDCP) for compression and security related operations, Radio-Link Control (RLC) for segmentation/concatenation, retransmissions, duplicate detection, and in-sequence delivery to higher layers, Medium-Access Control (M-AC) for the multiplexing of logical channels, hybrid-Automatic Requests (H-ARQ) retransmissions and scheduling, Physical Layer (PHY) for coding/decoding, modulation/demodulation, multi-antenna mapping.

2.1.3 EUTRAN-NodeB (eNB)

The LTE radio-access network uses a logical node base station architecture known as the eNodeB (eNB). The eNB is responsible for all radio-related functions in one or multiple

cells. The eNB is connected to the EPC by means of the S1 interface for both the user and control planes. Multiple eNBs are connected to each other via the X2 interface which provides functions such as multi-cell Radio Resource Management (RRM) to provide Inter-Cell Interference Coordination (ICIC). As the eNB is a logical and not a physical implementation, it allows operators to deploy scaled down versions to increase coverage and capacity. These are known as Macro (Urban:>100m), pico (Dense:<100m) and femto (Indoor:<50m) cells [6].

2.1.4 Physical transmission

The physical layer is responsible for coding, physical-layer hybrid-ARQ processing, modulation, multi-antenna processing, synchronization and resource mapping. It also handles mapping of transport channels to physical channels in the form of Transport Blocks (TB) at each Transmission Time Interval (TTI). Data transmission in downlink and uplink use the Down Link Shared (DL-SCH) and Uplink Shared (UL-SCH) transport channels, respectively. There are at most two transport blocks per TTI on a DL-SCH or UL-SCH. There are also physical control channels known as L1/L2 control channels [8].

The physical-channel types defined in LTE include [9]:

- The Physical Downlink Shared Channel (PDSCH) is the main physical channel used for downlink transmission of unicast data and paging information.
- The Physical Uplink Shared Channel (PUSCH) is the uplink counterpart to the PDSCH.
- The Physical Broadcast Channel (PBCH) carries part of the system information, required by the terminal to access the network.

- The Physical Multicast Channel (PMCH).
- The Physical Downlink Control Channel (PDCCH) is used for downlink control information used for scheduling related operations.
- The Physical Hybrid-ARQ Indicator Channel is used for acknowledgements and retransmission requests.
- The Physical Control Format Indicator Channel provides the terminals with information necessary to decode the set of PDCCHs.
- The Physical Uplink Control Channel (PUCCH) is used by the terminal to send channel-state information for downlink channel-dependent scheduling, and for requesting resources to transmit uplink data.
- The Physical Random-Access Channel (PRACH) is used for random access.
- Primary Synchronization Signal/Channel (PSS) and Secondary Synchronization Signal/Channel (SSS) are used for radio frame synchronization.

2.1.4.1 Frame Structure

LTE transmissions are organized into Time Domain Duplex (TDD) (Figure 2.2) or Frequency Domain Duplex (FDD) (Figure 2.3) radio frames 10 ms in length, each of which is divided into ten equally sized subframes of length 1 ms. Each subframe consists of two equally sized slots of length 0.5 ms, with each slot consisting $K = 7$ OFDM symbols including Cyclic Prefix (CP). The LTE OFDM subcarrier spacing is 15 kHz for both downlink and uplink which was chosen to carefully balance the overhead from cyclic prefix against sensitivity to Doppler spread and other types of frequency errors. The subcarrier spacing, assuming Fast Fourier Transform (FFT)-based implementation, translates to a

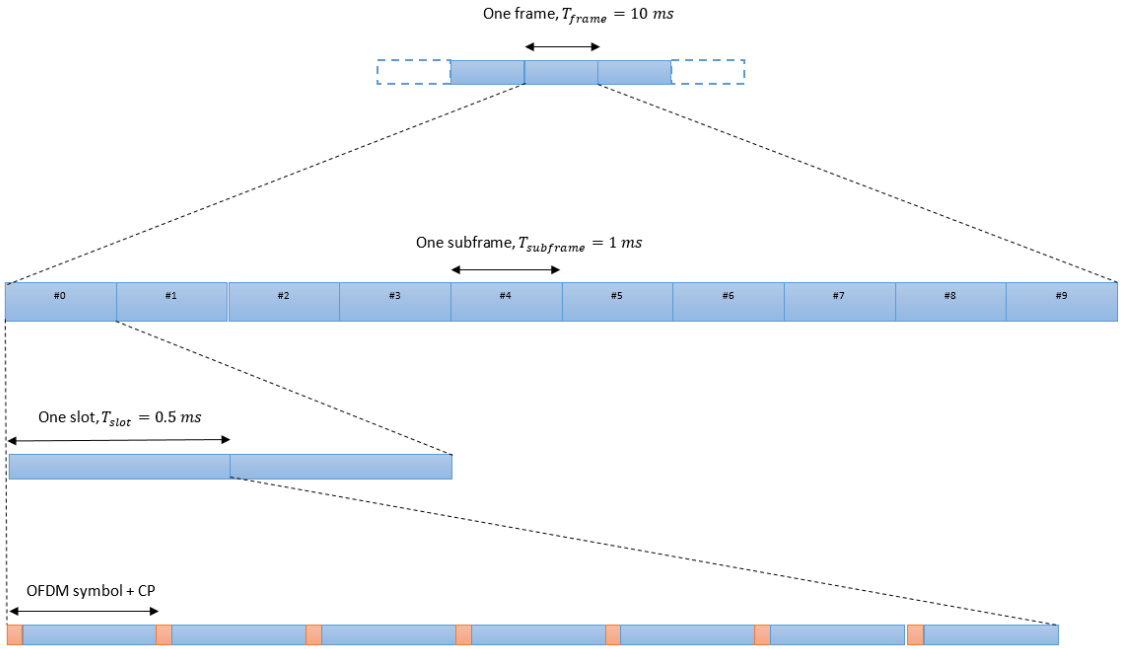

Figure 2.2: LTE time domain frame architecture

sampling rate and time $f_s = 1500 \cdot N_{FFT}$ and $T_s = 1/(15000 \cdot N_{FFT})$, respectively, where N_{FFT} is the FFT size [10].

The smallest physical resource in LTE is called Resource Element (RE), which consists of one subcarrier during one OFDM symbol. The RE are grouped into Resource Blocks (RB) N_{RB}, where each RB consists of 12 consecutive subcarriers in the frequency domain and one 0.5 ms (7 OFDM symbols each with cyclic prefix) slot in the time domain. Each RB thus consists of $7 \cdot 12 = 84$ RE's. The bandwidths and FFT sizes defined in LTE standard are shown in Table 2.1.

Table 2.1: LTE resource parameters defined in LTE standard

Channel bandwidth (MHz)	1.4	3	5	10	15	20
Number of resource blocks (N_{RB})	6	15	25	50	75	100
Number of subcarriers (N_{SC})	72	180	300	600	900	1200
IFFT (Tx)/FFT (Rx) size (N_{FFT})	128	256	512	1024	1536	2048
Sample rate (MHz)	1.92	3.84	7.68	15.36	23.04	30.72
Samples per slot	960	1920	3840	7680	11520	15360

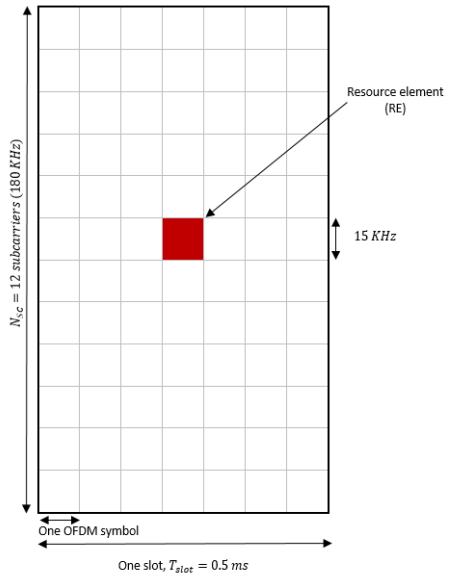

Figure 2.3: LTE time and frequency resource block

2.1.4.2 Synchronization

The PSS and SSS are used for radio frame synchronization. PSS are based on three 62-bit Zadoff-Chu sequences which are mapped to 72 active sub carriers in slot 0 and 10 in FDD, and slot 1 and 11. SSS is similar to PSS, however, they are made up of 62-bit 'm-sequence' scrambling sequences.

The eNB actively measures and sends a timing advance and frequency offset commands based on the difference between the received PUSCH, PUCCH and SRS. The received PSS and SSS commands are decoded by comparing with the three PSS sequences so as to obtain the sequence assigned to the cell, the Cell ID an group, as well as the primary synchronization offset. This process is repeated every 5 ms. The Cell ID is used to determine the pseudo-random sequence used for generating the reference signal in the cell. Once established, the (MIB) and (SFN) can be determined.

2.1.4.3 Uplink Physical-Layer Transmission

The LTE M-AC scheduler allocates a set of N_{RB} pairs which span $K = 14$ OFDM symbols in time (one subframe) to be used for the uplink transmission on the PUSCH physical channel. Two symbol periods are used for uplink demodulation reference signals for CSI and are thus not available for transmission. Furthermore, one additional symbol may be reserved for Sounding Reference Signals (SRS). SRS can also be used to estimate the downlink CSI assuming uplink/downlink reciprocity. This is especially of interest for TDD, where transmissions in downlink and uplink are on the same carrier frequency [11].

K blocks of N FFT-precoded symbols are mapped to the basic OFDM time-frequency grid, where $N = 12 \cdot N_{RB}$ is the assigned bandwidth in number of subcarriers. Mapping of the FFT-precoded signal to frequency-contiguous resource elements is preferred to retain good cubic-metric properties of the uplink transmission.

2.1.4.4 Downlink Physical-Layer Transmission

For downlink transmissions, up to two transport blocks of dynamic size are delivered to the physical layer and transmitted over the radio interface for each component carrier, depending on the configuration of the multi-antenna transmission scheme employed. The modulation schemes supported for the LTE downlink are QPSK, 16QAM, and 64QAM, respectively [12, 9, 13].

The modulation symbols are first mapped to N_L layers, corresponding to the number of antennas. The layers are then mapped to the antenna ports by means of the precoder functionality. The precoder relies on the Cell-Specific Reference Signals (CRS) for channel estimation for which there are at most four in each RB. This precoder/antenna

mapping can be described by a precoder matrix $\mathbf{W}$ of size $L \times N_L$, where L is the number of antenna ports. Thus the output of the precoder can be expressed as

$$\mathbf{x}_i = \mathbf{w}_i \mathbf{s}_i \qquad i \in L \tag{2.1}$$

where $\mathbf{x}_i$ is the precoded symbol at the i-th antenna output, $\mathbf{w}_i$ is the i-th precoding weight, and $\mathbf{s}_i$ is the i-th precoder input symbol. The antenna mapping can be configured depending on multi-antenna transmission scheme employed. These include transmit diversity, beam-forming and spatial multiplexing. The symbols of each antenna port are subsequently applied to the OFDM modulator [14].

Two classes of precoders are defined in LTE. These are Closed-Loop (CL) and Open Loop (OL) precoding, respectively. In case of CL precoding, the terminal selects and feeds back a suitable transmission rank and corresponding precoder matrix in the form of a Rank Indication (RI) and a Precoder-Matrix Indication (PMI), respectively. To limit the signalling overheads, only a limited set of codebook precoder matrices are defined for each transmission rank for a given number of antenna ports. OL precoding does not rely on any precoding. The precoder matrix is selected in a predefined and deterministic way known to the terminal in advance. The is especially important in high mobility scenarios where feedback is difficult [15, 16].

Similar to codebook-based precoding, non-codebook-based precoding is only applicable to DL-SCH transmission

2.1.5 Coordinated Multi-Point (CoMP)

CoMP is a technique introduce in LTE-A that enables the dynamic coordination of transmission and reception over different eNB's. The technique enables the Inter-Channel-

Interference (ICI) of neighbouring eNB's to be turned into useful signal, and thus results in improved overall system performance as well as efficient utilisation of the network. This is especially advantageous to cell edge users, who not only receive weaker signals from their serving eNB, but also high interferences from neighbouring eNBs. CoMP is divided into Joint Processing (JP) (Figure 2.4) and Coordinated Scheduling/Beamforming (CS/CB) (Figure 2.5) for both uplink and downlink [17, 18].

The downlink JP, data is transmitted to the terminal simultaneously from different eNBs so as to improve the received signal quality and strength, or actively cancel interference from transmissions that are intended for other terminals. This however, places a high demand onto the backhaul network because the data to be transmitted are shared to all participating eNBs. For downlink CS/CB, data to a single terminal is transmitted from one eNB, however, scheduling decisions are coordinated to control the interference. This reduces the backhaul signal in that only scheduling decisions are shared [19, 20].

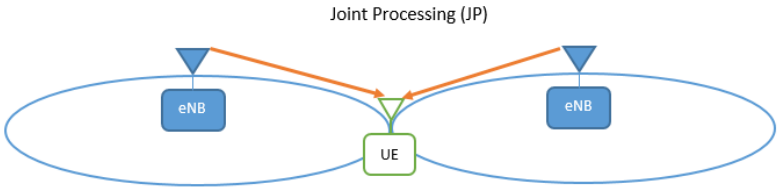

Figure 2.4: Joint Processing in Coordinated Multipoint

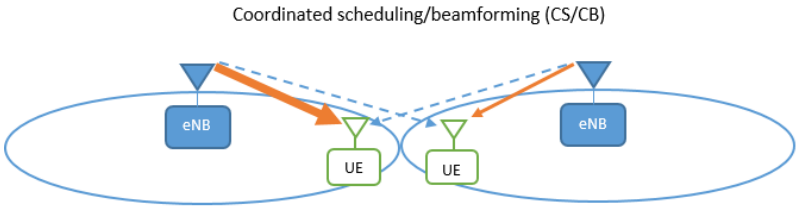

Figure 2.5: Coordinated Scheduling/Beamforming in Coordinated Multipoint

For uplink JP, multiple antennas at different eNBs are utilized to form a virtual antenna array. The signals received at the eNBs are then combined and processed to pro-

duce the final output signal. Uplink CS/CB operates by coordinating the scheduling decisions amongst the eNBs to minimise interference.

2.2 Multiple Access Techniques

Multiple Access allows multiple users to share a communication channel efficiently. The users transmit their signals independently to a common receiver via their respective channels. The transmissions must be within the total system bandwidth with individual user power constraints. Typically, the user transmissions are coordinated and synchronized by the base stations, such that the received signals are received coherently. MAS can be classified into two Orthogonal Multiple Access (OMA) and NOMA [21, 22, 23].

2.2.1 Orthogonal Multiple Access (OMA) Schemes

In OMA, multiple users transmit on orthogonal channels such that there is no interference in the users signal waveform. Thus, the receiver detects the signal for each user without interference from other users with the error performances similar to that of a single user. The total system resource/bandwidth W in time and frequency is divided into M frequency channels between the M users to ensure orthogonality. Examples of OMA techniques include time division multiple access (TDMA), frequency division multiple access (FDMA) (Figure 2.6), orthogonal division multiple access (OFDMA) and other MAC scheme which assign orthogonal signal waveforms.

2.2.1.1 Time Division Multiple Access (TDMA)

Time Division Multiple Access (TDMA) allows each user to transmit using the entire available bandwidth for a portion of the time [24]. Each frequency channel is divided

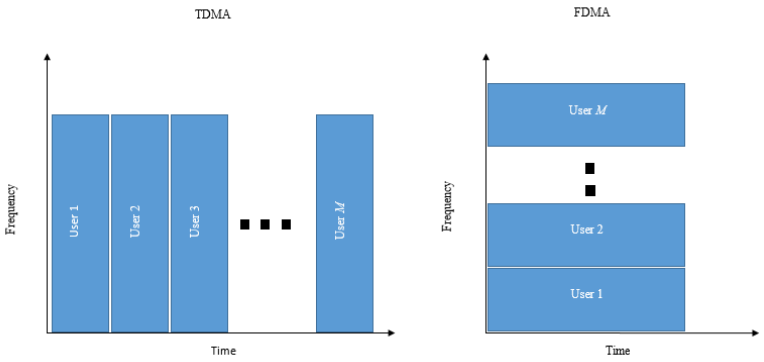

Figure 2.6: Orthogonal TDMA and FDMA resource allocation

into a number of periodically recurring time slots and multiple users are allocated a number of time slots which can vary according to their rate requirements. The number of slots in a frame, how many time slots are assigned to each user, and how this assignment is performed, depends on a number of factors such as permissible delay, available bandwidth, modulation technique etc.

2.2.1.2 Frequency Division Multiple Access (FDMA)

Frequency Division Multiple Access (FDMA) is the most classic MAC scheme used in mobile communications systems. The available system bandwidth W is divided into M equal narrow band frequency channels serving M users simultaneously where each user is allocated its exclusive channel. Frequency spacing between the user channels is required to minimize inter-channel interference caused by the non-linear effects of power amplifiers, operating near saturation which spread the signal bandwidth and generate inter-modulation frequencies [24, 4].

The basic challenges of classic FDMA are the requirement of M modulators and demodulators at the base station to serve M users simultaneously, which leads to excessive cost and complexity where the BS must handle large number of users (hundreds to thousands). Secondly, FDMA is not flexible in handling users with varying transmission

rate requirements due to the fixed allocation of narrowband channels. Thirdly, it suffers bandwidth wastage where no sub-channel is reallocated to other users if it is not in use by the assigned user [3, 25].

2.2.1.3 Orthogonal Frequency Division Multiplexing (OFDMA)

OFDM [26, 27] is a narrowband OMAS scheme used in 4G networks. In OFDM, the signals to be transmitted are mapped onto several parallel orthogonal sub-carriers (Figure 2.7). The orthogonality between subcarriers is ensured by spacing the subcarriers by n/T_s, where T_s is the symbol time and n is a non-zero integer usually chosen as one. Guard intervals called CP are added to each OFDM symbol to mitigate ICI. Furthermore, the bandwidth of each sub-carrier is narrower than the coherence bandwidth of the channel, which ensures flat fading in an otherwise frequency-selective channel. Practical implementations of OFDM is performed with a more efficient and faster Inverse Fast Fourier Transform (IFFT) for modulation, while fast fourier transform (FFT) is used for demodulation.

OFDMA [26, 28, 29] is a hybrid combination of FDMA and OFDM. It is currently used in wireless LAN, WiMAX (IEEE 802.16), and LTE downlink systems. The system bandwidth is divided into many sub-channels and each user is allocated multiple dedicated sub-channels, allowing M users transmit simultaneously. The number of sub-carriers allocated to each user is flexible dependent on its rate and QoS requirement. Additionally, sub-carrier allocation to different users can be either adaptive tor fixed [30, 31, 32, 33, 34, 35]. Fixed sub-carrier allocation does not adapt to users' channel conditions and remain unchanged throughout the communication session leading to a simpler implementation without incurring high overheard. Furthermore, the users can be allocated adjacent subcarriers, which simplifies frequency and time synchronization

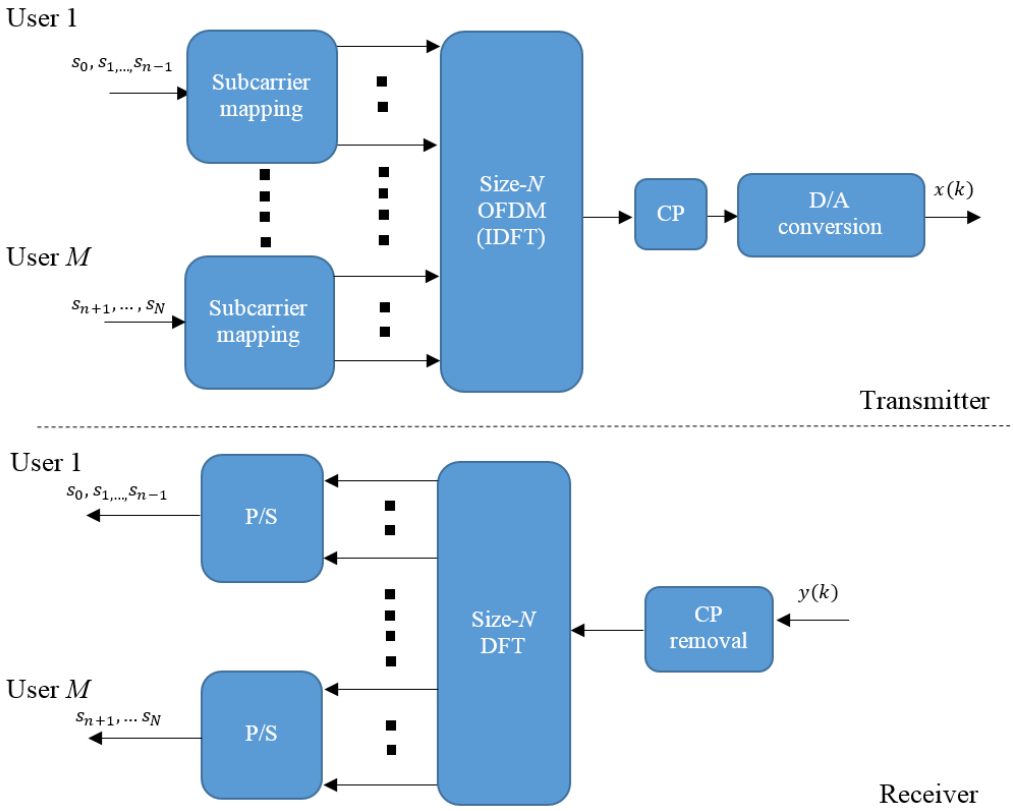

Figure 2.7: OFDMA resource allocation and modulation

on the expense of vulnerability to deep fading, or separated by more than the coherent bandwidth of the channel to exploit maximum frequency diversity, at the expense of a minimum separation between sub-carriers from different users requiring strict cross-user synchronization to avoid ICI.

Adaptive sub-carrier allocation dynamically allocates sub-carriers to users based on their channel condition so as to optimize some performance criteria.

The main challenges with OFDMA is that it suffers from a high Peak-to-Average Power Ratio (PAPR) which leads to inefficient operation of power amplifiers [36, 11, 31]. This is especially critical in uplink where user transmit powers are limited Secondly, OFDM is very sensitive to errors in time and frequency synchronization which leads to frequency and phase offset causing ICI and ISI.

2.2.1.4 Single Carrier-Frequency Division Multiple Access (SC-FDMA)

SC-FDMA can be described as normal OFDM with a FFT-based precoding to reduce the PAPR of the transmitted signal envelope [37, 38, 39, 40, 41, 42, 43, 44]. This is also known as DFTS-OFDM. A block of O modulation symbols from some modulation alphabet are first applied to a size-N DFT N_{DFT}. The output of the DFT is then mapped to consecutive subcarriers of an OFDM modulator where a size-K IFFT K_{IFFT} is implemented with $K_{IFFT} > N_{FFT}$. The unused IFFT subcarriers are set to zero. This is illustrated in Figure 2.8. A more computationally efficient radix-2 IFFT processing, $K_{IFFT} = 2^k$, for some integer k is used in place of IFFT. Similar to normal OFDM, a cyclic prefix is inserted for each transmitted block. When the FFT size M equals the IFFT size K, the FFT-IFFT

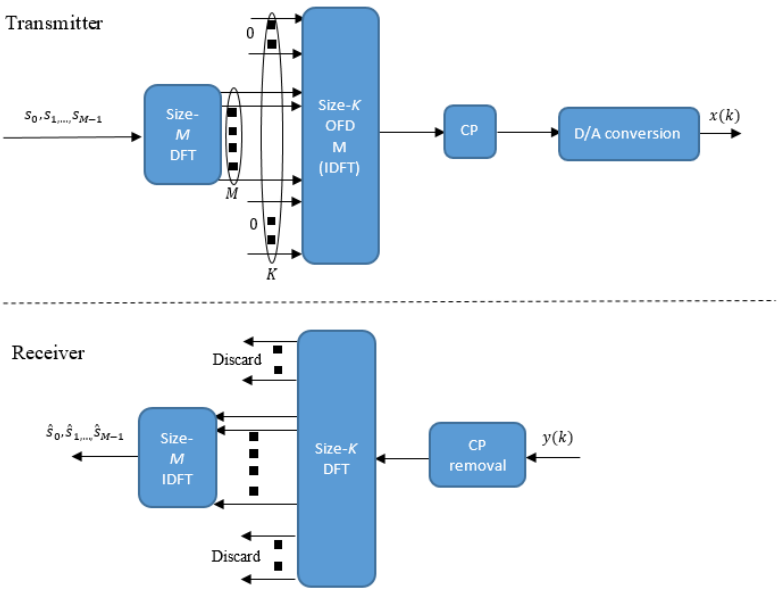

Figure 2.8: SC-FDMA resource allocation and modulation

processing would imply cancel each other out. However, when M is smaller than K with the remaining inputs to the IFFT set to zero, the output of the IFFT will be a signal with 'single-carrier'properties such as low power variations which increase power amplifier efficiency, and a bandwidth that depends on M.

2.2.2 Non-Orthogonal Multiple Access (NOMA) Schemes

NOMA is a promising technology that aims to increase the system throughput and capacity [45, 2, 46, 45, 47, 48]. NOMA allows multiple users to share time and frequency resources in the same spatial layer via simple linear superposition or code-domain multiplexing. The interference in NOMA is made controllable by non-orthogonal resource allocation, at the cost of slightly increased receiver complexity, where SIC or ML is employed. In OMA, although the orthogonally multiplexed users facilitates simple and interference-free Multi-User Detection (MUD) at receivers, it does not achieve the sum-rate capacity of a wireless system.

2.2.2.1 Power Domain NOMA (PD-NOMA)

PD-NOMA [2, 49, 50, 45, 1, 51, 52, 53, 48, 54] is a leading candidate for 5G multiple access. It is based on the principles of superposition coding where the transmitted signal is the sum of users' signals in the power domain, as illustrated in Figure 2.9. The scheme exploits the received power differences due to the near-far effect between users to solve the problem of detection ambiguity. i.e. the weaker users are allocated more power compared to the stronger users. Thus, the larger the difference in power level of the users'signals, the better the performance which outperforms the orthogonal schemes.

Consider a two user system where user 1 and user 2 are located far and near an eNB. Their transmit powers are P_1 and P_2. The received signals for the downlink, $y_m^{[DL]}$, and uplink $y^{[UL]}$ PD-NOMA systems can be expressed as

$$\mathrm{y}_m^{[DL]} = \mathrm{h}_m(\sqrt{\mathrm{P}_1}\mathrm{x}_1 + \sqrt{\mathrm{P}_2}\mathrm{x}_2) + \mathrm{z}_m = \mathrm{h}_m\mathrm{x} + \mathrm{z}_m \tag{2.2}$$

$$\mathrm{y}^{[UL]} = \mathrm{h}_1\sqrt{\mathrm{P}_1}\mathrm{x}_1 + \mathrm{h}_2\sqrt{\mathrm{P}_2}\mathrm{x}_2 + \mathrm{z} \tag{2.3}$$

where x_1, x_2 are the modulated symbols, h_1, h_2 the relative user complex channel coefficient between the eNB, and z the additive white Gaussian noise including ICI.

In downlink PD-NOMA, the same composite transmitted signal from the eNB is received at both users. This requires multi-user signal separation to be implemented at the UE so that each user can detect its component signal and decode its own data where non-linear receivers such as maximum likelihood detection or SIC can be employed. For SIC, the optimal order for decoding is in the order of the decreasing channel gain normalized by noise and ICI power, $|\mathbf{h}_m|^2/\mathbf{z}_0, m$. Thus, the i-th user can remove the inter-user interference from the j-th user where $|\mathbf{h}_j|^2/\mathbf{z}_0, j < |\mathbf{h}_i|^2/\mathbf{z}_0, i$. For the two-user case, assuming that $|\mathbf{h}_1|^2/\mathbf{z}_0, 1 > |\mathbf{h}_2|^2/\mathbf{z}_0, 2$, user 2 does not perform interference cancellation since it comes first in the decoding order. User 1 first decodes x_2 and subtracts its component from received signal y_1, then decodes x_1 without interference from x_2. In uplink PD-NOMA, the combined transmitted signal from the users are received at the eNB. The BS conducts SIC according to the descending order of channel gains, with the least power user detected interference free. A major disadvantage is the error propagation inherent in SIC.

For comparison, in OMA, the rates for each user can be expressed as

$$\mathrm{R}_1 < \alpha \log\left(1 + \frac{\mathrm{P}_1|\mathrm{h}_1|^2}{\alpha Z_0}\right) \tag{2.4}$$

$$\mathrm{R}_2 < (1-\alpha) \log\left(1 + \frac{\mathrm{P}_2|\mathrm{h}_2|^2}{(1-\alpha) Z_0}\right) \tag{2.5}$$

where α is the total time frequency resource. The term $(1-\alpha)$ ensures orthogonality is maintained by UE2 transmitting on different resources compared to UE1. In PD-NOMA,

the resources are share between the user and the rates become

$$R_1 < \log\left(1 + \frac{P_1|h_1|^2}{P_2|h_2|^2 + Z_0}\right) \tag{2.6}$$

$$R_2 < \log\left(1 + \frac{P_2|h_2|^2}{Z_0}\right) \tag{2.7}$$

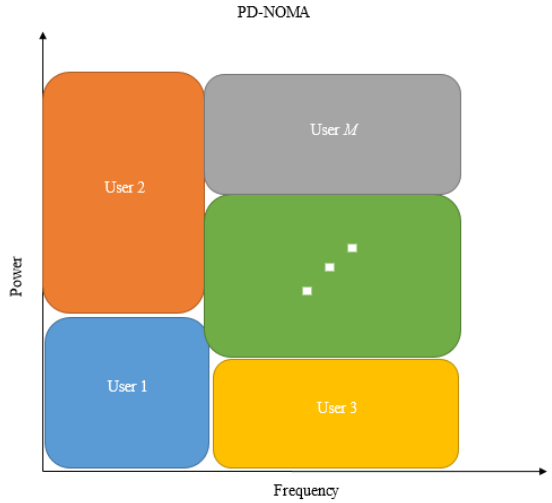

Figure 2.9: Power domain NOMA resource allocation

The main disadvantage of PD-NOMA is that although larger the difference in power level results in better the performance, the user throughput fairness is poor due to the rate of the weaker users becoming significantly lower than the stronger users as the power difference increases.

2.2.2.2 Coding Division Multiple Access (CDMA)

Coding Division Multiple Access (CDMA), illustrated in Figure 2.10, was initially developed for the military to allow multiple users M transmit on a network simultaneously. It is achieved by multiplying the data of each user with one out of W unique spreading sequences $\mathbf{W}^{[CDMA]}$ [55, 56, 57, 58, 59, 60]. The spreading code is normally composed of N chips which leads to a rate much higher than that of the user's which

leads to bandwidth expansion. The receiver, with a priori knowledge of the spreading codes, despreads the received signal back to its original bandwidth and in the process, cancels or minimize the interference from other users.

The wideband nature of CDMA makes it highly susceptible to a large delay spread between received paths which allows the receiver to reliably resolve a number of independent paths which are coherently combined to provide high path diversity, ensuring resilience to multipath fading. Furthermore, spreading the signal over large bandwidth results in a more resilience to interference and jamming due to signal level hidden in noise.

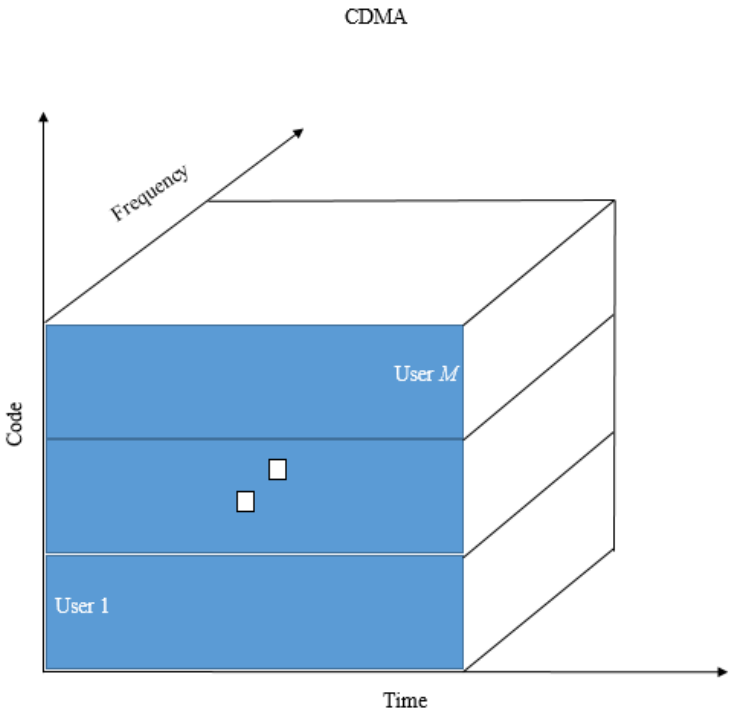

Figure 2.10: Code division multiple access resource allocation

The main disadvantage in CDMA is the bandwidth inefficiency due to bandwidth expansion. Additionally, the maximum number of users on a given channel with equal bit rate is limited by the number of sequences.

2.2.2.3 Low-Density Spreading (LDS)

Low-Density Spreading (LDS-CDMA) is an improved version of CDMA where sparse spreading sequences are used instead of conventional dense spreading sequences [61, 62, 63, 64, 65]. The number of non-zero spreading sequences are much less than that of CDMA which leads to less cross-sequence interference i,e. $\mathbf{W}^{[LDS]} << \mathbf{W}^{[CDMA]}$. While orthogonal spreading sequences would significantly reduce the inter user interference, they are generally not designed for channel overloading.

At the receiver, SIC or a simplified sequence detector known as Message-Passing Algorithm (MPA) can be employed for MUD. In MPA, a variable node represents the transmitted symbol, and a factor node corresponds to the received signal at each chip. The reliability of the symbols are exchanged between the nodes which improves error performance. Furthermore, assuming the maximum number of users superposed at the same chip is w, due to the LDS structure, the receiver complexity is $O(\mathbf{Q}^w)$ compared to $O(\mathbf{Q}^M); M > w$ for conventional CDMA where $\mathbf{Q}$ denotes the constellation order. Another advantage is that LDS-CDMA can directly be converted to LDS-OFDM, where the chips are replaced by subcarriers in OFDM.

2.2.2.4 Sparse-Code Multiple Access (SCMA)

Sparse-Code Multiple Access (SCMA) is an enhanced LDS where their principle of operation are similar [66, 67, 68]. However, in SCMA, bit streams are directly mapped to different sparse codewords. All codewords in the same codebook contain zeros in the same two dimensions, and the positions of the zeros in the different codebooks are distinct so as to facilitate the collision avoidance of any two users.

The key difference between LDS and SCMA is that a multi-dimensional constella-

tion for SCMA is designed to generate codebooks, which results in 'shaping'gain that is not possible for LDS. To simplify the design of the multi-dimensional constellation, a mother constellation can be generated by minimizing the average alphabet energy for a given minimum Euclidean distance between constellation points, and also taking into account the codebook-specific operations such as phase rotation, complex conjugate and dimensional permutation.

2.2.2.5 Multi-user Shared Access (MUSA)

Multi-User Shared Access (MUSA) [48, 69] is a NOMA spreading scheme where each users'modulated data symbols are spread by a specially designed sequence that facilitates robust SIC implementation. The design criteria is that the spreading sequences should have low cross-correlation and can be non-binary. The Users pick a random sequence from a pool of multiple spreading sequences. Furthermore, different spreading sequences may also be used for different symbols. This leads to improved performance via interference averaging. At the receiver, codeword-level SIC is used to separate data from different users. The complexity of codeword-level SIC is less of an issue in the uplink as the receiver needs to decode the data for all users anyway.

2.2.2.6 Pattern-Division Multiple Access (PDMA)

Pattern Division Multiple Access (PDMA) [70, 71, 72] has been proposed to exploit diversity without losing spectral efficiency. The technique uses non-orthogonal *"patterns"*, which are designed to maximize the diversity while minimizing the overlaps among multiple users. The diversity is not only actualized in the spatial domain, but also in time or frequency domain. The detection also uses a MPA to compute the marginal functions of the global code constraint by iterative computation of a local code constraint. Although

the codewords of PDMA do not have the low-density property in general, appropriate diversity order disparity can be observed where diversity order disparity leads to faster convergence of MPA. PDMA results in improved overall system capacity and error performance for each user, due to the diversity.

2.3 Multiple Antenna Techniques

Multiple antennas available at the transmitter and/or receiver can be utilized to increase the diversity and/or capacity of a communication system [73, 74, 75]. When the antennas are sufficiently placed apart, independent signal paths can be created where the channel between different transmit and receive antenna pairs fade independently. The required separation distance between antennas is dependent mainly on the carrier frequency f_c and the local scattering environment. For mobile equipment surrounded by many scatterers, the typical antenna separation is $0.5 \sim 1.0$ of carrier wavelength λ_c. For BS antennas placed on high towers, larger antenna separation of around 10's of wavelengths may be required.

Receive diversity is achieved by utilizing multiple receive antennas as in Single-Input Multi-Output (SIMO) scheme, while transmit diversity is achieved by utilizing multiple transmit antennas as in Multi-Input Single-Output (MISO) scheme Figure 2.11. When multiple transmit and receive antennas are employed such as MIMO, the capacity and diversity are increased significantly. This makes multi-antenna techniques an active area of research in order to meet the capacity and throughput requirements outlined for 5G. For example, massive MIMO techniques have recently been proposed which sees the number of antenna elements significantly increased (10-100x) so as to satisfy the requirements mentioned above (see Section 2.4.1).

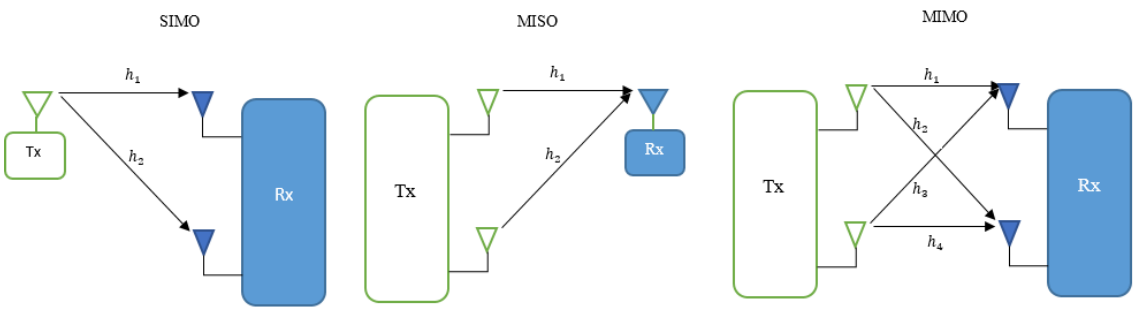

Figure 2.11: Multi-antenna techniques including SIMO, MISO and MIMO

2.3.1 Multiple Input Multiple Output (MIMO) Communications

MIMO communications exploits the spatial dimension through the use of multiple antennas at both the transmitter and receiver. This takes advantage of the rich scattering environment to allow for independent uncorrelated channels between any pair of receive-transmit antennas [76, 77, 78, 79, 80, 81, 82, 83]. MIMO system capacity and diversity gain increases linearly on the order of transmit/receive antennas $M_{min} = \min(M_t, M_r)$ and $M_t \times M_r$, respectively, without any power or bandwidth penalty. Furthermore, MIMO enables the realisation of spatial multiplexing (SM) where M_{min} independent transmissions are transmitted over the same bandwidth. Another form of SM, known as Vertical-Bell Labs Layered Space-Time (V-BLAST), is also employed to increase the system capacity rather than diversity.

MIMO systems are classified into Sinlge User MIMO (SU-MIMO) and Multiuser MIMO (MU-MIMO). In the following sections we will provide an overview of both SU-MIMO and MU-MIMO and explain various linear and non-linear precoding and detection techniques used in MIMO.

2.3.1.1 Single-User MIMO (SU-MIMO)

SU-MIMO is a point-to-point transmission where a single user equipped with M_t antennas transmits to a single receiver equipped with M_r antennas (Figure 2.12). The multiple

antennas at both the transmitter and receiver provide extra DoF which can be exploited to improve the system performance at the cost of hardware complexity. The received signal y is given by

$$\begin{bmatrix} y_1 \\ \vdots \\ y_{M_r} \end{bmatrix} = \begin{bmatrix} h_{11} & \dots & h_{M_t 1} \\ \vdots & \ddots & \vdots \\ h_{1M_r} & \dots & h_{M_t M_r} \end{bmatrix} \begin{bmatrix} x_1 \\ \vdots \\ x_{M_t} \end{bmatrix} + \begin{bmatrix} z_1 \\ \vdots \\ z_{M_r} \end{bmatrix} \Longleftrightarrow \mathbf{y} = \mathbf{H}\mathbf{x} + \mathbf{z} \tag{2.8}$$

where $\mathbf{y} \in \mathbb{C}^{M_r \times 1}$ is the complex $m \times 1$ received signal vector, $\hat{\boldsymbol{s}} = [\hat{s_1}, \dots, \hat{s_{M_t}}]$ is $M_t \times 1$ data vector, $\mathbf{H} \in \mathbb{C}^{M_t \times M_r}$ is the $M_t \times M_r$ complex channel matrix which assumed to be available at the receiver, $\mathbf{x} \in \mathbb{C}^{M_r \times 1}$ is $M_t \times 1$ complex transmitted symbol vector and $\mathbf{z} \in \mathbb{C}^{M_r \times 1}$ is $M_t \times 1$ noise vector of i.i.d complex Additive White Gaussian Noise (AWGN) with each element having variance σ^2.

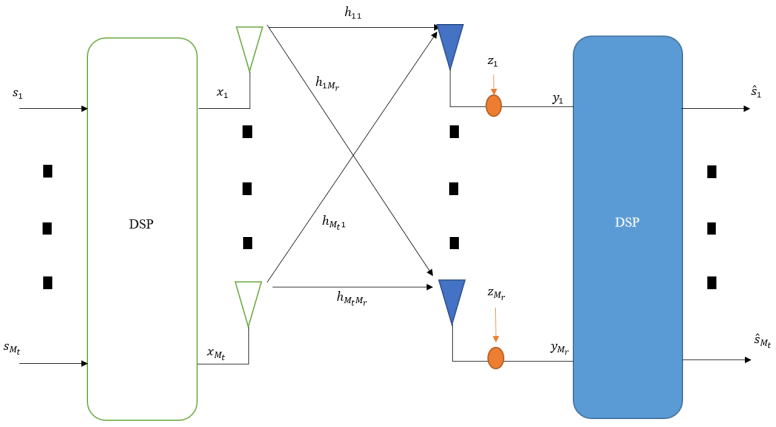

Figure 2.12: Single user MIMO system

The rank of MIMO channel is the algebraic rank of $\mathbf{H}$ which is the number of independent equations offered by the linear system ($rank \leq \min(M_t, M_r)$). Thus the number of streams that can simultaneously be transmitted using SU-MIMO is limited by the by $rank(\mathbf{H})$ and the availability of uncorrelated channels or the lack of dominant LOS.

Depending on the average received Signal-to-Noise Ratio (SNR), SU-MIMO can be used either to increase the reliability of data transmission through maximising spatial diversity gain or increase the system capacity through SM. The former is referred to in literature as D-BLAST while the latter is called V-BLAST.

In D-BLAST, redundancy between the data streams is introduced through the use of specialized Space-Time Block Coding (STBC) while in V-BLAST, serial data streams are divided into parallel data streams which are independently modulated and coded before being transmitted from different transmit antennas. In addition to SM gain, V-BLAST can achieves a diversity gain order up to M_r which varies depending in detection scheme employed. Numerous detection techniques including Zero Forcing (ZF) and Minimum Square Error (MMSE) has been proposed.

2.3.1.2 Multi-user MIMO (MU-MIMO)

MU-MIMO (Figure 2.13) is considered as an extension of SU-MIMO for the MAC to increase the spectral efficiency considerably. MU-MIMO exploits the spatial dimension in rich fading environment to enable the simultaneous communication of multiple users without subdivision in limited resources of time, frequency and codes. In the downlink however, since users can not jointly decode their data streams, precoding at the BS becomes necessary to implement Spatial Multiplexing (SM).

For uplink MU-MIMO, where M users each equipped with K antennas are chosen to communicate with a BS equipped with L antennas, the received signal y at the BS can be expressed as

$$\mathbf{y} = \sum_{m}^{M} \mathbf{H}_i \mathbf{x}_i + \mathbf{z} \tag{2.9}$$

where $\mathbf{x}_m$ is transmitted signal vector of the m-th user. $\mathbf{H}_m$ is complex Rayleigh flat

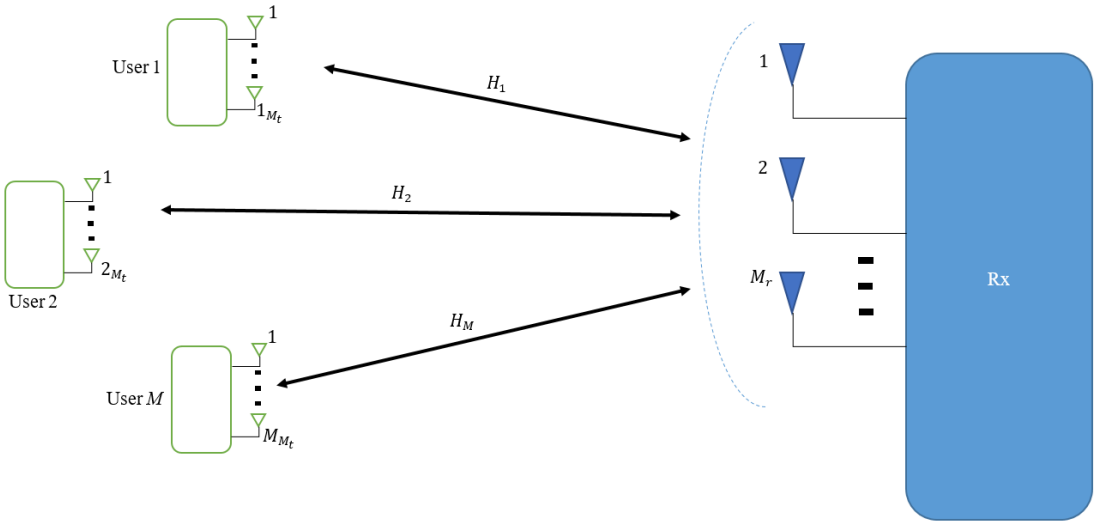

Figure 2.13: Multiuser MIMO system

fading channel matrix of the m-th user, which is assumed to be available at both communication ends, and $\mathbf{z}_m$ is vector of i.i.d complex AWGN with each antenna element having variance of σ^2. Each user is subject to an individual power constraint of P_m such that $tr(\mathbb{Q}_m) \leq \mathrm{P}_m$, where $m \in M$ where $\mathbb{Q}_m$ is the transmit covariance matrix of the m-th user defined as $\mathbb{Q}_m \triangleq \mathbb{E}[\mathrm{x}_m \mathrm{x}_m^T]$.

For the downlink, the received signal vector $\mathbf{y}_m$ at the m-th user is given as

$$\mathbf{y}_m = \mathbf{H}_m^T \sum_{m}^{M} \mathbf{x}_m + \mathbf{z} \tag{2.10}$$

where $\mathbf{x}$ is the superposition of modulated usersâĂŹ symbols transmitted from BS. $\mathbf{H}_m$ is complex Rayleigh flat fading downlink channel matrix for user m and assumed to be available at both communication ends, and $\mathbf{z}$ is vector of i.i.d complex AWGN at m-th user with each antenna element having variance of σ^2. The BS is under power constraint of $\mathrm{P} = \sum_m^M \mathrm{P}_m$ which is defined $tr(\mathbb{Q}) \leq \mathrm{P}$.

2.3.2 Precoding

When channel information is available at the transmitter, channel precoding can be used to achieve higher sum rates. Precoding is classified into linear and non-linear precoding[84, 85, 86, 87, 88, 89].

2.3.2.1 Linear Precoding

Multiuser linear precoders are jointly designed such that performance metrics for all users such as, sum rate and Signal-to-Interference-Plus-Noise Ratios (SINR), are maximized. Different precoding matrices $\mathbf{w}_m; m = 1, 2, \ldots, M$ are assigned to M active users at the transmitter. Example precoders are ZF and MMSE which invert the multiuser channel matrix [90]. The signal for each user $\mathbf{s}_m; m = 1, 2, \ldots, M$ is pre-multiplied the by ZF or MMSE precoding weights and thus, the received signal at the m-th user is given by

$$\mathbf{y}_m = \mathbf{H}_m^T \mathbf{w}_m \mathbf{s}_m \sum_{\substack{m=1 \\ i \neq m}}^{M} \mathbf{H}_m^T \mathbf{w}_m \mathbf{s}_m + \mathbf{z} \tag{2.11}$$

where the first and second terms represent the desired signal and the multiuser interference, respectively. The disadvantage in Equation (2.11) is that as the number of streams increase, performance decreases. A generalized ZF beamforming $\mathbf{w}_m$ is employed to solve this problem by pre-cancelling the interference ($\mathbf{H}_m^T \mathbf{w}_m = 0; \forall m \neq m$) at the transmitter.

2.3.2.2 Non-linear Precoding

Non-linear precoding involves extra signal processing compared with the linear version. The main methods used for non-linear precoding are based on spatial extension of Tomlinson-Harashima Precoding (THP) and the optimal Dirty Paper Coding (DPC).

[91, 92].

2.3.2.3 Singular Value Decomposition (SVD)

Singular Value Decomposition (SVD) [93, 94, 95] is a novel way of enabling spatial multiplexing to a single user employing MIMO type communication. SVD decomposes the the channel matrix $\mathbf{H}$ into a set of interference free parallel point-to-point channels capable of supporting a stream on each antenna, as illustrated in Figure 2.14. With appropriate power control and CSI available at both transmission points, SVD provides optimum MIMO performance. The channel matrix $\mathbf{H}$ can be decomposed into three separate matrices

$$\mathbf{H} = \mathbf{U}\Lambda\mathbf{V}^{*} \tag{2.12}$$

where $\mathbf{U} \in \mathbb{C}^{M_r \times M_r}$ and $\mathbf{V} \in \mathbb{C}^{M_t \times M_t}$ are the unitary rotation matrices and $\Lambda \in \mathbb{R}^{M_r \times M_t}$ is a rectangular matrix whose diagonal elements $\lambda_1 \geq \lambda_2 \ldots \lambda_{rank(\mathbf{H})}$ are real non-negative ordered singular values of the matrix $\mathbf{H}$, and off-diagonal, zero. Since

$$\mathbf{H}\mathbf{H}^{*} = \mathbf{U}\Lambda\Lambda^{T}\mathbf{U}^{*}, \tag{2.13}$$

the squared of the singular values λ_m^2 are the eigenvalues of the matrix $\mathbf{H}\mathbf{H}^{*}$ and $\mathbf{H}^{*}\mathbf{H}$. As there are $rank(\mathbf{H})$ singular values, the SVD can be rewritten as

$$\mathbf{H} = \sum_{m=1}^{M} \lambda_m \mathbf{u}_m \mathbf{v}_m^{*} \tag{2.14}$$

From Equation (2.14), the precoding matrix $\mathbf{V}$ and the post-coding matrix $\mathbf{U}^{*}$ can be applied at the transmitter and receiver, respectively, to transform the channel into parallel

channels weighted according to the matrix Λ expressed below

$$\mathbf{y} = \mathbf{U}^*(\mathbf{U}\Lambda\mathbf{V}^*)\mathbf{V}\mathbf{x} + \mathbf{U}^*\mathbf{z} \tag{2.15}$$

$$\mathbf{y} = \mathbf{I}\Lambda\mathbf{I}\mathbf{x} + \mathbf{U}^*\mathbf{z} \tag{2.16}$$

$$\mathbf{y} = \Lambda\mathbf{x} + \mathbf{U}^*\mathbf{z} \tag{2.17}$$

where $\mathbf{z} \sim \zeta\aleph(0, \mathrm{Z}_0\mathrm{I}_{M_r})$. The capacity of the decomposed MIMO channel can then be expressed as

$$\mathrm{C}_{SVD} = \sum_{m=1}^{rank(\mathbf{H})} \log(1 + \frac{p_m\lambda_m^2}{\mathrm{Z}_0}) \qquad bits/s/Hz \tag{2.18}$$

where p_m are the water-filling power allocation coefficients given as

$$p_m = (\mu - \frac{\mathrm{Z}_0}{\lambda_m^2})^+ \tag{2.19}$$

where μ is chosen to satisfy $\sum_m \mathrm{p}_m = \mathrm{P}$. Each element of Λ corresponds to the non-zero eigen-channel which supports a data stream, enabling spatial multiplexing of all $rank(\mathbf{H})$ streams.

The drawback in SVD is that it is mostly employed in single user MIMO communication due to the difficulty of decomposing multi-user channels. This is because at the eNB, the decomposition is performed on a single matrix populated with all the user channels to obtain a precoding matrix, while the users can only decompose and obtain their respective channels, which does not correlate with the multi-user channel post-coding matrix.

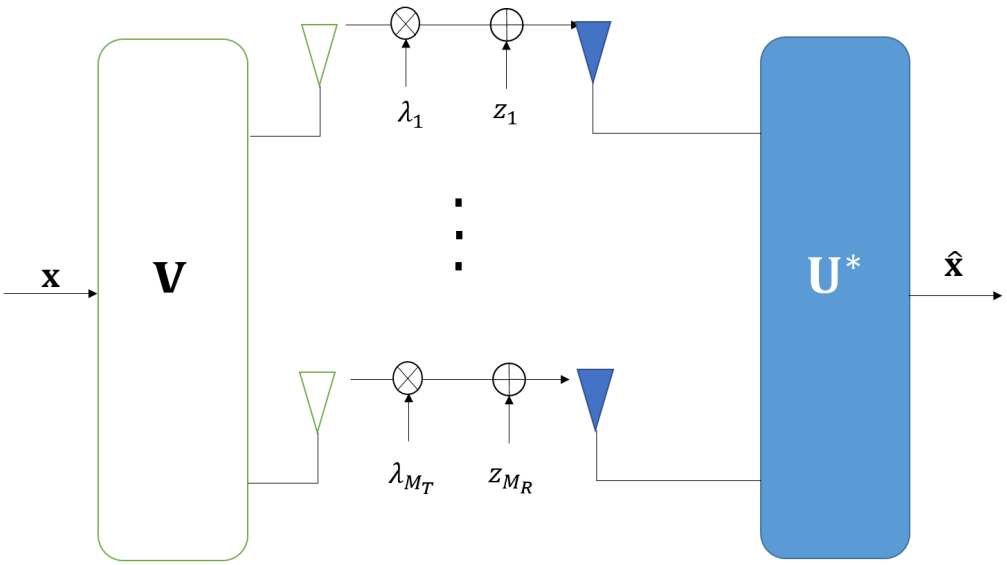

Figure 2.14: Spatial Multiplexing by singular value decomposition precoding

2.3.2.4 Block Diagonalization (BD)

Block Diagonalization (BD) has been proposed to enable SVD decomposition of multi-user MIMO channels [96, 97, 98, 99]. The BD method is an extension of zero forcing precoding which attempts to completely eliminate the MUI by twice SVD operations. The key idea of BD is to employ a precoding $\mathbf{V}$ such that

$$\bar{\mathbf{H}}_m \mathbf{V}_m = 0 \tag{2.20}$$

where $\bar{\mathbf{H}}_m$ is defined as the channel matrix of all users other that user m, expressed as

$$\bar{\mathbf{H}}_m = \bar{\mathbf{H}}_1^T, \ldots, \bar{\mathbf{H}}_{m-1}^T, \bar{\mathbf{H}}_{m+1}^T, \ldots, \bar{\mathbf{H}}_M^T]^T \tag{2.21}$$

Applying SVD to $\bar{\mathbf{H}}_m$ produces

$$\bar{\mathbf{H}}_m = \mathbf{U}_m \Lambda_m [\mathbf{V}_m^{(1)} \mathbf{V}_m^{(0)}]^* \tag{2.22}$$

where Λ_m is the diagonal matrix whose diagonal elements are the non-negative singular values of $\bar{\mathbf{H}}_m$ with dimensions of $rank(\bar{\mathbf{H}}_m)$. The matrices $\mathbf{V}_m^{(0)}$ and $\mathbf{V}_m^{(1)}$ contains the corresponding zero singular values and non-zero singular values of $\bar{\mathbf{H}}_m$, respectively. Therefore, $\mathbf{V}_m^{(0)}$ forms a orthogonal basis for the null space of $\bar{\mathbf{H}}_m$. Performing another SVD operation to $\bar{\mathbf{H}}_m\bar{\mathbf{V}}_m^{(0)}$ produces

$$\bar{\mathbf{H}}_m\bar{\mathbf{V}}_m^{(0)} = \bar{\mathbf{U}}_m\bar{\Lambda}_m[\bar{\mathbf{V}}_m^{(1)}\bar{\mathbf{V}}_m^{(0)}]^* \tag{2.23}$$

Thus, the total precoding matrix is defined as

$$\mathbf{V}^{BD} = [\bar{\mathbf{V}}_1^{(0)}\mathbf{V}_1^{(1)}, \bar{\mathbf{V}}_2^{(0)}\mathbf{V}_2^{(1)}, \ldots, \bar{\mathbf{V}}_M^{(0)}\mathbf{V}_M^{(1)}]\mathbf{D}^{1/2} \tag{2.24}$$

where $\mathbf{D}$ is a diagonal matrix whose elements scale the power transmitted on each column of $\mathbf{V}^{BD}$. The optimal power allocation coefficients of $\mathbf{D}$ are determined by water filling on the diagonal elements of Λ. Assuming total power constraint P_m, Λ can be expressed as

$$\Lambda = \begin{bmatrix} \Lambda_1 & \ldots & 0 \\ \vdots & \ddots & \vdots \\ 0 & \ldots & \Lambda_M \end{bmatrix} \tag{2.25}$$

Therefore, the sum capacity of a BD system can be expressed as

$$\mathrm{C}_{BD} = \max_{\mathbf{D}} \log(1 + \frac{\Lambda^2\mathbf{D}}{\sigma^2}) \tag{2.26}$$

2.3.3 Signal Detection

MUD [100, 101] techniques for MU-MIMO can be classified into linear and non-linear schemes. Linear MUD techniques such as low complexity ZF and MMSE provides limited performance due to the employment of linear front-end de-correlator **G** to separate data streams before individual demodulation. On the other hand, non-linear MUD methods such as ML can achieve optimal performance at cost of high computational complexity which increases exponentially as the number of users increase. Due to complexity issue, practical implementation of ML in overloaded system scenarios is prohibitive leading to search for suboptimal non-linear MUD techniques

2.3.3.1 Maximum Likelihood (ML) Detection

The optimal non-linear ML [102, 103] receiver performs signal decoding through exhaustive search for the most likely transmitted signals thus, minimizing the error probability at the cost of high computational complexity. For system of M users each equipped with single antenna and using the modulation alphabet size O,the number of computations is $Q = O^M$. ML receiver provides receive diversity of order M and the signal estimation is expressed as

$$\hat{\mathbf{x}} = \arg\Big(\min_{\substack{\mathbf{x}_q \in \mathbf{U} \\ q \in Q}} \|\mathbf{y} - \mathbf{H}\mathbf{x}_q\|^2\Big) \tag{2.27}$$

where $\mathbf{U} = [\mathbf{x}_1, \ldots, \mathbf{x}_q, \ldots, \mathbf{x}_Q]$ is the set of all possible transmitted signals vectors and $\mathbf{x}_q$ is the q-th possible vector.

2.3.3.2 Zero Forcing Detection

The linear ZF [104, 105, 106] receiver has a front-end $\mathbf{G}_{zf} = \mathbf{H}^{\dagger}$ where $\mathbf{H}^{\dagger} = (\mathbf{H}^{*}\mathbf{H})^{-1}\mathbf{H}^{*}$ denotes the Moore-Penrose pseudo-inverse of the channel matrix. The front-end are constructed from bank of M de-correlators where it decouples the matrix channel into parallel scalar channels where m-th decorrelator is the m-th column of $\mathbf{G}_{zf}$. When $\mathbf{H}$ is square and invertible, then $\mathbf{G}_{zf}$ is simply channel inversion. The output of a ZF receiver with perfect CSI at Receiver (CSIR) is thus given by

$$\mathbf{x} = \mathbf{G}_{zf}(\mathbf{H}\mathbf{x} + \mathbf{n}) = \mathbf{x} + \mathbf{H}^{\dagger}\mathbf{z} \tag{2.28}$$

The joint decoding decomposes the received signal into M streams which eliminates the Multiple User Interference (MUI). However, this comes at cost of noise enhancement.

2.3.3.3 Minimum Mean Squared Error (MMSE) Detection

The linear MMSE [107, 105] receiver maximizes the output SINR and minimize the mean square error in when estimating the transmitted signals. The front-end $\mathbf{G}_{mmse}$ of the receiver is constructed from bank of M-MMSE receivers given by

$$\mathbf{G}_{mmse} = (\mathbf{H}^{*}\mathbf{H} + \Gamma)^{-1}\mathbf{H}^{*} \tag{2.29}$$

where Γ is $M \times M$ diagonal matrix with entries of $\Gamma_m = 1/\lambda_m$, and $\lambda_m = \mathrm{P}_m/\mathrm{Z}_o$ is SNR of m-th user.

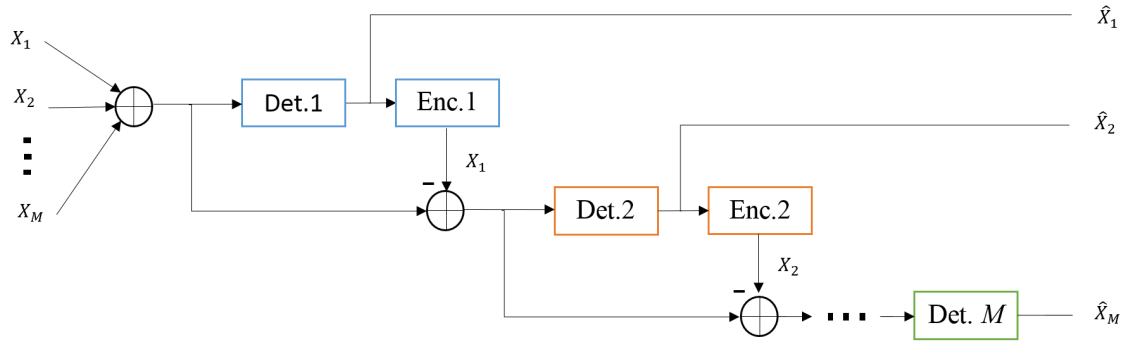

Figure 2.15: Successive interference cancellation (SIC) with power ordering $X_1 > X_2 > \ldots > X_M$

2.3.3.4 SIC Detection

The SIC receiver [108, 107, 49], illustrated in Figure 2.15, is one of the non-linear MUD methods which combines an iterative signal detection method and modulation. SIC can be used to detect users' signal where the received signals are arranged according to their SINR. The first stage of the receiver is used to decode the individual data stream s_1 with the highest SINR, assuming all the others as interference. Next, the re-encoded data of this user will be subtracted from the received vector. The second data stream will be detected using the same procedure until the last user who has the lowest signal power and no interference to deal with also detected. Since the lowest power users' data is detected last without interference from the others, it will achieve high diversity gain to mitigate the effects of channel fade. However, SIC is very sensitive to error propagation due to power ordering of users' signals and re-encoding of the estimated data in $M-1$ stages.

2.4 Future 5G

The amount of global mobile data traffic is expected to increase over a 100-fold in the coming decade, from under 3 exabytes in 2010 to well over 500 exabytes by 2020 [1].

This push has chiefly been driven by multimedia, M2M and cloud-based applications brought about by the migration to IPV6 address space. In addition, the number of connected devices are expected to increase 1000-fold and will continue to increase exponentially well into the tens of billions by the time 5G comes to fruition. To overcome these challenges, state-of-the art techniques and technologies need to be developed and the challenges of current LTE systems addressed and incorporated into 5G.

2.4.1 Requirements

Although no formal definition for 5G exists yet, the academia in collaboration with industry projects such as The Mobile and wireless communication Enablers for the Twenty-twenty Information Society (METIS) [109] and 5G Non-Orthogonal Waveforms (5GNOW) [110] have proposed 5G technical requirements as:

- Data Rate: $10-100$ times higher typical user data rate as compared to 4G, where typical user data rate will range from 1 Gbit/s to 10Gbit/s in high and low mobility scenarios, respectively. This translates into $1,000$ times more mobile data traffic per area (per user), where the volume per area (per user) will be over 100 Gbps/km^2;

- Capacity: To support $1,000x$ more connected devices, 5G will need to be able to efficiently accommodate with minimum performance degradation. With the expected rise of M2M systems, a single eNB may need to support $10,000$ or more low-rate devices along with its traditional high-rate mobile users. This will require radical changes to the signalling and network management compared to current 4G systems, whose overhead channels and state machines are not designed for such a diverse and large subscriber base

- Latency: Current 4G round-trip latencies are on the order of about 15 to 5 ms for LTE and LTE-A, respectively, which are based on the 1 ms subframe time with necessary overheads for resource allocation and access. Although sufficient for most current services, anticipated 5G applications including real-time two-way gaming, novel cloud-based technologies, virtual reality e.t.c. all require stringent low latencies. Thus, 5G will need to be able to support round trip latencies on the order of of about 1 ms.

- Energy and cost: 5G needs to be able to support longer user battery life. Although 5G costs and energy consumption is expected to decrease, data rates increasing by about 100-fold means that the Joules-per-bit and cost-per-bit will need to decrease by at least 100-fold.

2.4.2 Key Technologies and Challenges

To achieve the requirements as proposed in Section 2.4.1, the combined gains from three categories below need to be developed and harmonised such that the promises of 5G are achieved [18, 45, 46].

- Spectral Efficiency: Increased spectral efficiency, primarily through advances in multiple access and massive MIMO techniques to support more bits/s/Hz per node. Extreme densification, cell cooperation and offloading to increase the overall network capacity and area spectral efficiency.

- Bandwidth: Increased bandwidth by utilizing carrier aggregation, WiFi's unlicensed spectrum in the 5-GHz band, and moving toward the mmWave spectrum.

The dominant multiple access technique for high speed wireless communication has

been OFDM and OFDMA. They form the basis of most current standards such as WiFi, 4G, digital TV e.t.c. and is expected to be incorporated into 5G. This is due to the impressive characteristics they provide such as its natural ability to combat frequency selective fading, computationally efficient implementation via FFT/IFFT blocks, simple frequency-domain equalization, excellent pairing with MIMO without the added complication of Inter-Symbol Interference (ISI).

Despite the strengths of OFDM/OFDMA, there are several weaknesses inherent which could possibly become more pronounced in 5G networks. First, the PAPR is higher in OFDM than in other formats since the envelope samples are nearly Gaussian due to the summation of uncorrelated inputs in the IFFT. Although a Gaussian signal distribution is capacity achieving under an average power constraint, a high PAPR presents a poor trade-off between the linearity of the transmitted signal and the cost of the power amplifier. This problem largely overcome in LTE uplink DFT-OFDMA by precoding the OFDM signals at the cost of a slight power penalty and higher computational equalization process at the receiver. Secondly, although the spectral efficiency in OFDM is satisfactory, further relaxations of strict orthogonality and smaller CP could further improve performance.

To address OFDM's weaknesses, alternative approaches are being actively investigated in the research community. Most of these alternative are incremental changes to OFDM rather than a complete change to the signalling format. A key technology currently being researched is the harmonization of OFDM with multi carrier non-orthogonal multiple access, which is based on the principles of superposition coding where multiple access in provided in the power domain. The scheme provides superior performance compared to OFDMA by actively utilizing the near-far effect of geographically separ-

ated users with different power requirements. A key drawback to NOMA however, is the required large power separation between users which comes at a cost to the weaker users.

Other OFDM alternative technologies, although not the scope of this thesis are time-frequency packing and faster-than-Nyquist signalling to circumvent the limitations of strict orthogonality and CP, filterbank multi-carrier OFDM that does not require prior synchronization of distributed transmitters, universal filtered multi-carrier where filtering is performed on groups of adjacent subcarriers such that inter-carrier interference resulting from poor time/frequency synchronization is minimized, generalized frequency division multiplexing that adopts a shortened CP through the tail biting technique which provides attractive spectrum sharing characteristics where the frequency-domain holes are adaptively filled, single-carrier transmission due to the development of low-complexity non-linear equalizers implemented in the frequency domain.

Chapter 3

Uplink NOMA with Constellation Precoding (UL-NCPr)

3.1 Introduction

This chapter focuses on the multiple access interference and the problem of large power separation requirements so as to improve the error performance and sum rate capacity. This is achieved by introducing a novel NOMA scheme employing a new signal design where precoding is designed at the eNB, such that component users form a single and uniquely decodable composite constellation. As the composite constellation is as that of a single user transmitting that same constellation, MAI can be viewed as absent from the system which allows multiple users to transmit at their full rates. The precoding is designed by the eNodeB which searches and allocates power and phase rotations for each user that maximizes the minimum distance of the joint received signal constellation points. The resulting joint composite constellation belongs to higher constellation with rate equal to the number of multiplexed users. Users utilise a simple common periodic

pilot broadcasted by the eNB so as to adjust their transmissions adaptively to maintain the desired received composite signal. UL-NCPr provides a practical solution for implementing the Multiple Access Channel (MAC) in fading environments. The proposed scheme is evaluated with uplink SC-FDMA to show its compatibility and superior performance compared with conventional OMA and power domain NOMA schemes. It can also be easily integrated with conventional multiple access techniques to extend user capacity and improve link utilization.

The contributions of this chapter are as follows

- The requirement for large power separation has limited the flexibility of conventional PD-NOMA in terms of the DoF at the component user constellations and thus, by precoding in both power and phase domains, we allow multiple users transmit at their full rates leading to increased sum rates, subject to individual power constraints, compared to conventional NOMA schemes employing SIC

- As the individual users form a unique composite constellation, the receiver treats the received signal as that of a single users', thereby eliminating MAI perceived by conventional OMA and PD-NOMA with SIC. This enables our scheme achieve the optimum rate regions, rectangular in the case of 2 users transmitting with equal power.

- As the works in literature focus on rate maximization, by optimizing the power and phase of the component constellations, we provide superior bit error rates in terms of the minimum distance of the received composite constellation.

- Our scheme utilizes a common periodic pilot on which the users perform channel estimation. This reduces piloting overhead compared to current SC-FDMA/OMA

systems.

3.2 Motivation and Related Work

The design of efficient MAS for the 5G mobile system is crucial in improving system capacity to accommodate the anticipated massive number of connected devices. NOMA techniques have recently been proposed to complement existing OMA schemes so as to enable users share the same limited resources simultaneously [1].

In 4G OMA uplink schemes such as SC-FDMA, users are allocated exclusive resources thus there is no inter-user interference which leads to low complexity MUD at the base station [39]. SC-FDMA transmission is employed over OFDMA, which is used in the downlink, to reduce PAPR, which enables low complexity implementation of the mobile terminal [12].

OMA transmission is suitable for downlink as it can maximize the users' sum-rate. However, it is difficult to implement MUD techniques at the MS due to the limited processing power. For the uplink, OMA is sub-optimal in terms of spectral efficiency and hence NOMA techniques are proposed for future generation of mobile systems [2][53].

NOMA techniques such as CDMA [58][59], LDS, interleave division multiple access [111], SCMA [112], PDMA [45] add redundancy via spreading/coding to enable separation at the receiver at the cost of reduced spectral efficiency. The works in [113, 2, 114] investigated PD-NOMA by implementing Superposition Coding (SPC) with user power separation and SIC at the receiver. They showed that PD-NOMA with SPC outperforms OMA in terms of both system capacity and cell-edge user throughput. They also show that by choosing optimal power allocations for a specific user QoS, the performance could be further improved. Further capacity gains were investigated in [50] [115] by

employing PD-NOMA in a MIMO scheme, however, as the number of users increase, more antennas and/or RF chains are needed at the receiver which makes MUD at the receiver expensive. Furthermore, the amount of overhead increases with the number of users in terms of pilots needed for channel estimation, user scheduling and precoding. NOMA throughput gains were also investigated in uplink OFDMA system [116] where all the users transmit with equal power levels. An optimized cost function and Hungarian method were used to solve the problem of user pairing in such a way as to maximize either the user sum rate or weighted sum rate. The works in [117] and [118] further proposed opportunistic PD-NOMA beamforming while still guaranteeing a minimum capacity of the weakest user. [51] exploits user cooperation to improve reliability of the received signal due to SIC error propagation while [119] shows an improved ML-SIC MUD. Two user capacity regions for NOMA are presented in [1] which shows PD-NOMA significantly outperforming OMA in downlink. They showed performance gains in uplink, however the user throughput fairness was poor when the difference of the received powers of the users is large. This is due to the rate of the weak user being significantly lower than the stronger user. Performance gains were achieved in [114] where the authors proposed a fairness index based scheduling so as to guarantee gains for the weak user. It was shown in [120] and [121] that the rectangular capacity region can be achieved when multiple users transmits simultaneously so long as the MAI is perceived absent at the receiver i.e. each user sees no interference from the other. Due to the inherent nature of multiple access channels, the receiver will always see the signals from the users as interference when detecting the individual users using SIC and thus, the rectangular rate region is difficult to achieve.

3.3 Principles of Constellation Precoding

The key design principle for UL-NCPr is to allow multiple users share a common channel without the consequences of multiple access interference. This is possible so long as the transmissions from the users combine to produce a unique constellation pattern that belongs to a valid composite constellation known at the receiver. The minimum separation between these composite constellation points measured by the Minimum Euclidean Distance (d_{min}) should be sufficient to mitigate noise and enable successful detection. Thus, UL-NCPr combines signals from M different users $\mathbf{s}_m$ each using a b-bit linear modulation set $\mathbf{Q}_m, \mathbf{s}_m \in \mathbf{Q}_m$, to form a $\Omega = \prod_m \mathbf{Q}_m$ sized composite constellation $\mathbf{U} = [\mathbf{u}_1, \ldots, \mathbf{u}_\Omega]^T$, formed from the sum of all the possible permutations of the users signals. $\mathbf{U}$ can be expressed as

$$\mathbf{U} = \mathbf{V} \times \mathbf{W} \tag{3.1}$$

where $\mathbf{V} \in \mathbb{C}^{\Omega \times M}$ is a matrix whose rows represent the possible combinations of M signals and $\mathbf{W} \in \mathbb{C}^{M \times 1}$ is a precoding complex matrix whose entries represent the power and phase weights of these M users signals. Thus, any composite constellation $\mathbf{U}$ can exist for any M users so long as a precoding $\mathbf{W}$ exists for M.

Signal modulation and demodulation is a critical requirement in all telecommunications communication systems. They provide the means of conveying information efficiently by mapping a set of input bits b into a multi-level symbol. At the receiver, the symbol is demodulated by employing form of soft/hard ML detection [122]. Consequently, as the number of bits-per-symbol increases, so does the size of $\mathbf{Q}$, detection complexity and BER. Thus, for UL-NCPr, we get no increase in complexity for the same number of received constellation points. In fact, as the users are jointly decoded, the

operation is performed only once, compared to simultaneous multiple operations in traditional demodulation schemes, where each user is decoded separately. Therefore, we limit the size of the composite constellation to the highest modulation level supported in 5G; for any combination of number of of users and/or modulation Furthermore, as the composite constellation is a coherent addition of the users signal, we get a linear increase in the average symbol power which offsets the BER degradation.

3.4 Operational Example of UL-NCPr

The eNB as defined in LTE is responsible for all radio-related functions, including but not limited to scheduling, resource allocation and management, inference condition e.t.c. Thus, it holds a lot of information about the users in its cell such as the number of users, respective channel state informations, location, mobility e.t.c. This makes the eNB better suited for the signal design and implementation.

The basic UL-NCPr procedures are:

1. First, the eNB designs the signal constellations by employing an (off-line) exhaustive search algorithm to find power and phase precoding weights for any number of users, taking into account their QoS requirements (e.g. modulation order). To ensure the resulting composite constellations are optimized and fully decodable, the algorithm searches for the weights that maximizes the d_{min} between the composite constellation points. Furthermore, these computations can be carried out just once, reducing search complexity as compared to an on-line search which often requires some form of channel knowledge and/or feedback.

2. The weights are then indexed, tabulated and shared with the users such that the

eNB only signals the index and specific-user-order to the users, potentially minimizing overheads.

3. When multiple users request resources and QoS requirements to transmit their data, the eNB then looks up the corresponding weights and signals to the users as mentioned in item 2, along with any relevant information such as timing advance, frequency sync commands e.t.c.

4. If the eNB is equipped with multiple antennas, the receive antenna that requires the least total power spent on precoding and transmission is selected.

5. Next, the users estimate their channels from the common periodic pilots broadcasted by the eNB, assuming channel reciprocity in TDD systems.

6. The users then precode their data, apply SC-FDMA and wait for the appropriate timing commands before transmitting; the precoding converts the fading channel into a Gaussian channel.

7. The composite signal is then received by the eNB which first performs appropriate signal processing (e.g. SC-FDMA demodulation, CP removal).

8. Finally, eNB employs JML detection between the received signal and the designed constellation to extract the individual user data. This is an advantage over MUD detection like SIC where the detection process has several serial stages causing latency and unfairness due to error propagation.

9. The procedure is assumed to be repeated every subframe

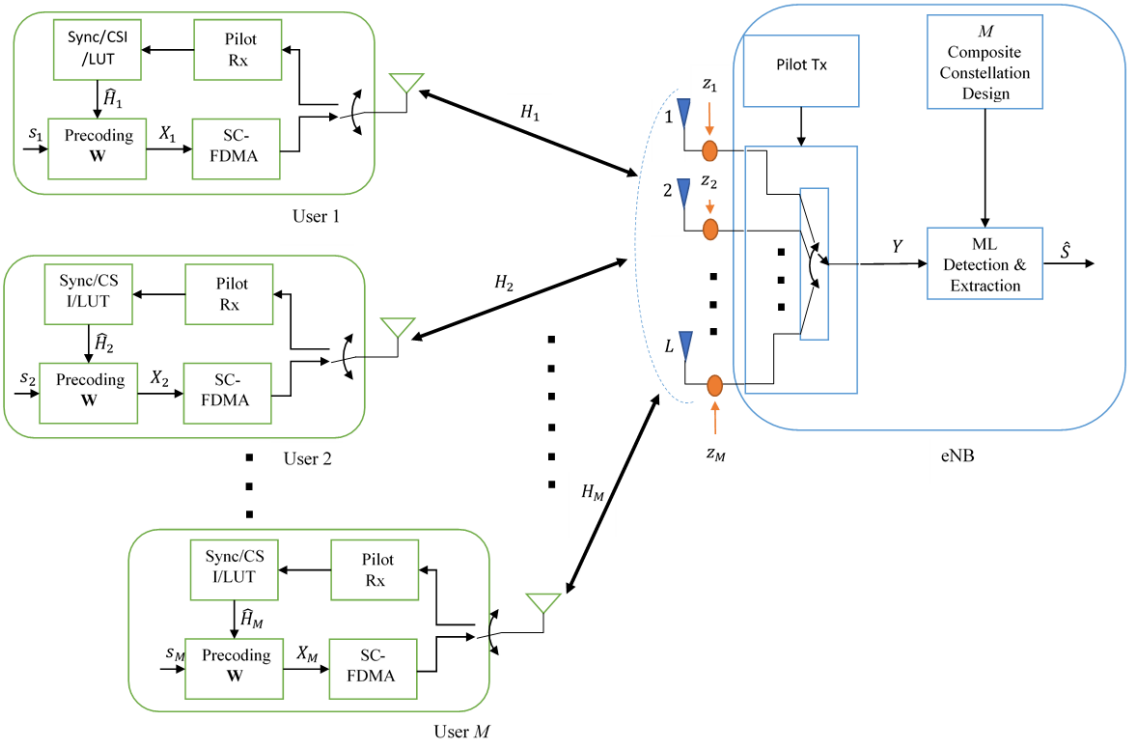

Figure 3.1: Uplink NOMA with Constellation Precoding system model with M users transmitting to an eNB equipped with L antennas.

3.5 System Model

The system block diagram of a baseband model of the proposed multiple access scheme in fading and additive white Gaussian noise is shown in Figure 3.1. At the transmitter side, M users employ SC-FDMA on N symbols as radio access method. The users are connected to an eNB equipped with L antennas, and their transmissions time and frequency synchronized such that they arrive at the eNB at the same time. It is assumed that each user is equipped with one antenna and has full CSI estimated from pilots broadcasted by the eNB. The users precode their data using indexes obtained from a pre-known Look Up Table (LUT). The joint received signal from all users is jointly decoded at the eNB by performing joint maximum likelihood. The precoding indexes are assumed to be signalled over the control channel and updated when a user drops or joins the transmission. This ensures that overhead signalling is kept to a minimum.

3.5.1 Channel Model

The users are typically located in a rich scattering environment where they experience Rayleigh multipath fading channel. This is enabled by the eNB being in an elevated position relative to the users where multiple objects scatter the signals. The channel is modelled as a complex Gaussian-distributed with zero-mean and unit variance. The baseband representation of $\mathbf{h}_{mln}$ is the channel from the m-th user at the l-th eNB antenna on the n-th SC-FDMA symbol, given by

$$\mathbf{h}_{mln} = \alpha_{mln} e^{-i\theta_{mln}} + \mathbf{z}_{ln} \tag{3.2}$$

where $\alpha_{mln} e^{-i\theta_{mln}} = \sum_t \alpha_{mlnt}(k) e^{-i2\pi mln\tau_l/N)}$ denotes the channel of the t-th path at the l-th antenna on the n-th SC-FDMA symbol of the m-th user; α, θ and τ_l represents the channel gain, phase and path delay, respectively, with the different paths assumed to be independent of each other. $\mathbf{z}_{ln}$ is a white complex Gaussian noise with zero mean and variance σ_{ln}^2

3.5.2 Signal Model

Consider M active single-antenna users communicating with an eNB such that their combined signals are received by ONE out of L receive antennas at the eNB. The precoding is designed at the eNB by computing power and phase rotations for each user such that the minimum distance of received composite constellation is maximized and fully decodable. To effectively precode their data to the designed weights, the users perform LMMSE channel state estimation from pilots with power P_p transmitted from the eNB. We assume the uplink/downlink channel reciprocity which is used in TDD systems. Furthermore, we assume total duration for transmission of symbols is less than

the minimum coherent time of the users channels i.e. the channels remain constant over the transmission period. Thus, we express the estimated channel as

$$\hat{\mathbf{h}}_{mln} = \mathbf{h}_{mln} + \epsilon_{mln} \tag{3.3}$$

where $\hat{\mathbf{h}}_{mln}$ is the estimated channel, and ϵ_{mln}, any estimation error in time, frequency and synchronization. ϵ_{mln} is modelled as a Gaussian distributed random variable with zero mean and variance $\sigma_\epsilon^2 = 1/(1 + P_p/z_o)$, making it the limiting factor on the precoding performance i.e. non-ideal conditions when $\epsilon \neq 0$. For the rest of this thesis, unless otherwise stated, we evaluate our proposed schemes in ideal conditions. This is to validate our design principles and serve as an upper-bound for future work in non-ideal conditions(see section 7.2).

Let $\mathbf{s}_{mn}$ denote the symbols at n-th symbol of the m-th UE with average constellation power fixed to one. By applying power and phase adjustment to ensure transmission power is fixed to the allocated power and phase values, the transmitted symbol becomes

$$\mathbf{x}_{mn} = \mathbf{w}_{mn}\mathbf{s}_{mn} \tag{3.4}$$

where $\mathbf{w}_{mn} = \sqrt{\mathrm{P}_{mn}}e^{-i\vartheta_{mn}}$ represents the power, P_{mn}, and phase, ϑ_{mn}, values respectively, at symbol n at each UE to ensure the received signal matches to the precoding indexes D_m and β_m assigned by the eNB. P_{mn} and ϑ_{mn}, determined by Channel Inversion (CI), are given as

$$\mathrm{P}_{mn} = \left[\frac{\mathrm{D}_m}{\alpha_{mn}}\right]^2 \tag{3.5}$$

$$\vartheta_{mn} = \beta_m - \alpha_{mn} \tag{3.6}$$

thus, the received signal y_{ln} at the l-th antenna on the n-th SC-FDMA symbol in frequency domain can thus be expressed as [123]

$$\mathbf{y}_{ln} = \sum_{m}^{M} \mathbf{h}_{mln}\mathbf{x}_{mln} + \mathbf{z}_{ln} \tag{3.7}$$

The channel inversion performed by precoder provides a simple way to compensate for fading locally using only a common periodic pilot. Although water-filling is proven to be the optimum adaptive modulation strategy in point-to-point single user systems, it is very difficult to apply for a multi-user case as considered in UL-NCPr. This is due to the channel dependent adaptation requiring users to change their constellations independently, which may result in excessive signalling and delays.

For the given signal model, the following assumptions are considered:

1. Perfect CSI is assumed for the users.
2. Channels remain constant for the duration of transmissions i.e. each subframe.
3. Perfect user synchronization such that their transmissions arrive at the eNB at the same time.
4. Per-antenna power constraints at the users.
5. Designed precoding weights LUT available at the users.
6. Users do not drop or join in active frames, but scheduled in the next sub-frame.

3.5.3 Constellation Design

3.5.3.1 Design Objectives and Considerations

The objective for our constellation design is performing a search to find power allocation D_m and phase rotation value β_m for each user that MAXIMIZES the minimum distance of the combined received constellation points. This enables a non-ambiguous QAM constellation to be formed which makes detection possible. However, several important design criteria and considerations are made with regards to the constellation design as follows

1. According to permutation theory [124], for any system with M users each having binary information bit of $b_m \in [0, 1]$, there are 2^M possible permutations of their signals. .

2. With each user employing standard BPSK or Ω-QAM modulation there exist a matrix $\mathbf{V} \in \mathbb{C}^{\Omega \times M}$ which contains all the possible permutations [125, 126] of the modulated signals, with the size of $\mathbf{U}$ being equal to number of unique permutations Ω.

3. The sum of the rows of $\mathbf{V}$ produces a point in a constellation diagram that represents the combined sum of individual user symbols in a specific permutation sequence, with the sum of all rows producing the composite vector $\mathbf{U}$.

4. Without any form of signal weighting, there may be ambiguity in the values of $\mathbf{U}$, where several points have the same value i.e the composite vector is non-unique with zero d_{min}.

5. For any defined range of power and phase weights, there exists a permutation matrix of all possible combinations of the weights.

6. Employing power and phase weights may form a non-ambiguous constellation points in **U**, however, finding the the values that maximize the d_{min} ensures increased error rate performances.

7. As several users have different QoS requirements, our constellation design needs to accommodate both equal and variable-rate type component constellations.

8. As some component combinations produce large composite constellations, we limit the size of **U** either by adjusting the modulation level **Q** and/or M, to practical standards.

9. As when a user drops in active frame causes total transmission collapse i.e. composite constellation no longer valid at eNB, scheduling should be carried out on a per-subframe basis such that the eNB can actively re-schedule the other active users, or continue when no drop occurs. This minimizes the duration of the collapse-state. The same can be applied when other users request to join.

3.5.3.2 Constellation Search Algorithm and Procedures

Let $\bar{\mathbf{U}}_i[\bar{\mathbf{D}}_i, \bar{\beta}_i]$ denote the multidimensional vector containing the i-th possible composite constellation $\bar{\mathbf{U}}_i$ derived from the i-th possible combination of power, $\bar{\mathbf{D}}_i = [\bar{\mathrm{D}}_1, \bar{\mathrm{D}}_2, ..., \bar{\mathrm{D}}_M]$, and phase, $\bar{\beta}_i = [\bar{\beta}_1, \bar{\beta}_2, ..., \bar{\beta}_M]$ weights, respectively. Furthermore, define the search ranges as $\bar{\mathrm{D}}_m = [0 \rightarrow 1]$ and $\bar{\beta}_m = [0 \rightarrow \pi]$. Then the criteria for finding the power and phase values that maximize the d_{min} can be defined as

$$\mathbf{U}[\mathrm{D}, \beta] = \arg \max_{d_{min}} \{\bar{\mathbf{U}}_i[\bar{\mathrm{D}}_i, \bar{\beta}_i]\} \quad \forall i \tag{3.8}$$

where $\mathbf{U}[\mathrm{D}, \beta]$ is the vector containing the composite constellations points that maximize the d_{min} of $\mathbf{U}$ at specific values of $\mathbf{D} = [\mathrm{D}_1, \ldots, \mathrm{D}_M]$ and $\beta = [\beta_1, \ldots, \beta_M]$. Each iteration in Equation (3.8) can be expressed by employing Equation (3.1) as

$$\mathbf{U}_i = \mathbf{V} \times \bar{\mathrm{D}}_{mi} e^{j\bar{\beta}_{mi}} \quad \forall i \tag{3.9}$$

As an example, for a 2-user UL-NCPr system with each user employing BPSK modula-

Table 3.1: Algorithm variable definitions including their notation, size and search range.

Notation	Definition	Size	Search Range
M	Number of users	-	M
m	m-th user	-	$1 \ldots m \ldots M$
$\mathbf{V}$	Matrix of all possible permutations of the users input constellations	$\Omega \times M$	-
i	i-th vector of all possible combinations of power and phase i.e. $\mathbf{W}_i$	-	$1 \ldots i \ldots$ -
$\mathbf{D}_m$	Power allocation for the m-th user (Final)	-	-
$\bar{\mathrm{D}}_m$	Power allocation for the m-th user (Search)	-	$0 : \Delta\bar{\mathrm{D}}_m : 1$
$\Delta\bar{\mathrm{D}}_m$	Power allocation search resolution	-	-
$\bar{\mathbf{D}}_i$	i-th Vector of all user Power allocations (Search)	$1 \times M$	$1 \ldots i \ldots$
β_m	Phase allocation for the m-th user (Final)	Scalar	-
$\bar{\beta}_m$	Phase allocation for the m-th user (Search)	$1 \times M$	$0 : \Delta\bar{\beta}_m : \pi$
$\Delta\bar{\beta}_m$	Phase allocation search resolution	-	-
$\bar{\beta}_i$	i-th Vector of all user Phase allocations (Search)	$1 \times M$	$1 \ldots i \ldots$
$\mathbf{W}$	Large matrix of all possible combinations of Power and Phase allocations	$i \times M$	-
$\mathbf{W}_i$	i-th vector of all user Power and Phase allocations (Search)	$1 \times M$	$1 \ldots i \ldots$
Ω	Size of all possible composite constellation points of M users	-	-
$\mathbf{U}$	Vector of all possible composite constellation points (Final)	$\Omega \times 1$	-
$\bar{\mathrm{U}}$	Vector of all possible composite constellation points (Search)	$\Omega \times 1$	-
$\bar{\mathrm{U}}_i$	i-th vector of all possible composite constellation points (Search)	$\Omega \times 1$	$1 \ldots i \ldots$

tion i.e $[-1, 1]$, for the search ranges of D_m and β_m can be expressed as

$$\mathrm{D}_m \rightarrow [0, 0.1, 0.2, \ldots, 1] \quad \forall m \tag{3.10}$$

$$\beta_m \rightarrow [0, 1, 2, 3, 4, 5, \ldots, 90] = [0, \tfrac{\pi}{180}, \ldots, \pi] \quad \forall m \tag{3.11}$$

we can then rewrite Equation (3.9) as

$$\mathbf{U}_i = \begin{bmatrix} 1 & 1 \\ 1 & -1 \\ -1 & 1 \\ -1 & -1 \end{bmatrix} \begin{bmatrix} \bar{\mathrm{D}}_{1i} e^{j\bar{\beta}_{1i}} \\ \bar{\mathrm{D}}_{2i} e^{j\bar{\beta}_{2i}} \end{bmatrix} \forall i \tag{3.12}$$

Assuming the values that maximize all the points in $\mathbf{U}$ from Equation (3.8) are $D_1 = D_2 = 1.0$ and $\beta_1 = 0, \beta_2 = 90$, we can then find $\mathbf{U}$ from Equation (3.12) as

$$\begin{bmatrix} 1+j \\ 1-j \\ -1+j \\ -1-j \end{bmatrix} = \begin{bmatrix} 1 & 1 \\ 1 & -1 \\ -1 & 1 \\ -1 & -1 \end{bmatrix} \begin{bmatrix} e^{j0} \\ e^{j\frac{\pi}{2}} \end{bmatrix} \tag{3.13}$$

We employ the exhaustive search Algorithm 1 to find the precoding values that maximize d_{min} of our composite constellation. The algorithm variables, their sizes, as well as the search ranges are defined in Table 3.1. For clarity, we summarize the algorithm steps as below

1. We begin by initializing our algorithm by defining the number of users and our power and phase search resolutions of 0.1 and $\pi/180$, respectively.

Algorithm 1 Search algorithm used in computing the power and phase values that maximize the minimum distance of the composite constellation points.

1: $Initialize: M =$ number of users; $\bar{\mathrm{D}}_m \leftarrow 0 : 0.1 : 1; \bar{\beta}_m \leftarrow 0 : \pi/180 : \pi$
2: $Generate$ Complex component symbols $\mathbf{V}$
3: **while** $m \neq 1$ **do**
4: Find all possible combinations $\mathbf{W}$ of $[\min \bar{\mathrm{D}}_m \rightarrow \max \bar{\mathrm{D}}_m]$ with $[\bar{\beta}_m \rightarrow \max \bar{\beta}_m]$ for all m
5: **for** $i \leftarrow$ All possible combinations **do**
6: $\bar{\mathrm{U}}_i \leftarrow \mathbf{V} \cdot \mathbf{W}_i$
7: **end for**
8: Compute d_{min} for all $\bar{\mathrm{U}}_i$
9: Find $\mathrm{U}[\mathrm{D}_m, \beta_m] \leftarrow \arg\max_{d_{min}}\{\bar{\mathrm{U}}[\mathbf{W}]\}$
10: **end while**

2. Based on the number of users in step 1 and the users' QoS requirements i.e equal or variable rate component constellations, we generate binary stream matrix $\mathbf{V}$, containing all the possible values of the users signals. We then modulate the respective component signals based on $\mathbf{Q}_m$.

3. The next step is to find all the i-th possible combination of power and phase weight values $\mathbf{W}_i = \bar{\mathbf{D}}_i \bar{\beta}_i$.

4. Iterate $\mathbf{W}_i$ from step 3 to find the i-th composite vector $\mathbf{U}_i = \mathbf{V} \times \mathbf{W}_i$.

5. Find the d_{min} of all the points in composite vector $\mathbf{U}_i$.

6. Based on step 5, select the i-th weights $\mathbf{W}_i$ that maximize the points in the composite vector $\bar{\mathbf{U}}_i$

7. Test the weights by employing Equation (3.8) to check if the criteria and considerations in Section 3.5.3.1 are met.

We set our search intervals to obtain as much resolution as possible while reducing search complexity, without significant impact on the d_{min}. It is assumed that the computations are carried out only once, and the corresponding maximum d_{min} values, based

on the number of users, are stored and indexed both at the eNB, and the users in a LUT.

3.5.3.3 Equal Power, Unequal Power and Rotated Component Constellations

In this section, we investigate the impact of of Equal Power (EP) allocation, Unequal Power (UP) allocation, and phase rotations on the d_{min} to our composite constellation design. For a 2-user UL-NCPr employing BPSK system with EP allocation, the modulation sets $\mathbf{s}_m \in [1,-1] \forall m$ with $\mathbf{V} = [1,1;1,-1;-1,1;-1,-1]^T$ produces an ambiguous composite constellation of $\mathbf{U} = [2,0,0,-2]^T$ with $\Omega = 3$ constellation points and $d_{min} = 0$ which makes successful detection impossible. i.e the zeros produce ambiguity. Applying phase rotation to the second user with $\mathbf{s}_2 \in [j,-j]$, the possible combination vector $\mathbf{V}$ becomes $\mathbf{V} = [1,j;1,-j;-1,j;-1,-j]^T$ producing $\mathbf{U} = [1+j, 1-j, 1+j, -1-j]^T$ with $d_{min} = 2$ and $\Omega = 4$ non-ambiguous composite constellation points which enables successful detection.

Table 3.2: UL-NCPr constellation design example for a 2 to 4 user equal power (EP) allocation case. The table shows the component and composite constellations. The phase precoding and d_{min} of the composite constellations are given for each case. The amplitude is assumed equal to one for all users

M	Component Constellation	Phase rotation (degrees)	Received Composite Constellation Ω-QAM	d_{min}
2	BPSK	$\beta_1 = 0, \beta_2 = 62$	4-QAM	2
	4-QAM	$\beta_1 = 0, \beta_2 = 30$	16-QAM	0.7321
3	BPSK	$\beta_1 = 0, \beta_2 = 36$ $\beta_3 = 72$	8-QAM	1.2361
	4-QAM	$\beta_1 = 0, \beta_2 = 18$ $\beta_3 = 35$	64-QAM	0.4181
4	BPSK	$\beta_1 = 0, \beta_2 = 30$ $\beta_3 = 60, \beta_4 = 90$	16-QAM	1.0353
	4-QAM	$\beta_1 = 0, \beta_2 = 8$ $\beta_3 = 26, \beta_4 = 81$	256-QAM	0.2790

Table 3.2 shows an example of two to four equal power (EP) users each employing BPSK and 4-QAM, where only phase rotation is considered. The composite constellations with their d_{min} are also shown. As an example, for three users all employing BPSK, by applying relative phase shifts of $\beta_1 = 0°, \beta_2 = 36°, \beta_3 = 72°$, a composite 8-QAM constellation with d_{min} of 1.2361 is formed. For the case of all users employing 4-QAM, a relative phase shift of $\beta_1 = 0°, \beta_2 = 18°, \beta_3 = 35°$, produces 64-QAM composite constellation with d_{min} of 0.4181.

Table 3.3: UL-NCPr constellation design example for unequal power (UP) 2-user and 3-user cases each employing BPSK and/or 4-QAM. The size of the composite constellation, power allocation, phase rotation and the d_{min} of the composite constellations are also provided.

M	Component Constellation	Power Allocation	Phase rotation (degrees)	d_{min}
2	BPSK	$D_1 = 1.0, D_2 = 1.0$	$\beta_1 = 0, \beta_2 = 62$	2
	4-QAM	$D_1 = 1.0, D_2 = 1.0$	$\beta_1 = 0, \beta_2 = 30$	0.7321
3	BPSK	$D_1 = 1.0, D_2 = 0.7$ $D_3 = 1.0$	$\beta 1 = 0, \beta_2 = 45$ $\beta_3 = 90$	1.400
	4-QAM	$D_1 = 1.0, D_2 = 0.9$ $D_3 = 0.9$	$\beta 1 = 0, \beta_2 = 52$ $\beta_3 = 72$	0.4236

Table 3.3 shows the minimum distance comparison of two and three unequal power (UP) users each employing BPSK and 4-QAM. Both power allocation and phase rotation searches are considered. It is shown that for the case two users, EP allocation achieves the maximum d_{min}. For the case of three BPSK users, the power and phase allocations of $D_1 = 1.0, D_2 = 0.7, D_3 = 1.0$ and $\beta_1 = 0°, \beta_2 = 45°, \beta_3 = 90°$, results in an 11.7% increase in d_{min}. This is illustrated in Figure 3.2(a) and Figure 3.2(b) where both the component and composite constellations are superimposed.

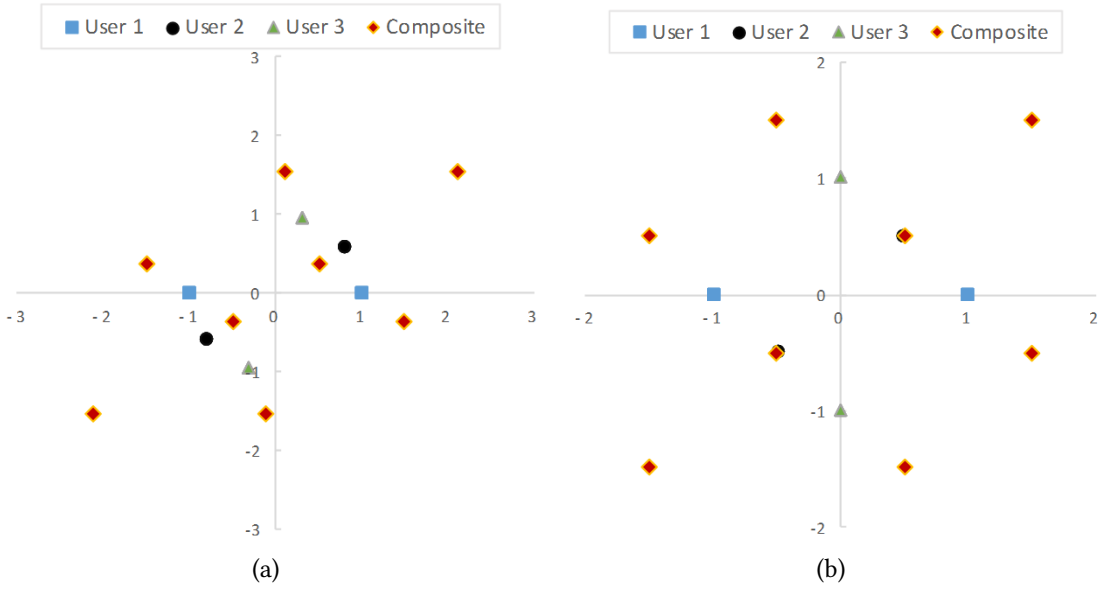

Figure 3.2: Superimposed component and composite constellation of three users each employing BPSK. Base component constellation reference of $(0°, 180°)$ is assumed. (a) Superimposed component constellations of EP users with phase allocations of $\beta_1 = 0°, \beta_2 = 36°, \beta_3 = 72°$. (b) Superimposed component constellations of UP users with UP and phase allocations of $D_1 = 1.0, D_2 = 0.7, D_3 = 1.0$ and $\beta_1 = 0°, \beta_2 = 45°, \beta_3 = 90°$, respectively.

In Figure 3.2(a), only phase rotation is applied while in Figure 3.2(b), both power and phase rotations are applied. For three users all employing 4-QAM, the UP and phase allocations of $D_1 = 1.0, D_2 = 0.9, D_3 = 0.9$ and $\beta_1 = 0°, \beta_2 = 52°, \beta_3 = 72°$, results in a 1.3% increase in d_{min}. This is illustrated in Figure 3.3(c) and Figure 3.3(d) and compared to EP allocations in Figure 3.3(a) and Figure 3.3(b) .

3.5.3.4 Equal Rate Component Constellations

We employ our search algorithm proposed in Section 3.5.3.2 and the power allocation strategies in [113] for PD-NOMA to find the power and phase values that maximize the distance of the composite constellation produced from equal rate component constellations i.e all users employ same component constellation e.g BPSK or 4-QAM e.t.c.

Table 3.4 and Table 3.5 shows the impact of power and phase optimizations for BPSK and 4-QAM users, respectively, compared to power optimizations only in conventional

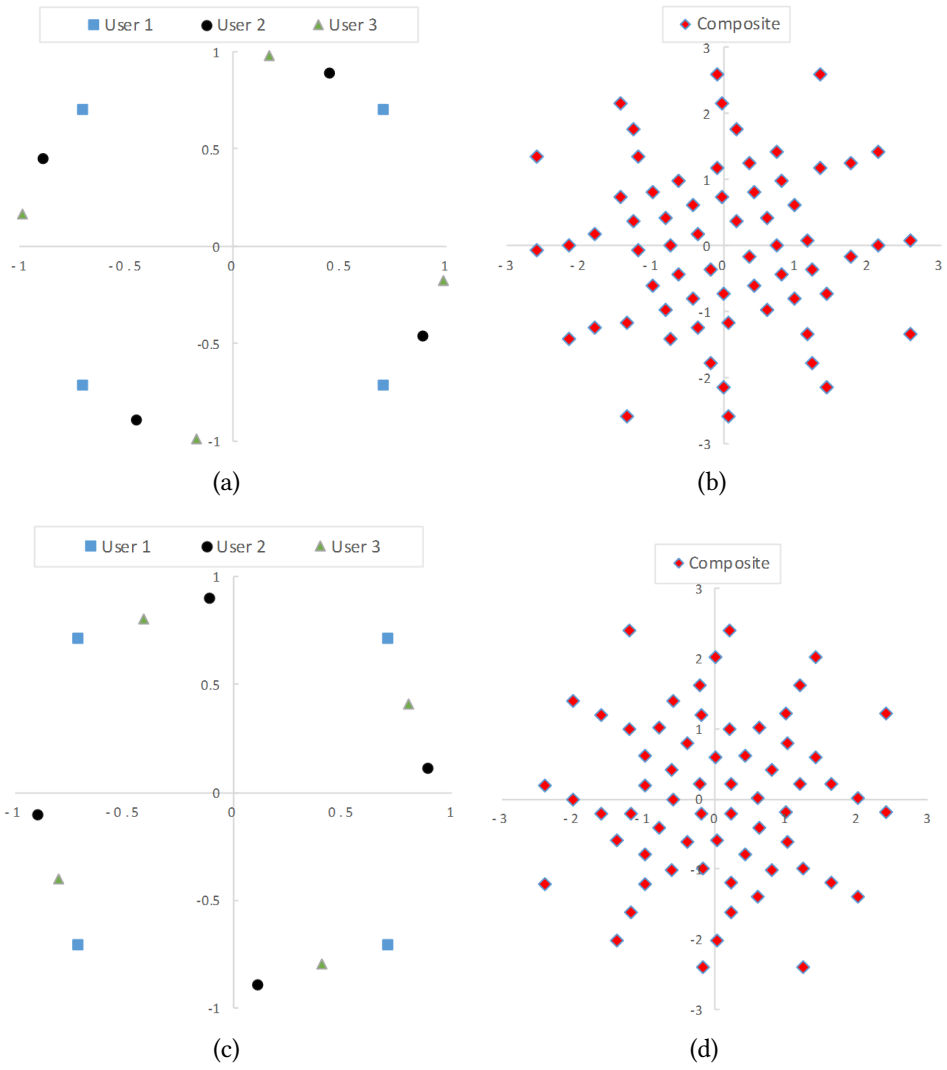

Figure 3.3: Superimposed component and composite constellation of three users each employing 4-QAM. (a) Superimposed component constellations of EP users with phase allocations of $\beta_1 = 0°, \beta_2 = 18°, \beta_3 = 35°$. (b) Composite constellation of EP users. (c) Superimposed component constellations of UP users with UP and phase allocations of $D_1 = 1.0, D_2 = 0.9, D_3 = 0.9$ and $\beta_1 = 0°, \beta_2 = 52°, \beta_3 = 72°$, respectively. (d) Composite constellation of UP users.

NOMA which leads to significantly better error performance.

3.5.3.5 Variable Rate Component Constellations

As the individual user QoS may vary, we employ our search algorithm to search for power and phase values that maximize the d_{min} of the composite constellation formed from different component constellations e.g user 1 employs 4-QAM while user 2 employs 16-QAM. This enables a more robust and adaptive system compared to only equal rate

Table 3.4: UL-NCPr example of two to four users all employing BPSK. Their individual power allocations, relative phase shifts and the size of their composite constellation are given. The PD-NOMA with power allocation only is also given for comparisons. The composite constellation d_{min} for both schemes are presented

M	Scheme	Power Allocation	Phase Rotation	Rx Composite Constellation	d_{min}
2	PD-NOMA	$D_1 = 1.0, D_2 = 0.5$	$\beta_{1\to2} = 0$	4-PAM	1.0
	UL-NCPr	$D_1 = 1.0, D_2 = 1.0$	$\beta_1 = 0, \beta_2 = 30$	4-QAM	2.0
3	PD-NOMA	$D_1 = 1.0, D_2 = 0.6$ $D_3 = 0.8$	$\beta_{1\to3} = 0$	8-PAM	0.4
	UL-NCPr	$D_1 = 1.0, D_2 = 0.7$ $D_3 = 1.0$	$\beta_1 = 0, \beta_2 = 45$ $\beta_3 = 90$	8-QAM	1.4
4	PD-NOMA	$D_1 = 1.0, D_2 = 0.1$ $D_3 = 0.2, D_4 = 0.4$	$\beta_{1\to4} = 0$	16-PAM	0.2
	UL-NCPr	$D_1 = 1.0, D_2 = 0.5$ $D_3 = 0.6, D_4 = 1.0$	$\beta_1 = 0, \beta_2 = 0$ $\beta_3 = 40, \beta_4 = 70$	16-QAM	1.0

Table 3.5: UL-NCPr example of two and three users all employing 4-QAM. Their individual power allocations, relative phase shifts and the size of their composite constellation are given. The composite constellation d_{min} for both schemes are presented

M	Scheme	Power Allocation	Phase Rotation	Rx Composite Constellation	d_{min}
2	PD-NOMA	$D_1 = 1.0, D_2 = 0.5$	$\beta_{1\to2} = 0$	16-QAM	0.70
	UL-NCPr	$D_1 = 1.0, D_2 = 1.0$	$\beta_1 = 0, \beta_2 = 30$		0.73
3	PD-NOMA	$D_1 = 1.0, D_2 = 0.7$ $D_3 = 0.5$	$\beta_{1\to3} = 0$	64-QAM	0.28
	UL-NCPr	$D_1 = 1.0, D_2 = 0.9$ $D_3 = 0.9$	$\beta_1 = 0, \beta_2 = 40$ $\beta_3 = 20$		0.4

component constellations.

Table 3.6 shows an example of two to three users all employing variable component modulations. The individual power and phase values, composite constellation and their respective d_{min} are illustrated. The component and resulting composite constellation

Table 3.6: UL-NCPr example of two users all employing variable component modulations. Their individual power allocations, relative phase shifts and the size of their composite constellation are given. The composite constellation d_{min} for both schemes are presented

M	Component Constellation	Power Allocation	Phase Rotation	Rx Composite Constellation	d_{min}
2	BPSK+4-QAM	$D_1 = 0.5, D_2 = 1.0$	$\beta_1 = 50, \beta_2 = 5$	8-QAM	1.00
	BPSK+8-QAM	$D_1 = 1.0, D_2 = 1.0$	$\beta_1 = 60, \beta_2 = 5$	16-QAM	0.82
	BPSK+16-QAM	$D_1 = 1.0, D_2 = 0.8$	$\beta_1 = 10, \beta_2 = 4$	32-QAM	0.51
	4-QAM+8-QAM	$D_1 = 1.0, D_2 = 0.6$	$\beta_1 = 75, \beta_2 = 30$	32-QAM	0.50
	4-QAM+16-QAM	$D_1 = 1.0, D_2 = 0.6$	$\beta_1 = 52, \beta_2 = 60$	64-QAM	0.32
	8-QAM+16-QAM	$D_1 = 0.6, D_2 = 1.0$	$\beta_1 = 50, \beta_2 = 45$	128-QAM	0.21

for the values in Table 3.6 are illustrated in Figures 3.4(a) to 3.4(f). For example, it can be seen that for BPSK and 4-QAM component constellations, applying the precoding weights produces a non-rectangular 8-QAM composite with d_{min} of 1. For BPSK and 8-QAM component constellations, a non-rectangular 16-QAM composite constellation with d_{min} of 0.82 is produced. Furthermore, as the number component constellation points increase, the d_{min} decreases. Thus there is a trade-off between error performance and QoS demands.

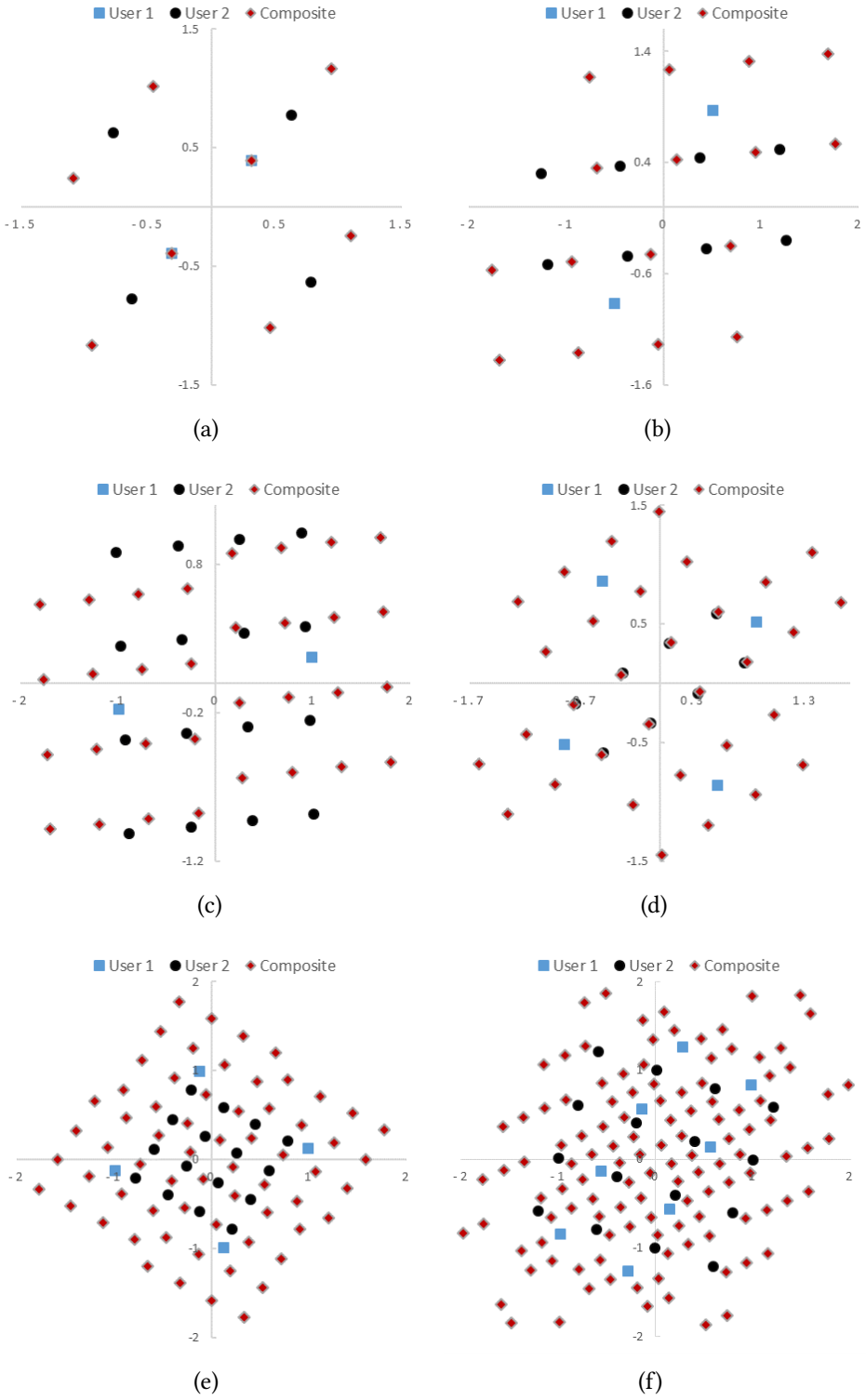

Figure 3.4: Superimposed component and composite constellation of two users employing variable component constellations. (a) Users 1 and 2 employing BPSK and 4-QAM, respectively, producing 8-QAM composite constellation. (b) Users 1 and 2 employing BPSK and 8-QAM, respectively, producing 16-QAM composite constellation. (c) Users 1 and 2 employing BPSK and 16-QAM, respectively, producing 32-QAM composite constellation. (d) Users 1 and 2 employing 4-QAM and 8-QAM, respectively, producing 32-QAM composite constellation. (e) Users 1 and 2 employing 6-QAM and 16-QAM, respectively, producing 64-QAM composite constellation (f) Users 1 and 2 employing 8-QAM and 16-QAM, respectively, producing 128-QAM composite constellation

3.5.4 Antenna Selection

In order to conserve power at the user terminals, the eNB selects the antenna q that requires the least total transmit power from all the users to maintain a fixed signal to noise (SNR). The total received power at the l-th receive antenna can be defined as

$$\mathrm{P}_{tot}^{(l)} = \sum_{m=1}^{M} \frac{\mathrm{D}_m}{\sum_1^N |\mathbf{h}_{mln}^2|} \tag{3.14}$$

where D_m is the assigned transmit power of user m, subject to per-antenna power constraint. Thus the least total transmit power to selected antenna t can be defined as

$$\mathrm{P}_{tot}^{(t)} = \arg \min_{l=1 \to L} \{\mathrm{P}_{tot}^{(l)}\} \tag{3.15}$$

3.5.5 Joint Maximum Likelihood Detection

The non-linear JML detection for the composite received signals is employed at the eNB. It is optimal in the sense of minimizing the error probability by searching for the most likely transmitted signals and since fading is compensated at the transmitter, the detection process is reduced to that of JML detection in AWGN channels. Furthermore, as the received constellation is designed by the eNB, the JML detector uses $\mathbf{U}$ as a reference to compare with the received signal y_n with no CSIR required. The detector performs an exhaustive search between the received signal and all constellation points in $\mathbf{U}$ to find the constellation point which is the closest to y_n in terms of Euclidean distance. For an M user system each with modulation set $\mathbf{Q}$, there are $\Omega = \mathbf{Q}^M$ for equal rate, and $\Omega = \prod_m \mathbf{Q}_m$ for variable rate composite constellation, possible signal vectors at the

channel input given as

$$\bar{\mathbf{x}}_{(\bar{q})} = [\mathbf{x}_1^{(q)} \dots \mathbf{x}_m^{(q)} \dots \mathbf{x}_M^{(q)}]; \qquad q \in \mathbf{Q}_m \tag{3.16}$$

where $\mathbf{x}^{(q)}$ is the q-th possible transmitted symbol from the modulation set of the m-th user and $\bar{\mathbf{x}}_{(\bar{q})} \in \mathbf{U}$ is the $\bar{q}$-th composite signal at the channel input. By employing the minimum distance criterion, the estimated signal at the eNB can be expressed as

$$\hat{\mathbf{x}} = \arg\left[\min_{\mathbf{U}}(\|\mathbf{y}_n - \bar{\mathbf{x}}_{(\bar{q})}\|^2)\right]; \qquad \bar{q} = 1, \dots, \Omega \tag{3.17}$$

where $\|\mathbf{y}_n - \bar{\mathbf{x}}_{(\bar{q})}\|^2$ is the distance between the received signal an the possible transmitted vector $\bar{\mathbf{x}}_{(\bar{q})}$.

As mentioned in section 3.3, the number of calculations needed to perform JML is the same as that of a single user employing the same order constellation. This presents a trade-off between user throughput and system capacity. For example, assume a single user in LTE employs the highest allowed modulation of 128-QAM, for a two user equal rate component constellations in UL-NCPr, the maximum rate achievable for both users is then $\mathbf{Q}_1 \cdot \mathbf{Q}_2 <$ 128-QAM. However, as our designed composite constellation is a coherent addition of the users signal, we get a linear increase in the average symbol power which offsets the channel capacity as well as BER degradation. Furthermore, proposed schemes such as sphere decoding [127, 128] and multi-stage ML detection [129] can employed to significantly reduce the complexity of ML.

3.6 Signalling and Synchronization

3.6.1 Common Periodic Pilot (CPP)

Communication in UL-NCPr is divided into TDD subframes which assumes uplink/ downlink channel reciprocity. The eNB broadcasts a periodic high SNR BPSK signal with power and phase known to all users at the beginning of each subframe as illustrated in Figure 3.5. The users employ least mean minimum square error estimator to extract CSI of their respective channels. The users precode and transmit their data on the PUSH. Common Periodic Pilot (CPP) in UL-NCPr has several advantages over traditional forward channel training approaches.

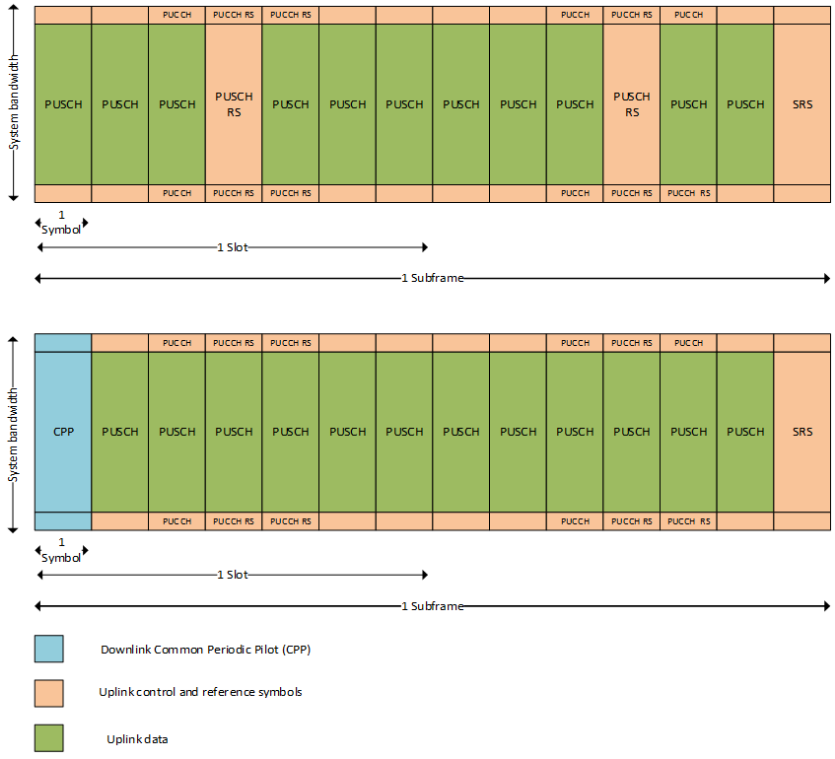

Figure 3.5: LTE uplink structure (top) compared to UL-NCPr uplink structure (bottom); CPP-Common periodic pilot, PUSCH- Physical uplink shared channel, SRS-Sounding reference signal, RS- reference signal, PUCCH- Physical uplink control channel

- Due to more power available at the eNB, better quality CSI measurements can be made by the users.

- The orthogonality of pilots must be maintained for PUSCH reference signal which leads to higher overhead and detection complexity while the CPP reverse piloting relaxes the orthogonality constraints and is common to all users.

- SC-FDMA users typically allocate $20-25\%$ of their total power to reference signals for channel estimation at the receiver while in UL-NCPr, CPP is utilized only at the transmitter for CSI without the need at the receiver.

3.6.2 Synchronization

UL-NCPr utilizes synchronization in LTE where primary synchronization signal and secondary synchronization signals are periodically broadcasted from eNB which enables a closed loop tracking control procedure to maintain synchronization [130]. The UE connects to the cell and detects the system information block (SIB) which is broadcasted through the downlink PBSH by the eNB. From the SIB, the UE detects the PRACH parameters which are required to generate PRACH preamble for random access procedure. Random access procedure is used by the UE to request for uplink resources and the eNB only assigns resources to if it is time/frequency synchronized. The eNB estimates the initial timing advance from PRACH preamble sent by the UE and transmits timing advance to users which is defined as the time period that a UE has to wait before it starts transmitting.

3.7 Performance Analysis

3.7.1 Capacity

The channel capacity of 2-users in AWGN is considered in this subsection since the general properties and the relative performance of different multiple access techniques are the same as M or $\mathbf{Q}$ increases [131].

In information theory, the capacity of a memoryless AWGN point to point channel with input x and output y can be defined as [120]

$$\mathrm{C} = \max_{p_x} I(\mathrm{x};\mathrm{y}) \tag{3.18}$$

where the maximization is over the input distributions subject to average power constraint. For a 2-user system, x_m where $m = 1, 2$, and a given independent input distribution of $\rho(x_1)$ and $\rho(x_2)$, the sum capacity defines the pentagon $\varsigma(p_{x_1}, p_{x_2})$ as the set of all rate pairs satisfying the constraint

$$\mathrm{R}_1 < I(\mathrm{x}_1;\mathrm{y}|\mathrm{x}_2) = B\log_2\left(1 + \frac{\mathrm{P}_1}{B\mathrm{Z}_o}\right) \tag{3.19}$$

$$\mathrm{R}_2 < I(\mathrm{x}_2;\mathrm{y}|x_1) = B\log_2\left(1 + \frac{\mathrm{P}_2}{B\mathrm{Z}_o}\right) \tag{3.20}$$

$$\mathrm{R}_1 + \mathrm{R}_2 < I(\mathrm{x}_1, \mathrm{x}_2; y) = B\log_2\left(1 + \frac{\mathrm{P}_1 + \mathrm{P}_2}{B\mathrm{Z}_o}\right) \tag{3.21}$$

where Z_o is noise power density. In Equation (3.19) and Equation (3.20), the individual user rate cannot exceed the capacity of an AWGN system where the interferences from either user are absent. In Equation (3.21), the sum rate cannot exceed the capacity of AWGN with the received power being sum of the two users. Due to the inherent nature of MAC, the users always see interferences from each other which makes achieving

the optimum rectangular region difficult to achieve. In conventional PD-NOMA with SIC, the weak user is decoded by subtracting its signal from the dominant strong user while the strong user is detected with the weak user as interference. This enables rate maximization for the stronger user while the weaker user can still achieve a non-zero rate. Downlink NOMA takes advantage of the near-far effect due to the distances of the users relative to the eNB, to maximize the sum rates [113, 1]. Assuming user 2 is the strongest, the rates can thus be defined as

$$\mathrm{R}_1 < I(\mathrm{x}_1;\mathrm{y}) = B\log_2\left(1+\frac{\mathrm{P}_1}{B\mathrm{Z}_o}\right) \tag{3.22}$$

$$\mathrm{R}_2 < I(\mathrm{x}_2;\mathrm{y}|\mathrm{x}_1) = B\log_2\left(1+\frac{\mathrm{P}_2}{\mathrm{P}_1+B\mathrm{Z}_o}\right) \tag{3.23}$$

For UL-NCPr, multiple users combine to form a single composite constellation. From the receiver point of view, this is analogous to a single user transmitting that constellation where the multiple users provide power gain to the single user constellation. In this case, many virtual users combine as a single user in an AWGN channel with received power as the sum of the individual user powers subject to their respective power constraint, e.g. for 2 user UL-NCPr, we get 3 dB power gain, assuming unit noise $\sigma^2 = 1$. This means that the multiple users contribute their full rates to achieve a fixed composite constellation. Consequently, MAI can then be viewed as absent in the system which enables joint detection as though the received signal is that of a single user, subject to eNB post processing where the individual users are separated. This then relaxes the constraint in Equation (3.21) and defines the sum capacity of the system as

$$\mathrm{R}_n = I(\mathrm{x}_n;\mathrm{y}_n) = \sum_{m=1}^{M}\log_2\left(1+\frac{\mathrm{P}_{mn}}{\mathrm{Z}_n}\right) \tag{3.24}$$

The channel capacity R_n serves as an upper-limit for any Gaussian distributed signal constellation at the MAC input. However, for any practical communication system employing independent and equally likely Ω modulation levels, the maximum achievable throughput can be found by calculating the mutual information between transmitted signal vector and received signal vector. This is known as the Constellation Constrained Capacity (CCC) and defined by [121]

$$R = \max_{\rho(\bar{\mathbf{x}}_{(\bar{q})} \cdots \rho(\bar{\mathbf{x}}_{(\Omega)})} \sum_{q=1}^{\Omega} \rho(\bar{\mathbf{x}}_{(\bar{q})}) \int_{-\infty}^{\infty} \rho(\mathbf{y}|\bar{\mathbf{x}}_{(\bar{q})}) \log_2 \left[\frac{\rho(\mathbf{y}|\bar{\mathbf{x}}_{(\bar{q})})}{\sum_{i=1}^{\Omega} \rho(\bar{\mathbf{x}}_{(\bar{i})}) \rho(\mathbf{y}|\bar{\mathbf{x}}_{(\bar{i})})} \right] d\mathbf{y} \tag{3.25}$$

where $\rho(\bar{\mathbf{x}}_{(\bar{q})})$ is the probability associated with $\bar{\mathbf{x}}_{(\bar{q})}$, and $\rho(\mathbf{y}|\bar{\mathbf{x}}_{(\bar{q})})$ the conditional probability of received composite symbol given for two dimensional expressed as

$$\rho(\mathbf{y}|\bar{\mathbf{x}}_{(\bar{q})}) = \frac{1}{2\pi\sigma^2} e^{-\left(\frac{\|\mathbf{y}-\bar{\mathbf{x}}_{(\bar{q})}\|^2}{2\sigma^2}\right)} \tag{3.26}$$

Assuming improbable occurrence for all symbols $\rho(\bar{\mathbf{x}}_{(\bar{q})}) = 1/\Omega$, the capacity in bits/s/Hz can be derived as

$$R = \log_2 - \frac{1}{\Omega} \sum_{q=1}^{\Omega} \mathbb{E}\left[\log_2 \sum_{q=1}^{\Omega} e^{-\left(\frac{\|\mathbf{y}-\bar{\mathbf{x}}_{(\bar{q})}\|^2 - \|\mathbf{z}\|^2}{2\sigma^2}\right)} \right] \tag{3.27}$$

3.7.2 Bit Error Rate

Due to the composite constellation formed from the superposition of M users being non-rectangular QAM, it is hard to derive error rates since it depends on the d_{min} of the composite constellation. However, an upper bound for each composite constellation can be derived from the closest constellation points defined as $d^2_{min_n}$ and the bits per symbol,

ψ. This can be expressed as

$$P_b \approx \frac{P_e}{\psi}, P_e < (\Omega - 1)Q_c(\sqrt{\left(\frac{d^2_{min_n}}{Z_n}\right)} \tag{3.28}$$

where P_b and P_e are the bit and symbol error probabilities, respectively, and Q_c is the complimentary error function.

For calculating the error rate for each of our composite constellation, we divide the constellation into F rings. The number of constellation points on the f-th ring having the same symbol energy is defined as J_f. The j-th symbol on the f-th ring is denoted by $u(f, j)$ where $f \in F$ and $j \in J_f$. We then calculate the Symbol Error Rates (SER) for each ring (assuming received symbol belongs to that ring) and then calculate the total SER over all rings. Assuming all symbols are equally likely, the probability of symbols on the f-th ring is then $\gamma = J_f/\Omega$. Thus we can derive the SER of our composite constellation as

$$P_e \approx \sum_f \gamma \sum_{b \neq 1} Q_c\left(\sqrt{\frac{d^2_{u(f,1),u(f,b)}}{Z_n}}\right) + \sum_f \gamma \sum_{v \neq f} \sum_{b=1} Q_c\left(\sqrt{\frac{d^2_{u(f,1),u(v,b)}}{Z_n}}\right) \tag{3.29}$$

where the first term in Equation (3.29) is the summation of the distances between constellation points on the same ring and the second term is the distances between constellation points on different rings all averaged by the PDF of respective rings.

As an example, we derive the SER of a three equal rate BPSK users producing 8-QAM composite constellation. Due to the symmetry of the composite constellation, we can choose any symbol on each ring for the following analysis and define according to Figure 3.6

$d^2_{u(1,1),u(1,2)}$ = distance between the symbol 1 and 2 on ring 1

$d^2_{u(1,1),u(2,j)}$ = distance between symbol 1 on ring 1 and any other symbol on ring 2

$d^2_{u(1,1),u(3,j)}$ = distance between symbol 1 on ring 1 and any other symbol on ring 3

$d^2_{u(2,1),u(1,j)}$ = distance between symbol 1 on ring 2 and any other symbol on ring 1

$d^2_{u(2,1),u(2,j\neq 1)}$ = distance between the symbol 1 and $j \neq 1$ on ring 2

$d^2_{u(2,1),u(3,j)}$ = distance between symbol 1 on ring 2 and any other symbol on ring 3

$d^2_{u(3,1),u(1,j)}$ = distance between symbol 1 on ring 3 and any other symbol on ring 1

$d^2_{u(3,1),u(2,j)}$ = distance between symbol 1 on ring 3 and any other symbol on ring 2

$d^2_{u(3,1),u(3,2)}$ = distance between the symbol 1 and 2 on ring 3

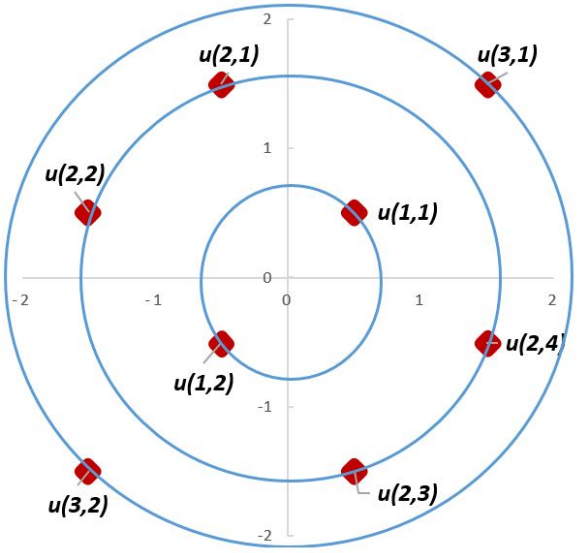

Figure 3.6: Ring format (R, J) for three BPSK component signals combined to form 8-QAM composite constellation

Thus we can derive SER expression for 8-QAM as from Equation (3.29) as

$$P_{e_{(8-QAM)}} \approx \frac{1}{4}\left(Q_c\left(\sqrt{\frac{d^2_{u(1,1),u(1,2)}}{Z_n}}\right)+\sum_{j=1}^{4}Q_c\left(\sqrt{\frac{d^2_{u(1,1),u(2,j)}}{Z_n}}\right)+\sum_{j=1}^{2}Q_c\left(\sqrt{\frac{d^2_{u(1,1),u(3,j)}}{Z_n}}\right)\right)$$
$$+\frac{1}{2}\left(\sum_{j=1}^{2}Q_c\left(\sqrt{\frac{d^2_{u(2,1),u(1,j)}}{Z_n}}\right)+\sum_{j\neq 1}^{4}Q_c\left(\sqrt{\frac{d^2_{u(2,1),u(2,j)}}{Z_n}}\right)+\sum_{j=1}^{2}Q_c\left(\sqrt{\frac{d^2_{u(2,1),u(3,j)}}{Z_n}}\right)\right)$$
$$+\frac{1}{4}\left(\sum_{j=1}^{2}Q_c\left(\sqrt{\frac{d^2_{u(3,1),u(1,j)}}{Z_n}}\right)+\sum_{j=1}^{4}Q_c\left(\sqrt{\frac{d^2_{u(3,1),u(2,j)}}{Z_n}}\right)+Q_c\left(\sqrt{\frac{d^2_{u(3,1),u(3,2)}}{Z_n}}\right)\right) \tag{3.30}$$

3.8 Simulation Modelling and Results

3.8.1 Simulation Modelling

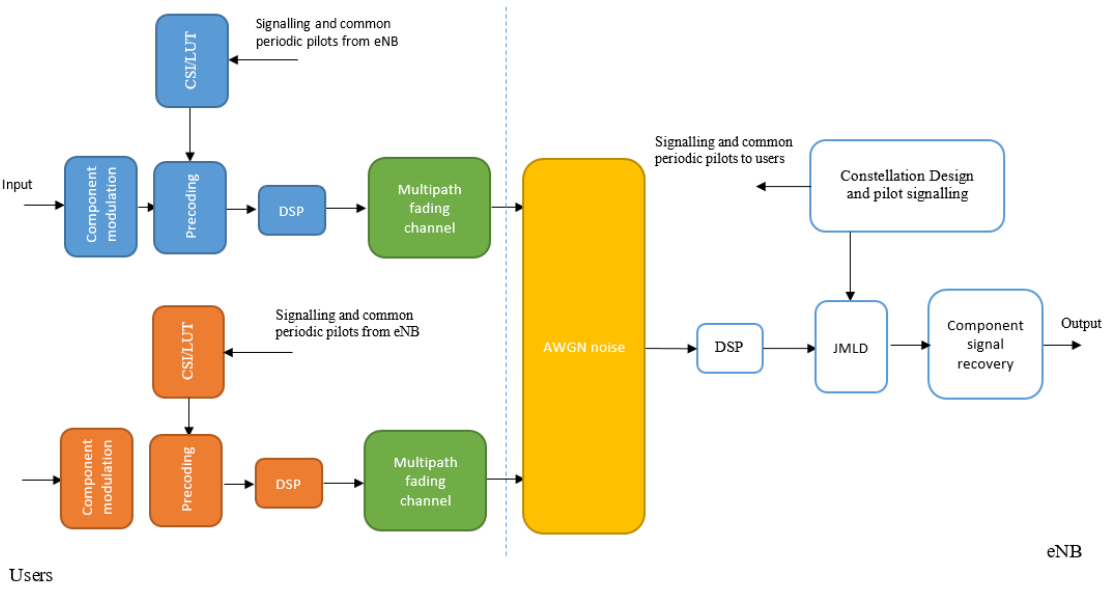

Figure 3.7: UL-NCPr MATLAB simulation Model

A Monte-Carlo simulation is carried out in MATLAB to compare the performance of our proposed scheme. The simulation model is illustrated in Figure 3.7. For simplicity, BPSK, 4-QAM and 8-QAM component modulations are employed on each SC-FDMA symbol

at each user. First, the users employ component modulations to their input data with respect to their QoS requirements. It is assumed that the eNB grants and signals the precoding indexes to be employed based on the user requests, to the eNB antenna that requires the least transmit power from the users. Next, the users perform CSI measurements from the CPP broadcasted by the eNB. Furthermore, they look up the corresponding precoding values based on the signalled indexes. Subsequently, they precode their symbols. As there is no bandwidth expansion inherent in UL-NCPr, due to the DFT and IDFT operations cancelling out, the precoded symbols are appended with CP. The users are assumed to fulfil any timing and synchronization requirements before transmitting the symbols over the channel. Independent and uncorrelated flat fading channels are assumed for all the users. AWGN noise is applied to joint received signal at the eNB. The eNB then performs JML detection with the reference constellation and extracts the respective composite signals. The system performance is evaluated in terms of BER and capacity bounds in multipath channel over thousands of symbol periods. We compare our proposed scheme with that of a single user employing SC-FDMA OMA with and without CI, MIMO SM scheme with SIC and ML detection and conventional PD-NOMA. Full channel state information is assumed to be available for the comparisons.

3.8.2 Results

Figure 3.8 shows the BER performance of UL-NCPr with the precoding values in Table 3.4. It can be seen that for two users employing BPSK, we get the same error rate performance compared to a single user employing 4-QAM. We also get 8.3 dB and 20.8 dB difference compared to 2x2 MIMO with ML and SIC detections BER of 10^{-4}, respectively. This difference is due to our scheme employing CI. The single user employing 4-QAM SC-FDMA

with ML detection in fading is also shown for comparison.

Figure 3.9 shows the BER performance when user 1 and 2 employ 4-QAM and 8-QAM component constellations, respectively. For 4-QAM component constellation, we get 0.1 dB gain compared to a single user employing 16-QAM constellation while for 8-QAM component constellations, we achieve a 7.5 dB gain. This is due to the power gain of the composite constellation, compared to average power of one for the single user. The performance of 2x2 MIMO SM with SVD precoding is shown for comparison. The SVD precoding results in fading channel performance as the channel gains are limited by the eigenvalues of the channel matrix.

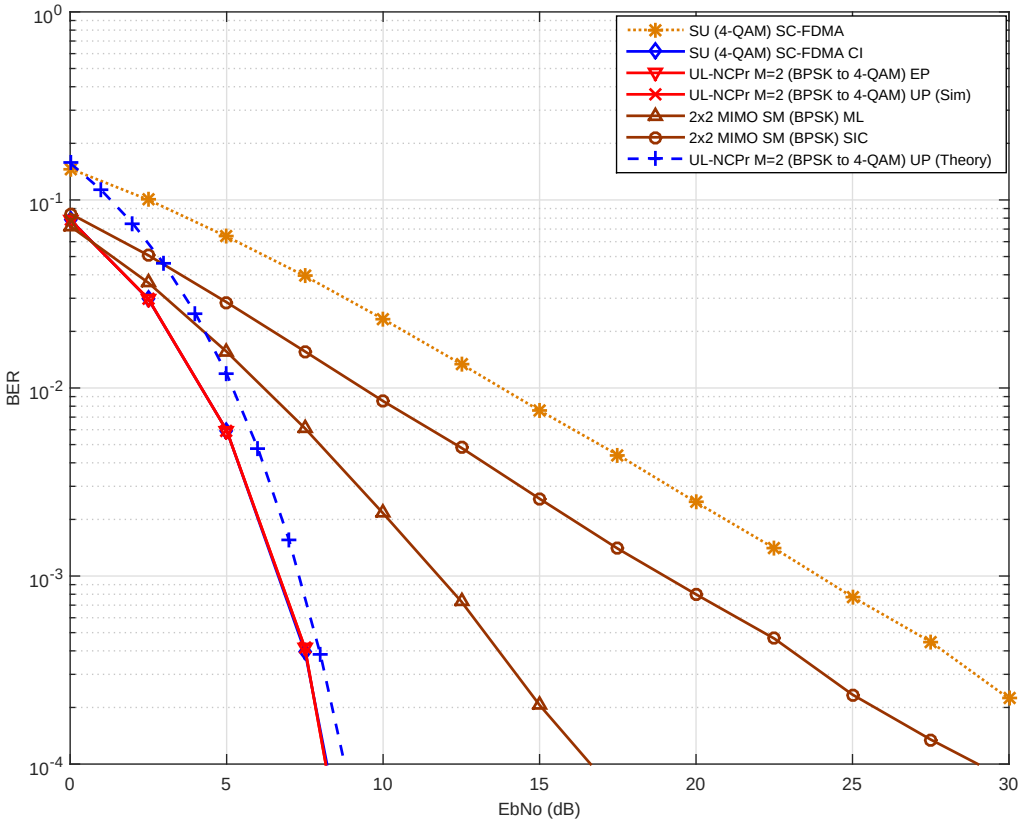

Figure 3.8: Two user UL-NCPr EP and UP compared to single user in SC-FDMA employing 4-QAM with and without channel inversion, and MIMO 2x2 spatial multiplexing with ML and SIC detection schemes

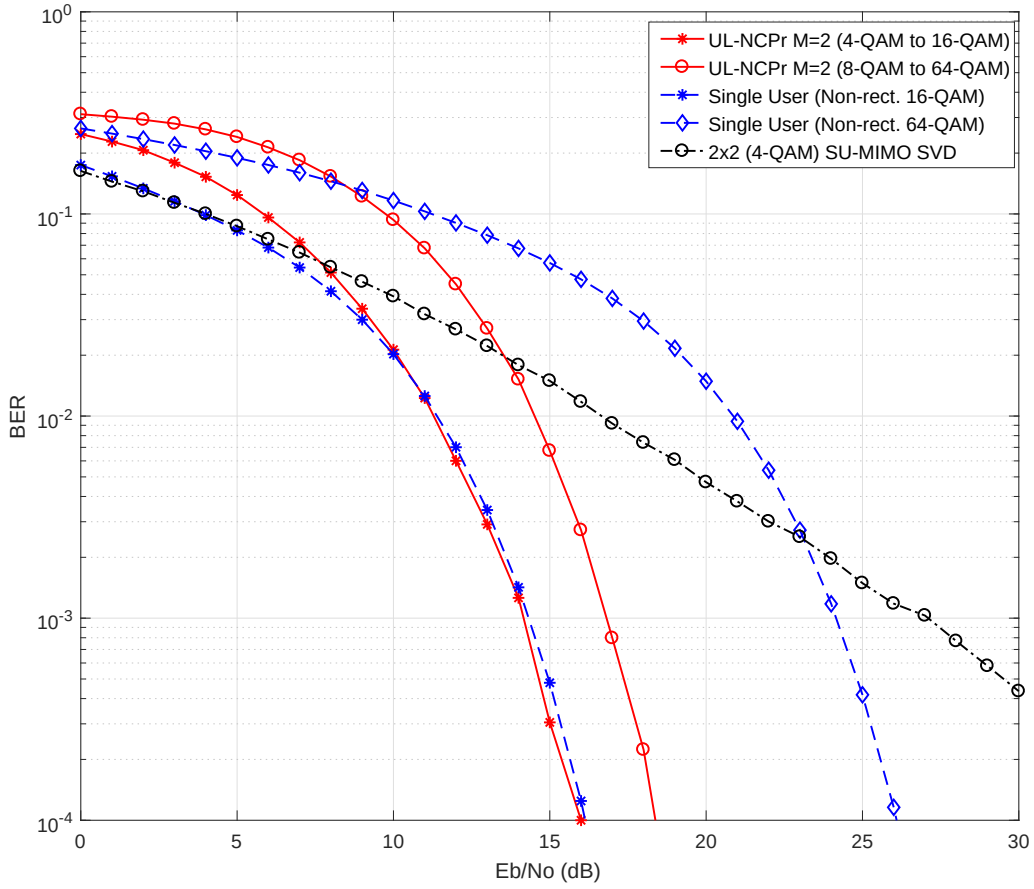

Figure 3.9: Two user UL-NCPr with users employing 4-QAM and 8-QAM component constellations, respectively. This is compared to single user in SC-FDMA employing 4-QAM with channel inversion, and a 2x2 MIMO SM SVD with CSIT&R

For three users each employing BPSK with UP allocation, we get 1.6dB gain compared to EP allocation as illustrated in Figure 3.10.

Figure 3.11 shows the error performance for two to five users each employing BPSK with power and phase adjustment in Table 3.4. It can be seen that as the size of the number of users increases, the size of the composite constellation increases, while the BER performance decreases. These results show that we can superpose multiple users on the same time/frequency resource and still maintain decodability at the receiver, without the need for CSIR.

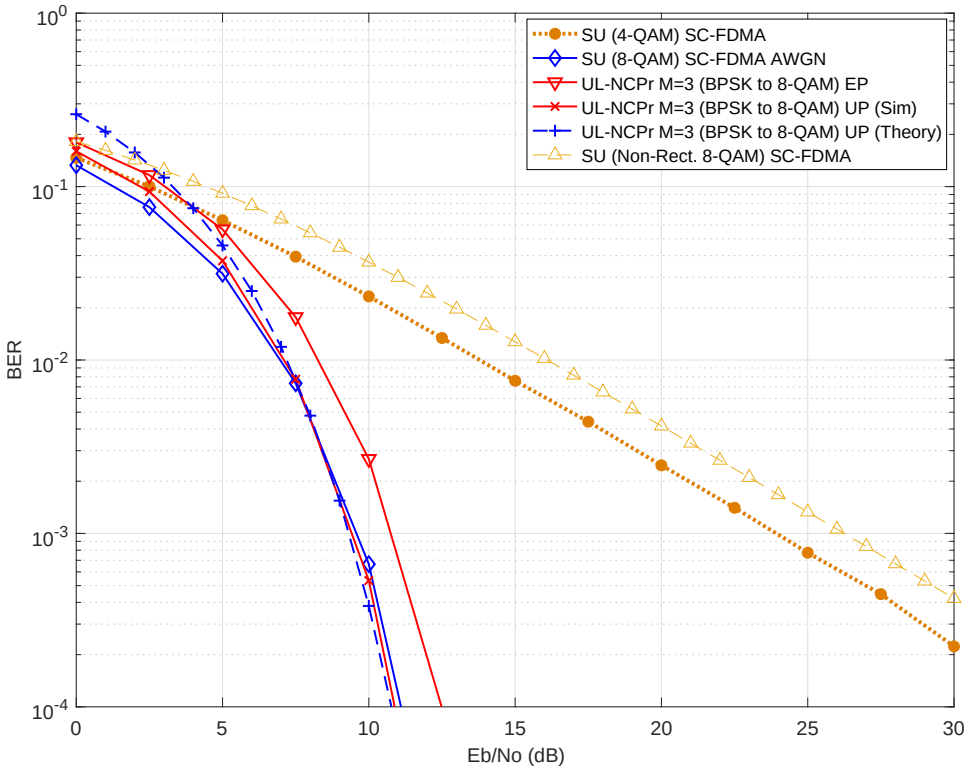

Figure 3.10: Three user UL-NCPr EP and UP compared to single user SC-FDMA employing 8-QAM with and without channel inversion schemes

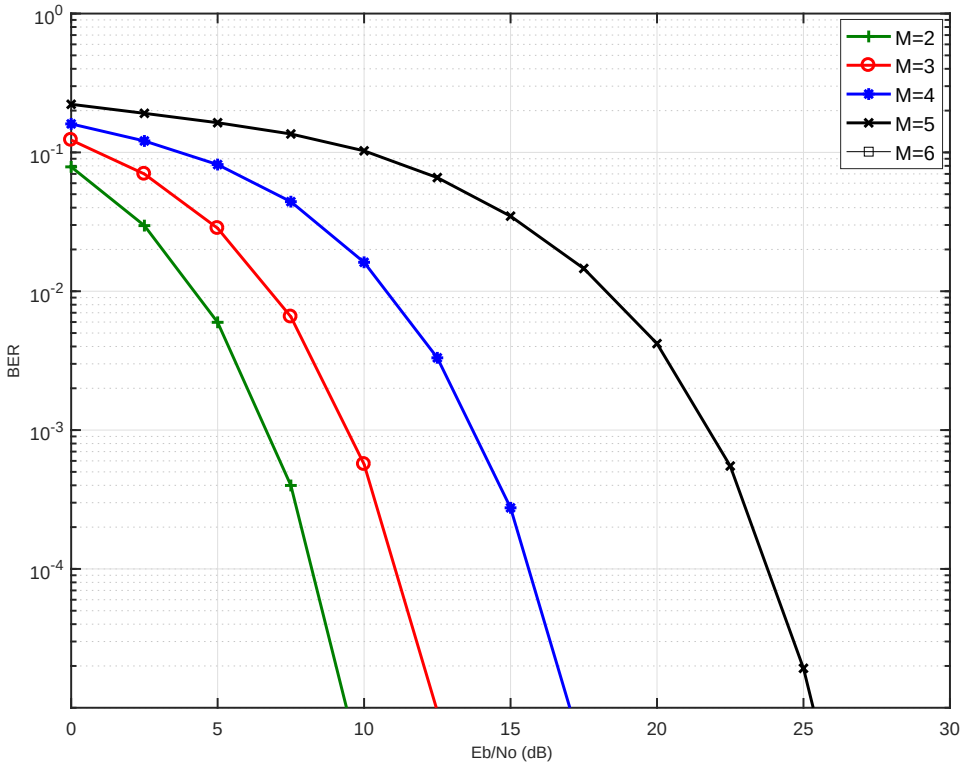

Figure 3.11: BER performance of UL-NCPr UP system for two to five users employing BPSK component constellations using the power and phase allocations given in Table 3.4

Figure 3.12 shows 2-user rate regions for UL-NCPr compared to PD-NOMA and OFDMA schemes. As two users in UL-NCPr contribute their full rates and form a single constellation, we get 3 dB power gain, assumming $\sigma^2 = 1$. Thus, our scheme achieves sum rate of 2 bps/Hz, the optimal point as compared to OFDMA EP and uplink PD-NOMA employing SIC, with sum rates of 1.585 bps/Hz and 1.322 bps/Hz, respectively [120][121].

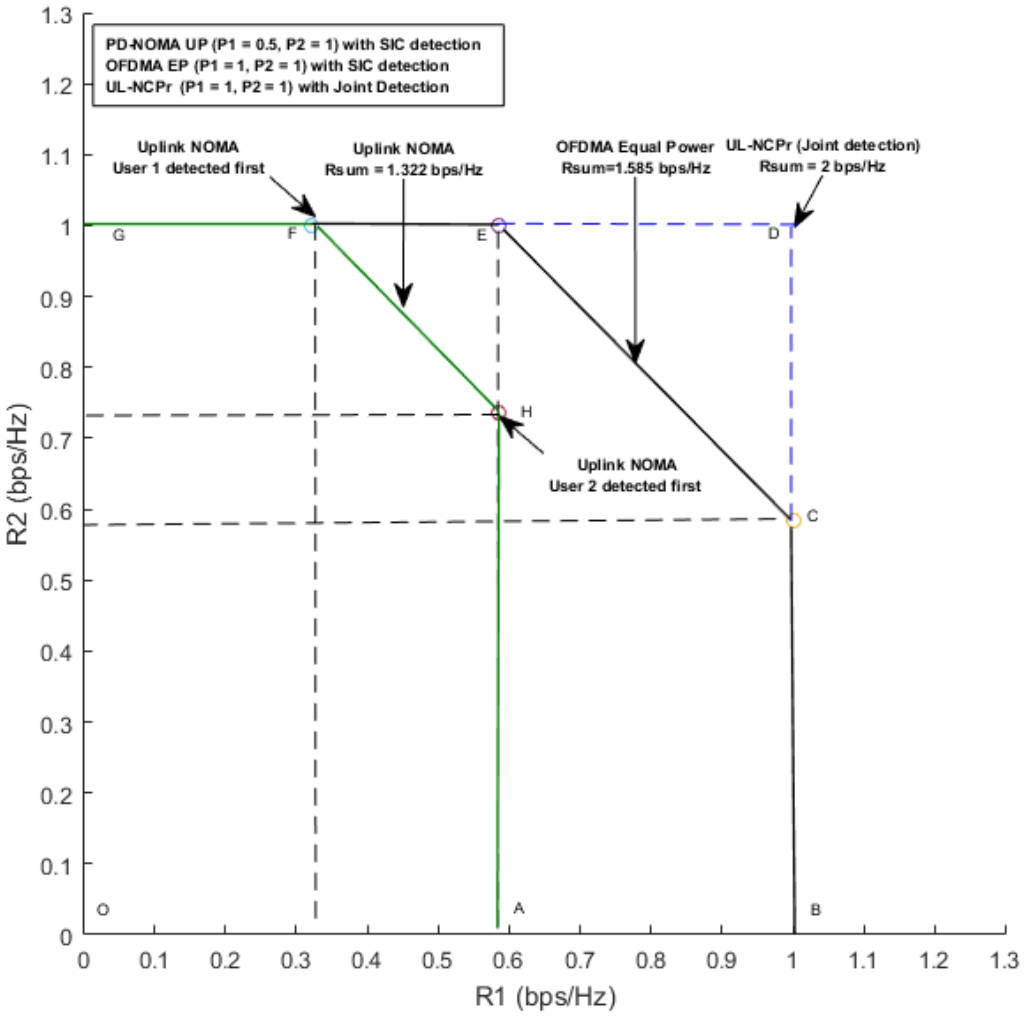

Figure 3.12: Two user capacity region for UL-NCPr compared to PD-NOMA and OFDMA schemes. The power allocations for UL-NCPr and PD-NOMA are given in Table 3.4. OFDMA uses equal power. The variance is set to unity i.e $\sigma^2 = 1$. PD-NOMA and OFDMA employ SIC while UL-NCPr joint detection

Figures 3.13 and 3.14 shows the two user UL-NCPr constellation constrained capacity compared with conventional PD-NOMA and a single user SC-FDMA/OMA with Gaussian MAC as upper bound. It can be seen that for both component modulations, we achieve performance close to two-user Gaussian MAC (GMAC) bound. Furthermore, due to the power gain achieved by combining the two-users powers, we achieve increased capacity compared to the single user in OMA. The poor performance of PD-NOMA for the weak user can also be seen, where more than 10 dB SNR is required to achieve 1 bps/Hz capacity. This is as a result of large power separation requirements in PD-NOMA,

consequently degrading sum-rate capacity. For comparison, the maximum supported channel capacity (Shannon Capacity) is illustrated in Figure 3.15, which further shows the impact of large power separation in PD-NOMA. This shows UL-NCPr can multiplex the two users without the consequence of MAI and still achieve full rate.

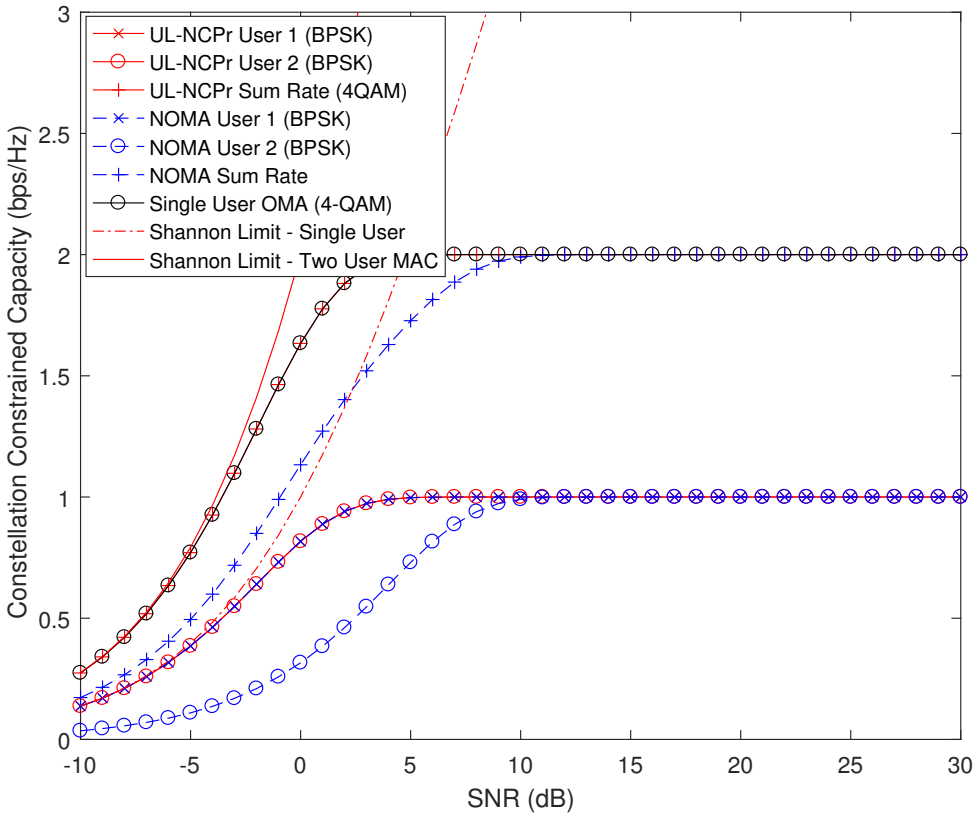

Figure 3.13: Constellation constrained capacity of two users in UL-NCPr each employing BPSK, compared with conventional PD-NOMA, a single user OMA and Shannon limit Gaussian MAC as upper bound

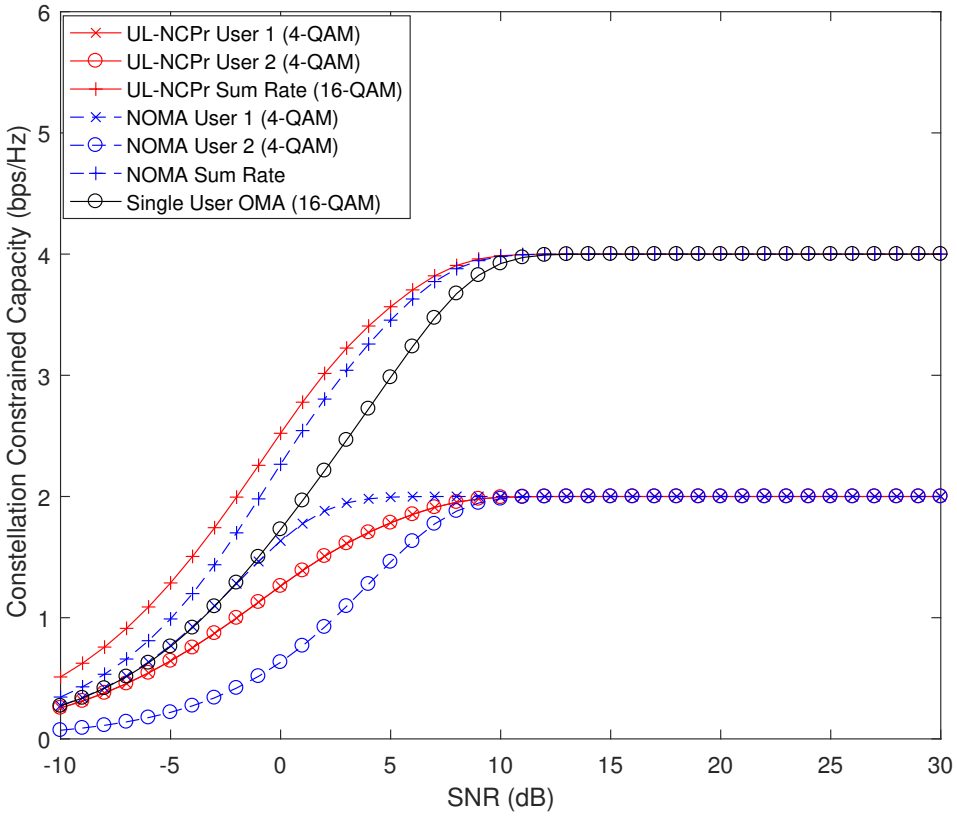

Figure 3.14: Constellation constrained capacity of two users in UL-NCPr each employing 4-QAM, compared with conventional PD-NOMA and a single user OMA

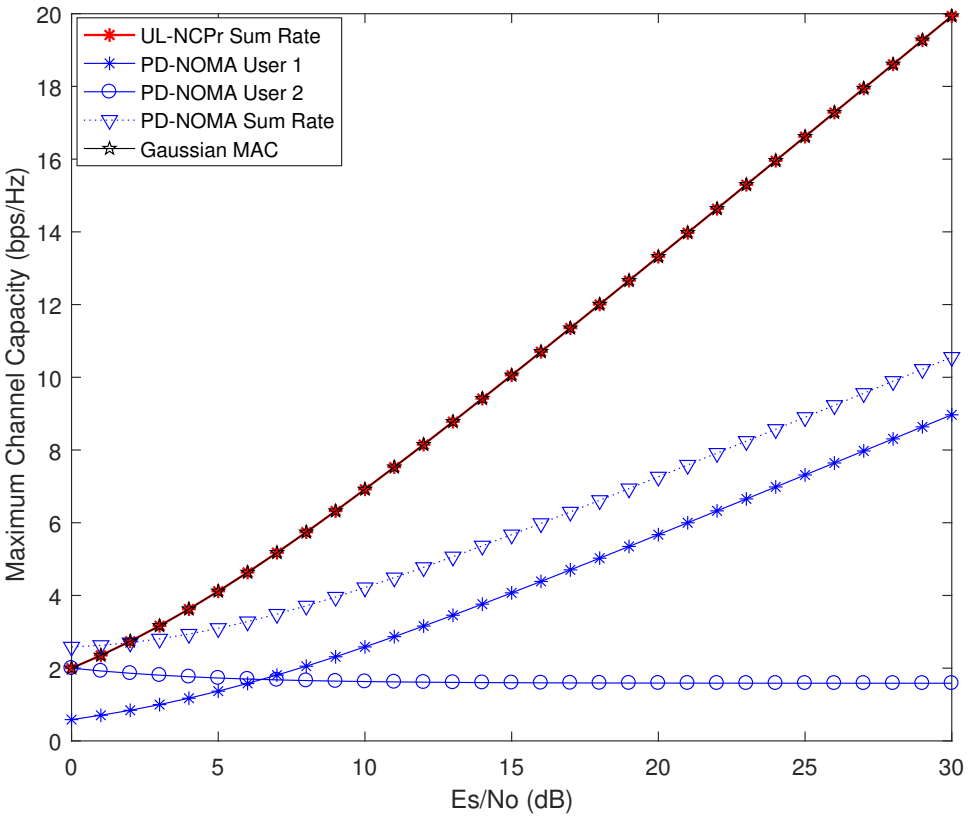

Figure 3.15: Two user UL-NCPr shannon capacity compared with conventional PD-NOMA and a single user SC-FDMA with Gaussian MAC as upper bound

Figure 3.16 shows the constellation constrained capacity for three BPSK users in UL-NCPr compared to PD-NOMA and single user OMA employing the same size constellation as our composite constellation. Similar to the two-user case, it can be see that we achieve power gain due to the sum of users powers compared to a single user OMA. For weak user in PD-NOMA, a SNR of up to 12 dB is required to achieve full rate. However, it can be seen UL-NCPr does not achieve Gaussian bound performance as for the two-user case. This is due to power allocations discussed earlier.

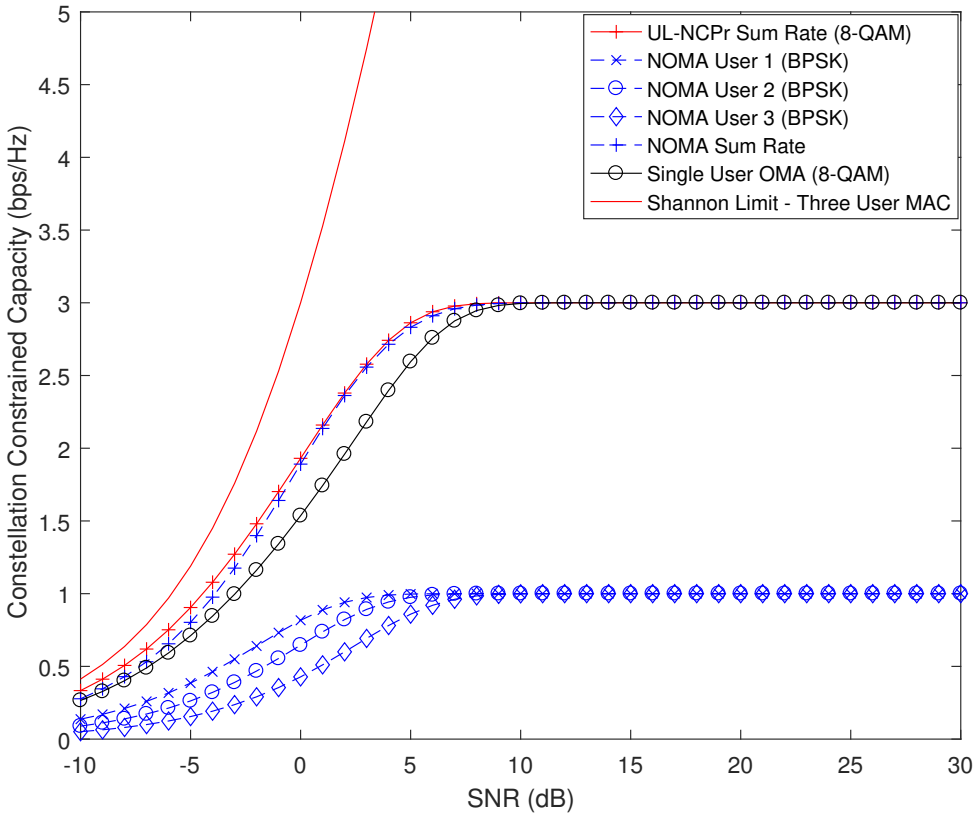

Figure 3.16: Constellation constrained capacity of three users in UL-NCPr each employing BPSK, compared with conventional PD-NOMA, a single user OMA and Shannon limit Gaussian MAC as upper bound

3.9 Conclusion

This chapter introduces a novel NOMA precoding scheme where multiple uplink users are scheduled in both power and phase domain such that they combine to produce a single and uniquely decodable composite constellation. The precoding is designed by the eNB which allocates the power and phase rotation for each user that maximizes the minimum distance of the joint received signal constellation. As the composite constellation is as that of a single user transmitting that same constellation, MAI can be viewed as absent from the system which allows multiple users to transmit at their full rates. Furthermore, we relax the large power separation requirement inherent in PD-NOMA by additional precoding in the phase domain. Our scheme operates with minimal overhead signalling without the need for channel state information at the receiver.

Compared to traditional MIMO SM employing SVD, we achieve up to 8.3 dB gain in BER performance. This is due to the channel gains in SVD precoding channel gains being limited by the eigenvalues of the channel matrix. As our composite users are jointly decoded as a single constellation (which eliminates MAI), we get close to optimum GMAC rates bound for the 2-user scenario. Furthermore, we achieve significant increase in sum rate compared to PD-NOMA. This is due to larger power separation required as the number of users increase, which significantly degrades the sum rates. The scheme also ensures higher rates for the weaker users due to the relaxation on the power separation requirement. This makes our MAC scheme compatible and complimentary with current LTE and future 5G.

Chapter 4

Downlink NOMA with Constellation Preforming

4.1 Introduction

In this chapter, we extend our novel NOMA constellation design and apply it in downlink multi-user broadcast channel. The key difference compared to our uplink NOMA scheme in Chapter 3 is that the users component constellations are superposed/preformed prior to transmission, compared to the channel-based superposition UL-NCPr.

Channel precoding in traditional SIMO broadcast schemes is difficult to employ due to the channel matrix being non-invertible. However, due to all users receiving the same signal constellation in NCPf, the fading can be compensated locally so that the users can detect and extract their component signals.

We employ the signal preforming in Section 4.2 where multiple user signals are combined and transmitted on a single transmitter. This is achieved by an off-line search to determine individual user power and phase weights, subject to the eNB power constraints,

with the objective of maximizing the minimum distance of the composite constellation. The preformed composite constellation belongs to a higher constellation with rate equal to the number of multiplexed users. The users decode their signals by comparing the received signal with the designed constellation. By superposing in both power and phase domains, we relax the power separation constraint inherent in PD-NOMA and achieve increased sum capacity. As the individual users form a single and unique composite constellation, the users treat the received signal as interference-free thereby eliminating multi-user interference compared to conventional OMA and PD-NOMA with SIC.

The contributions of this chapter are as follows:

- Efficient utilization of a single transmitter to transmit multi-user signals on the same time/frequency resource. This is in comparison to spatial multiplexing schemes where each stream requires separate antennas/RF-chains.
- Interference elimination by multi-user signal preforming. The users see the received signal as a single composite signal without interference from other users' signals.
- Increased channel capacity compared to OFDMA and power domain NOMA.

4.2 NOMA with Constellation Preforming (NCPf)

4.2.1 Principles of NCPf

Similar to our UL-NCPr signal design in Chapter 3, the design principle for NCPf is to enable multiple users share a common channel without the consequences of multiple access interference. The key differences are that the user signals are superposed at the eNB

prior to transmission, compared to channel-based superposition in the uplink. This results in the transmissions being subject to the total eNB constraints, unlike per-antenna power constraints in uplink. Furthermore, the broadcast nature in the downlink makes it less stringent on timing and synchronization requirements. Consequently, the composite constellation is broadcasted and received by all the active users. The eNB also signals the users an LUT index notifying them the active constellation to be used for MLD, and their specific-user-order for extraction. As the preforming is performed at eNB, the users do not need the pre-design weights for detection, but only the transmitted composite constellation. Upon reception, the users estimate their respective channel gains so as to compensate for the fading on the received signal. They then perform the MLD with the pre-known constellation. As the detected symbol is a composite of the all the preformed users, they extract their respective data and discard the rest.

4.2.2 System Model

4.2.2.1 Signal Model

The system block diagram of a baseband model of the proposed NCPf broadcast scheme is shown in Figure 4.1. The eNB, equipped with a single antenna, broadcasts superimposed data on N OFDM subcarriers to M users, each equipped with one antenna. It is assumed that all users have perfect CSI, estimated from reference signal transmitted by the eNB. We also assume that the total duration for transmission of symbols is less than the minimum coherent time of the users channels i.e. the channels remain constant over the transmission period. Furthermore, the users are assumed to be located in increasing distance from the eNB, such that the first user has the strongest, and the last user has the weakest channel, respectively.

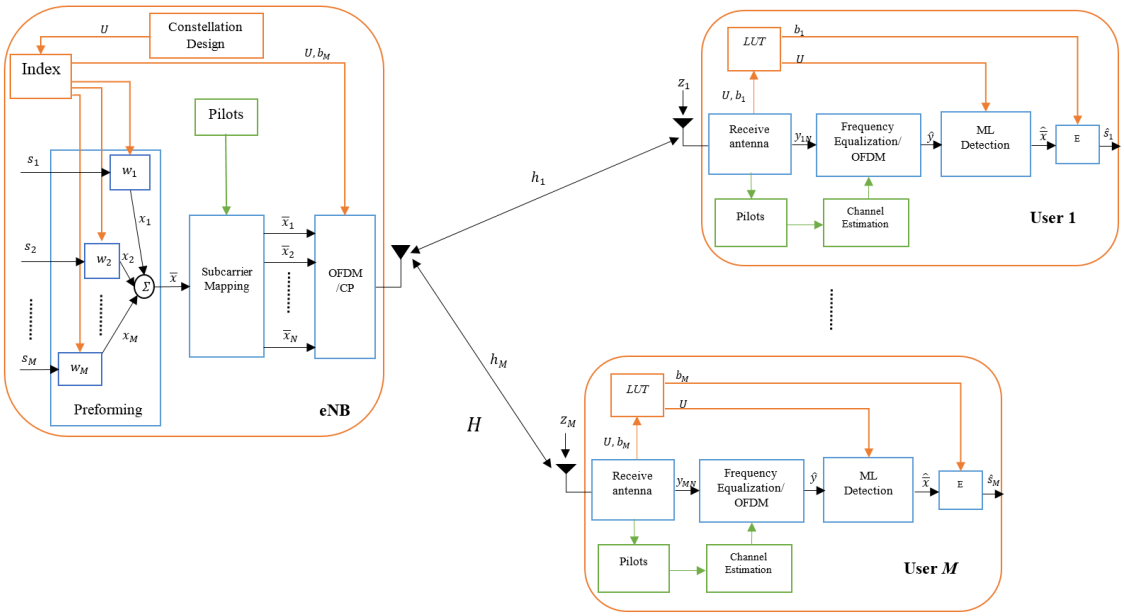

Figure 4.1: System Model of the proposed downlink NOMA with constellation preforming scheme. The figure shows the eNB equipped with a single antenna broadcasting preformed superimposed data to multiple M users also equipped with a single antenna. The channel and noise are also illustrated. It is assumed the eNB transmits on N orthogonal subcarriers.

The composite constellation is designed at the eNB by an off-line search of the power and phase rotations weights for each user such that the transmitted constellations' minimum distance is maximized and fully decodable. At the receiver, the received signal at each user is decoded by performing MLD from a channel equalized pre-known composite constellation signalled by the eNB.

Let $\mathbf{s}_{mn}$ denote the complex component signal of the m-th user on the n-th subcarrier, by applying power and phase preforming weights, $\mathbf{w}_{mn}$, to each component user, the transmitted symbol becomes

$$\bar{\mathbf{x}}_n = \sum_m \mathbf{w}_{mn}\mathbf{s}_{mn} = \sum_m \sqrt{\mathbf{p}}_{mn} e^{j\theta_{mn}} \mathbf{s}_{mn}, \tag{4.1}$$

where $\sqrt{\mathbf{p}}_{mn}$ and $e^{j\theta_{mn}}$ represents the power and phase, weights respectively.

The received signal at the m-th user on the n-th subcarrier can thus be expressed as

$$\mathbf{y}_{mn} = \mathbf{h}_{mn}\bar{\mathbf{x}}_n + \mathbf{z}_{mn} \tag{4.2}$$

where $\bar{\mathbf{x}}_n$, is the complex composite symbol of M users with power constraint $E[|\bar{\mathbf{x}}_n|^2] \leq \mathbf{P}$. The term $\mathbf{h}_{mn}$ denotes the channel from the eNB antenna to the m-th user on subcarrier n. The term, $\mathbf{z}_{mn}$, is a white complex Gaussian noise at the m-th user with zero mean and variance σ^2_{mn}.

For the above signal model, the following assumptions are considered:

1. Perfect CSIR and estimate at the users.
2. Channels remain constant for the duration of transmissions i.e. each subframe.
3. The users are located in increasing distance (decreasing channel gain) from the eNB.
4. Per-eNB power constraints i.e. the total power is shared between the users.
5. Design objectives an considerations outlined in section 3.5.3.1.
6. Designed preforming constellation and the specific-user-order for signal extraction are available at the users.
7. The eNB does not add or remove users in an active subframe; can be scheduled in the next sub-frame.

4.2.2.2 Constellation Preforming and Algorithm

We employ our search algorithm proposed in Section 3.5.3.2 to find the power and phase values that maximize the distance of the composite constellation. The key design differ-

ence compared to the uplink search algorithm is that in downlink, the total eNB power is shared by the users, compared to per-antenna power constraint for the users in uplink. This makes the power search function as a fraction of $\mathbf{P}$. Therefore, we modify the power allocation strategy in Algorithm 1 and generate Algorithm 2 to obtain the weights. The algorithm variables are as defined in Table 3.1.

Algorithm 2 Search algorithm used in computing the power and phase values that maximize the minimum distance of the composite constellation points.

1: $Initialize: M =$ number of users; $\mathbf{P} \leftarrow 1; \bar{\mathrm{D}}_m \leftarrow (0 : 0.1 : 1)\mathbf{P}; \bar{\beta_m} \leftarrow 0 : \pi/180 : \pi$
2: *Generate* Complex component symbols $\mathbf{V}$
3: **while** $m \neq 1$ **do**
4: Find all the possible combinations of all the user powers $\mathbf{D}_i = [\bar{\mathrm{D}}_{1i} \ldots \bar{\mathrm{D}}_{Mi}]$ as a fraction of $\mathbf{P}$
5: Find all possible combinations $\mathbf{W}_i$ of $\mathbf{D}_i$ with $[\bar{\beta}_1 \rightarrow \bar{\beta}_M]$
6: **for** $i \leftarrow$ All possible combinations **do**
7: $\bar{\mathbf{U}}_i \leftarrow \mathbf{V} \cdot \mathbf{W}_i$
8: **end for**
9: Compute d_{min} for all $\bar{\mathrm{U}}_i$
10: Find $\mathbf{U}[\mathrm{D}_m, \beta_m] \leftarrow \arg\max_{d_{min}}\{\bar{\mathbf{U}}[\mathbf{W}]\}$
11: **end while**

The algorithm steps are summarized as below

1. We begin by initializing our algorithm by defining the number of users and our power and phase search resolutions of $0.1\mathbf{P}$ and $\pi/180$, respectively.

2. Based on the number of users in step 1 and the users' QoS requirements i.e equal or variable rate component constellations, we generate binary stream matrix $\mathbf{V}$, containing all the possible values of the users input signal. We then modulate the respective component signals based of $\mathbf{Q}_m$.

3. Find all the possible combinations of all the user powers $\mathbf{D}_i = [\bar{\mathrm{D}}_{1i} \ldots \bar{\mathrm{D}}_{Mi}]$ as a fraction of $\mathbf{P}$

4. The next step is to find all the i-th possible combination of power and phase weight

values $\mathbf{W}_i = \mathbf{D}_i\bar{\beta}_i$.

5. Iterate $\mathbf{W}_i$ from step 4 to find the i-th composite vector $\mathbf{U}_i = \mathbf{V} \times \bar{\mathrm{D}}_i e^{j\bar{\beta}_i}$.

6. Find the d_{min} of all the points in composite vector $\bar{\mathbf{U}}_i$.

7. Based on step 6, select the i-th weights $\mathbf{W}_i$ that maximize the d_{min} of the composite constellation points.

Table 4.1: Example of two and three users all employing BPSK. Their individual power allocations as a fraction of **P**, relative phase shifts and the size of their composite constellation are given. The composite constellation d_{min} for both schemes are presented

M	Scheme	Power Allocation	Phase Rotation	Composite Constellation	d_{min}
2	PD-NOMA	$\mathrm{D}_1 = 0.3\mathrm{P}, \mathrm{D}_2 = 0.7\mathrm{P}$	$\beta_{1\to2} = 0$	4-PAM	0.6
	NCPf	$\mathrm{D}_1 = 0.5\mathrm{P}, \mathrm{D}_2 = 0.5\mathrm{P}$	$\beta_1 = 60, \beta_2 = 0$	4-QAM	1.0
3	PD-NOMA	$\mathrm{D}_1 = 0.1\mathrm{P}, \mathrm{D}_2 = 0.3\mathrm{P}$ $\mathrm{D}_3 = 0.6\mathrm{P}$	$\beta_{1\to3} = 0$	8-PAM	0.2
	NCPf	$\mathrm{D}_1 = 0.3\mathrm{P}, \mathrm{D}_2 = 0.3\mathrm{P}$ $\mathrm{D}_3 = 0.4\mathrm{P}$	$\beta_1 = 90, \beta_2 = 44$ $\beta_3 = 8$	8-QAM	0.5

Table 4.2: Example of two and three users all employing 4-QAM. Their individual power allocations as a fraction of **P**, relative phase shifts and the size of their composite constellation are given. The composite constellation d_{min} for both schemes are presented

M	Scheme	Power Allocation	Phase Rotation	Composite Constellation	d_{min}
2	PD-NOMA	$\mathrm{D}_1 = 0.3\mathrm{P}, \mathrm{D}_2 = 0.7\mathrm{P}$	$\beta_{1\to2} = 0$	16-QAM	0.4
	NCPf	$\mathrm{D}_1 = 0.3\mathrm{P}, \mathrm{D}_2 = 0.7\mathrm{P}$	$\beta_1 = 5, \beta_2 = 0$		0.4
3	PD-NOMA	$\mathrm{D}_1 = 0.1\mathrm{P}, \mathrm{D}_2 = 0.2\mathrm{P}$ $\mathrm{D}_3 = 0.7\mathrm{P}$	$\beta_{1\to3} = 0$	64-QAM	0.1
	NCPf	$\mathrm{D}_1 = 0.2\mathrm{P}, D_2 = 0.2\mathrm{P}$ $\mathrm{D}_3 = 0.6\mathrm{P}$	$\beta_1 = 65, \beta_2 = 5$ $\beta_3 = 0$		0.2

Tables 4.1 and 4.2 illustrates an example of two and three users all employing BPSK and 4-QAM, respectively. The composite constellations with their d_{min} are also shown. As

an example, for two users employing BPSK, we achieve a 40% increase in d_{min} compared to PD-NOMA [113]. Furthermore, by applying a phase rotation of $\beta_1 = 60, \beta_2 = 0$ to the component users signal, we relax the power separation requirement for PD-NOMA and both users transmit with equal powers. This results in fair rates for both users, compared with poor rates for the weak user in PD-NOMA. Similarly, for three users employing BPSK, we achieve $d_{min} = 0.5$ for NCPf compared to $d_{min} = 0.2$ for PD-NOMA. We also achieve fairer rates for the users compared to PD-NOMA, were the weaker user rates are significantly poorer than the strong user. For two users employing 4-QAM, we get equal performance with PD-NOMA.

For three 4-QAM users, we achieve $d_{min} = 0.2$ compared to $d_{min} = 0.1$ for PD-NOMA. Furthermore, the weaker users get increased rates. The difference in the shape of the constellation design can be seen in Figures 4.2(a) and 4.2(b).

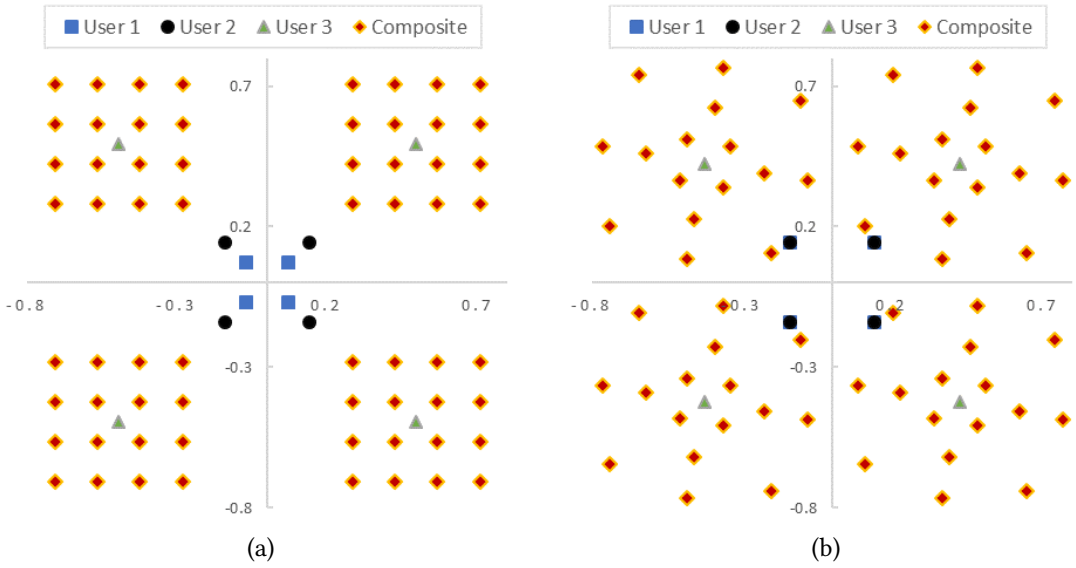

Figure 4.2: Superimposed component and composite constellation of three users each employing 4-QAM. (a) Superimposed component constellations of PD-NOMA users with power allocations of $D_1 = 0.1P, D_2 = 0.2P, D_3 = 0.7P$. (b) Superimposed component constellations of NCPf users with power and phase allocations of $D_1 = 0.2P, D_2 = 0.2P, D_3 = 0.6P$ and $\beta_1 = 65, \beta_2 = 5, \beta_3 = 0$, respectively.

Table 4.3: UL-NCPr example of two users all employing variable component modulations. Their individual power allocations, relative phase shifts and the size of their composite constellation are given. The composite constellation d_{min} for both schemes are presented

Scheme	Component Constellation	Power Allocation	Phase Rotation	Composite Const.	d_{min}
PD-NOMA	BPSK+4-QAM	$D_1 = 0.4P, D_2 = 0.6P$	$\beta_1 = 0, \beta_2 = 0$	8-QAM	0.5
NCPf		$D_1 = 0.3P, D_2 = 0.7P$	$\beta_1 = 43, \beta_2 = 0$		0.6
PD-NOMA	4-QAM+8-QAM	$D_1 = 0.4P, D_2 = 0.6P$	$\beta_1 = 0, \beta_2 = 0$	32-QAM	0.2
NCPf		$D_1 = 0.2P, D_2 = 0.8P$	$\beta_1 = 13, \beta_2 = 0$		0.3

Table 4.3 shows an example of two users employing variable component constellations. When either the first and second users employ BPSK and 4-QAM (Figures 4.3(a) and 4.3(b)) or 4-QAM and 8-QAM (Figures 4.4(a) and 4.4(b)), respectively, we achieve a 0.1 increase in d_{min} for both strategies. However, this comes at the cost of larger power separation for NCPf. Due to the users employing joint detection, the sum capacity offsets the power separation issue.

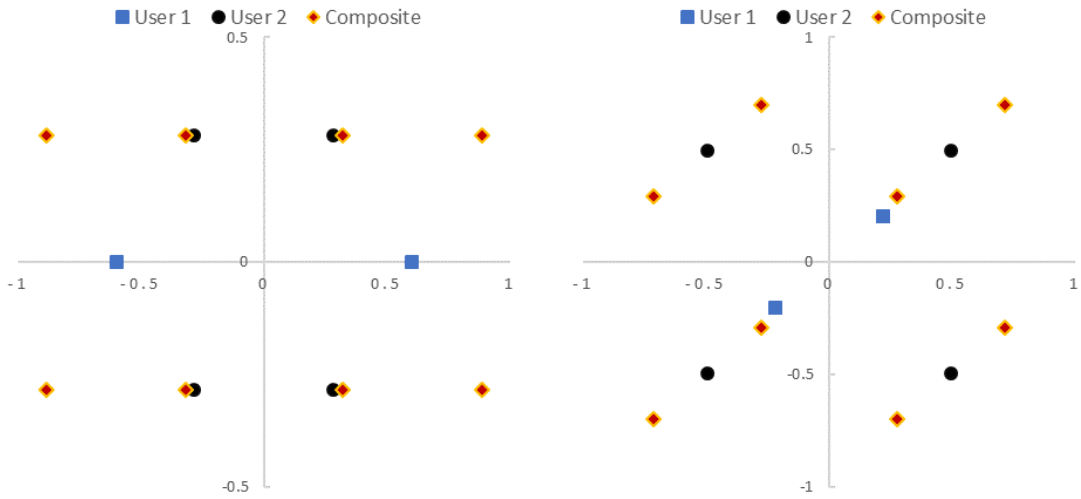

(a) (b)

Figure 4.3: Superimposed component and composite constellation of two users employing variable rate BPSK and 4-QAM. (a) Superimposed component constellations of PD-NOMA users with power allocations of $D_1 = 0.4P, D_2 = 0.6P$. (b) Superimposed component constellations of NCPf users with power and phase allocations of $D_1 = 0.3P, D_2 = 0.7P$ and $\beta_1 = 43, \beta_2 = 0$, respectively.

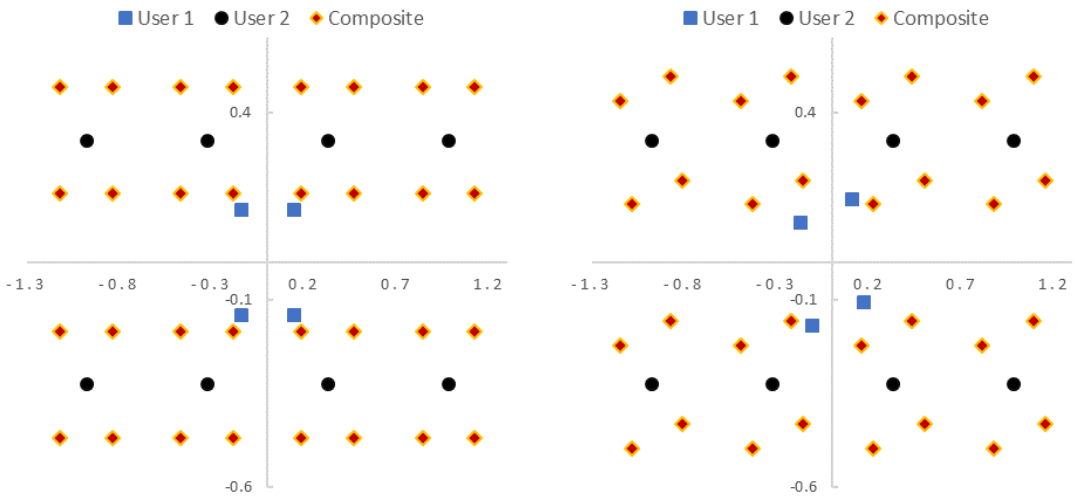

(a) (b)

Figure 4.4: Superimposed component and composite constellation of two users employing variable rate 4-QAM and 8-QAM. (a) Superimposed component constellations of PD-NOMA users with power allocations of $D_1 = 0.4P, D_2 = 0.6P$. (b) Superimposed component constellations of NCPf users with power and phase allocations of $D_1 = 0.3P, D_2 = 0.7P$ and $\beta_1 = 43, \beta_2 = 0$, respectively.

4.2.2.3 Joint Maximum Likelihood Detection and Recovery

At the receiver, the users performs channel estimation and frequency domain equalization from orthogonal pilots broadcasted from the eNB. JML detection is then employed at the receiver using the designed constellation as reference. The detector carries out a search between the received signal and reference constellation points to find the minimum Euclidean distance between the two distances as defined as

$$\hat{\mathbf{x}}_n = \arg\left[\min_{\mathbf{U}}(\|\mathbf{y}_{mn} - \mathbf{u}_i \mathbf{h}_{mn} \mathbf{h}^*_{mn}\|^2)\right] \quad \forall i \tag{4.3}$$

where $\mathbf{h}_{mn}$ is the complex conjugate of the downlink channel. The users extract their signals from the detected composite signal. Let $\bar{b}$ denote the user order in computation of $\mathbf{V}$, assuming the users are ordered from $1,...,M$, then the signal vector of the m-th user, $\hat{\mathbf{s}}_{mn}$, can be defined as the $\bar{b}$-th column of $\hat{\mathbf{x}}_n$.

4.3 Performance Analysis

For NCPf, multiple users combine to form a single composite constellation. From the user point of view, the received constellation sees no interference from other users. Thus, multiple users combine as a single user with the transmitted power as the sum of the individual user powers, subject to eNB power constraint. This results in the system capacity defined as point-to-point system with the SNR the power sum of the individual users defined as

$$C_{|\text{NCPf}} = \sum_{m=1}^{M} \mathbb{E}\left(\log_2\left(1 + \frac{|\mathbf{h}_m|^2\mathbf{P}}{\sigma_m^2}\right)\right) \tag{4.4}$$

where $\mathbf{P} = \sum_m \mathrm{D}_m$ is the sum of the individual users component signal power. Furthermore, modifying the CCC formula in eq. (3.27), we express the downlink CCC as

$$R = \log_2 - \frac{1}{\Omega}\sum_{q=1}^{\Omega} \mathbb{E}\left[\log_2 \sum_{q=1}^{\Omega} e^{-\left(\frac{\|\mathbf{y}-\mathbf{H}\bar{\mathbf{x}}_{(\bar{q})}\|^2 - \|\mathbf{z}\|^2}{\sigma^2}\right)}\right] \tag{4.5}$$

where $\mathbf{y} = \mathbf{H}\bar{\mathbf{x}} + \mathbf{z}$ is the received signal defined in Equation (4.2).

Similar to our error rate analysis in Section 3.7.2, it is hard to derive a BER since it depends on the d_{min} of the received composite constellation. Thus, we derive an upper bound approximation to the error rates. As the receive signal at each of the users is as a point-to-point transmission in fading, we modify Equation (3.29) and express the probability of error as

$$P_e^{DL} \approx \sum_f \gamma \sum_{b\neq 1} Q_c\left(\sqrt{\frac{|h_m|^2 d^2_{u(f,1),u(f,b)}}{Z_n}}\right) + \sum_f \gamma \sum_{v\neq f}\sum_{b=1} Q_c\left(\sqrt{\frac{|h_m|^2 d^2_{u(f,1),u(v,b)}}{Z_n}}\right) \tag{4.6}$$

4.4 Simulation Modelling and Results

4.4.1 Simulation Model

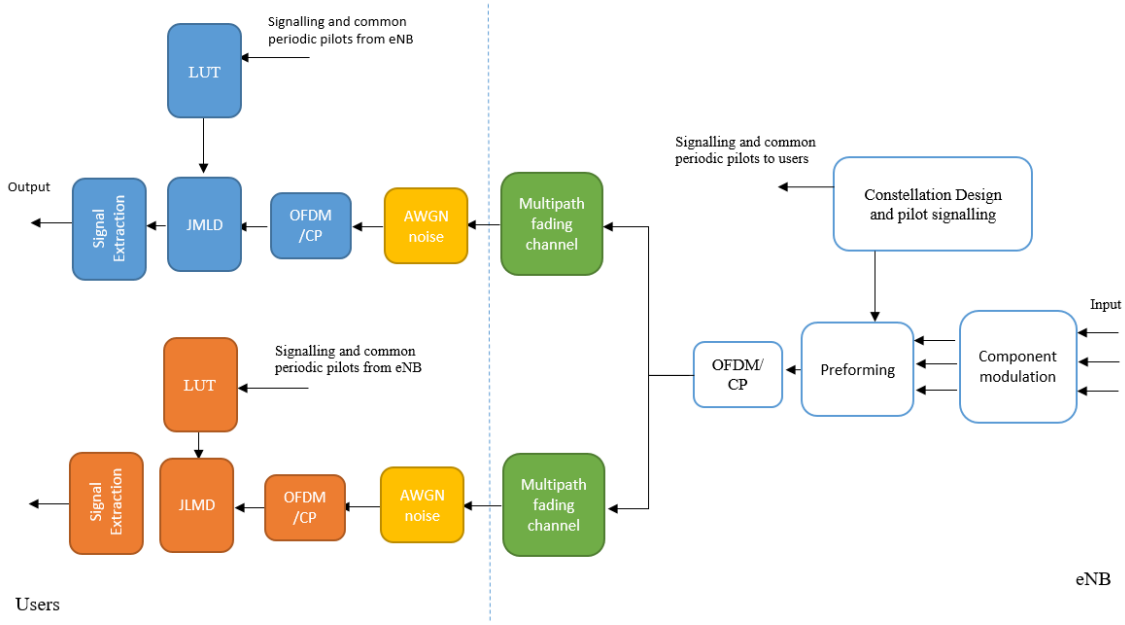

Figure 4.5: NCPf simulation Model

A Monte-Carlo simulation is carried out in MATLAB to validate the performance of our proposed scheme. For simplicity, a two and three user system are considered. It is assumed that the users are located in increasing distance from the eNB. Thousands of user input streams are first modulated with the component modulation to be simulated. The symbols for each user are then mapped to N RE. The users signal on the n-th RE are then preformed, such that each subcarrier is composed of the M user signals. Next we employ IFFT and CP. The signals are then transmitted in to an uncorrelated multipath fading channel, with AWGN noise applied at the users. The signals are received by the users who then perform ML detection with the designed constellation as reference. It is assumed that the users have full channel state information. The system performance is evaluated in terms of BER, capacity bounds and throughput over thousands of symbols. We compare our proposed scheme with conventional OMA and PD-NOMA schemes.

4.4.2 Results

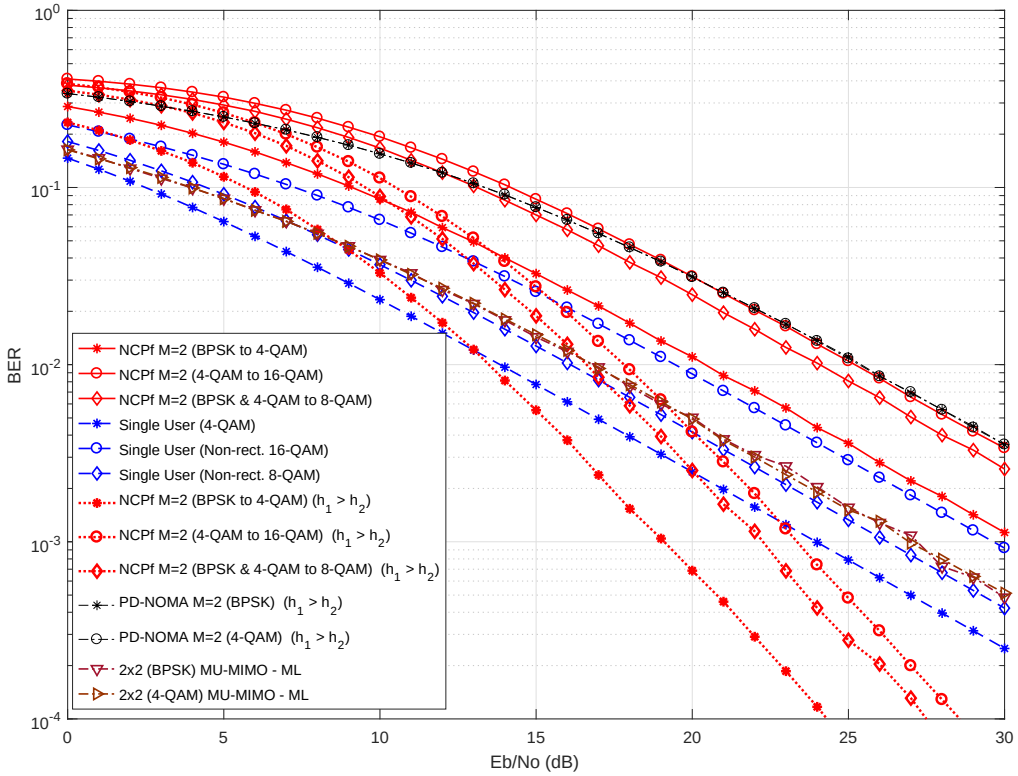

Figure 4.6: BER vs Eb/No performance of 2-user NCPf system compared to single user OMA and 2-user PD-NOMA employing SIC.

Figure 4.6 illustrates the BER performance for NCPf compared with OMA and PD-NOMA employing SIC. Due to multiple users forming a single constellation with the same power constraint as a single OMA user, we trade d_{min} performance for increased spectral efficiency. However, due to the NOMA principle of distance-dependent multiplexing, when the channels are ordered from the strongest to the weakest i.e. $\mathbf{h}_1 > \mathbf{h}_2$, we offset the loss in BER achieving higher performance for the strongest user, while the weak users have a slightly lower BER performance. For the two users employing either BPSK or 4-QAM component constellation to produce 4-QAM and 16-QAM composite, respectively, it can be seen that at high SNR, we start to gain BER performance for the strong NCPf user compared to the single user. For example, at BER of 10^{-3} , we get 5 dB and 7 dB

BER improvements for all BPSK and all 4-QAM component constellations, respectively. While we lose about 6 dB for the weak user, we achieve double the spectral efficiency compared to the single user. Furthermore, due to the error propagation performance of SIC, the performance of the strong PD-NOMA user is the same with the weak NCPf user.

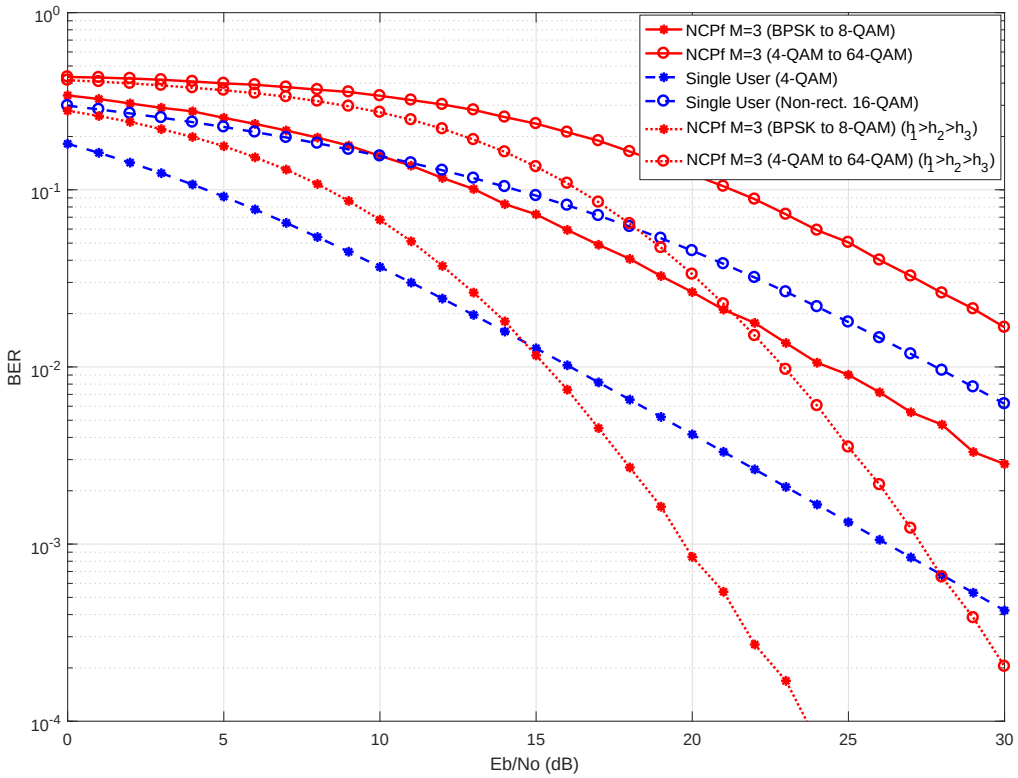

Figure 4.7: BER vs Eb/No performance of 3-user NCPf system compared to single user OMA.

Similarly, for three users employing either BPSK or 4-QAM component constellation to produce 8-QAM and 64-QAM composite, respectively, it can be seen that at higher SNR, we gain BER performance for the strong NCPf user compared to the single user. For example, at BER of 10^{-3} , we get of 7 dB BER improvement for all BPSK component constellations, compared to a single user employing non-rectangular 8-QAM. For all 4-QAM component constellations, we achieve 5 dB improvement at BER of 10^{-2} compared to a single user employing non-rectangular 64-QAM. For the weak user, we lose 8 dB for

all BPSK component constellations. However, we get 3x the channel capacity compared to the single user.

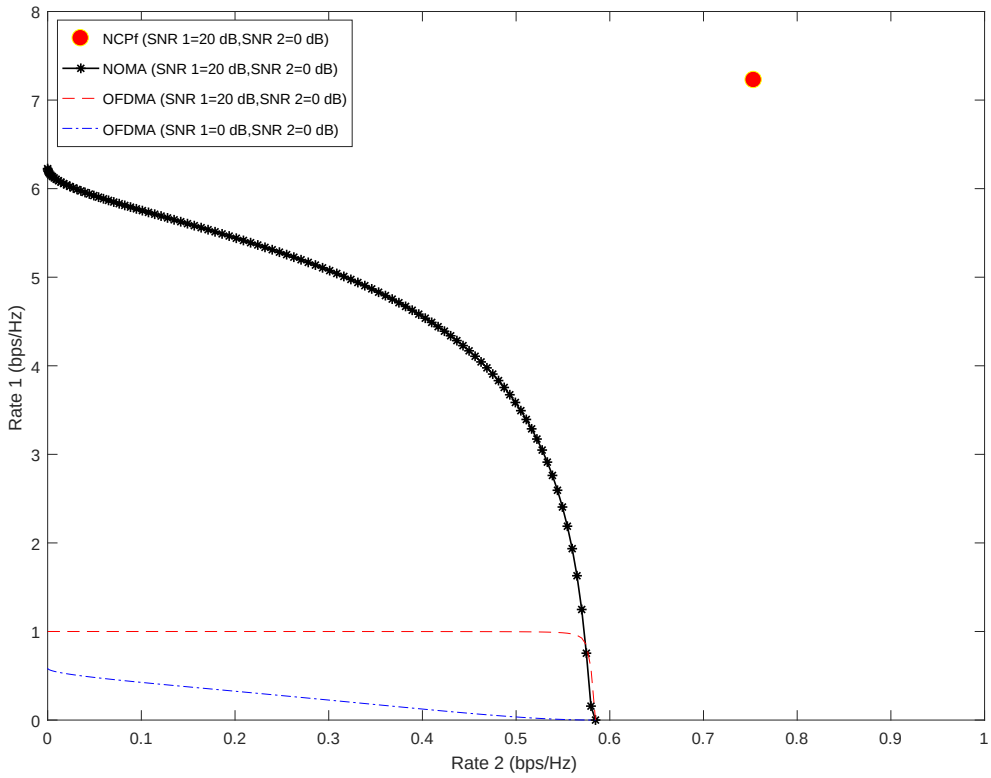

Figure 4.8: 2-user rate region illustrating the performance of NCPf compared to OMA and PD-NOMA. The variance is set to unity i.e $\sigma^2 = 1$. PD-NOMA and OFDMA employ SIC while UL-NCPr joint detection

Figure 4.8 shows the two user rate regions illustrating the achievable sum capacities for NCPf, OMA and PD-NOMA. For NCPf, at received $\text{SNR}_1 = 20$ dB for the strong user and $\text{SNR}_2 = 0$ dB, we get sum capacity of 8 bps/Hz. It can be seen NCPf outperforms PD-NOMA and OMA.

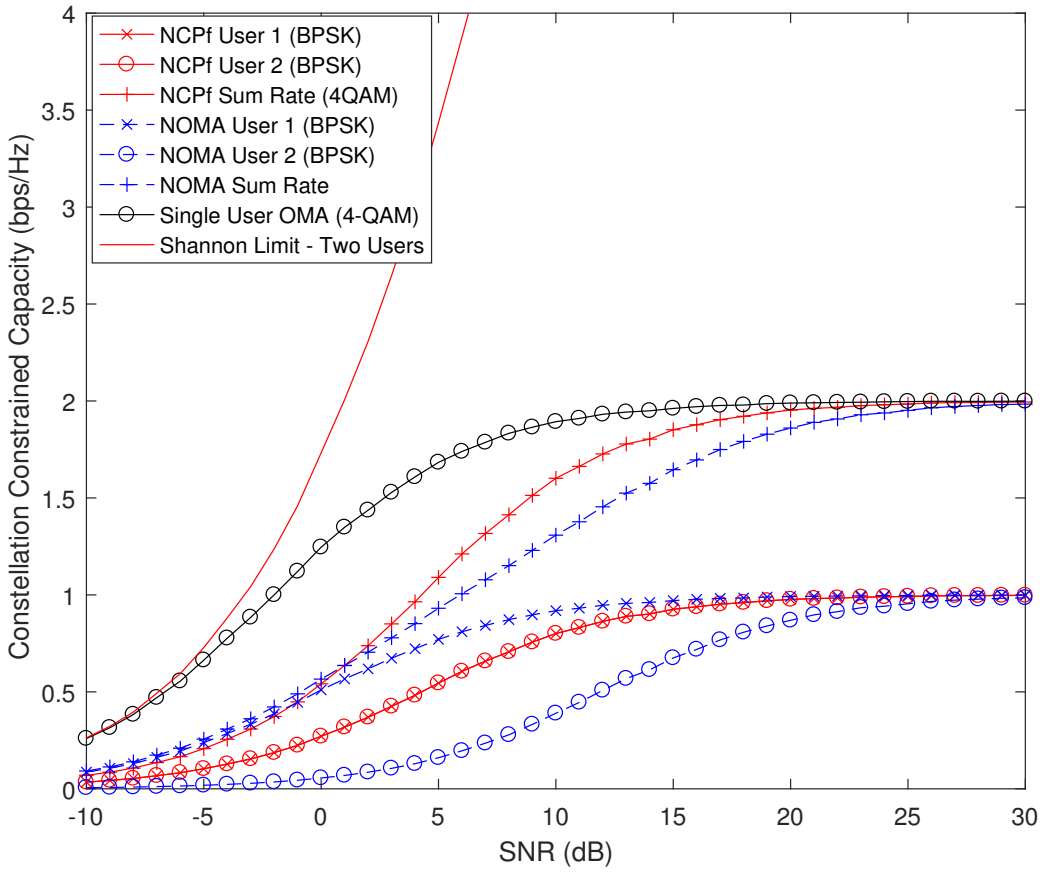

Figure 4.9: 2-user constellation constrained capacity performance for NCPf, compared to OMA and PD-NOMA with the users employing BPSK component constellations, respectively. Shannon bound is included for comparison.

Figures 4.9 and 4.10 shows the two-user CCC performance for NCPf, OMA and PD-NOMA with the users employing BPSK and 4-QAM component constellations, respectively. For the BPSK component constellations, it can be seen that SNR of 10 dB, we get 0.3 bps/Hz increase in capacity compared to PD-NOMA. Although the strong PD-NOMA user achieves increased capacity compared to each of the NCPf users e.g. 0.22 bps/Hz at 5 dB, we achieve increased sum-rate. This is due to the poor rate of the weak user resulting in degraded sum-rate and poor fairness, where a significant $\geq$ 30 dB SNR is needed for the PD-NOMA weak user to achieve full rate of 1 bps/Hz. The same performance trend applies to 4-QAM component constellations. The Shannon Limit for single user

employing the same size composite constellation with average power $|\mathbf{x}|^2 = 1$ is shown for comparison. Note that we achieve less rates compared to the single OMA user due to total average power constraint $\sum_m |\bar{\mathbf{x}}_m|^2 = 1$ for all users in NCPf. This constraint applies to subsequent results.

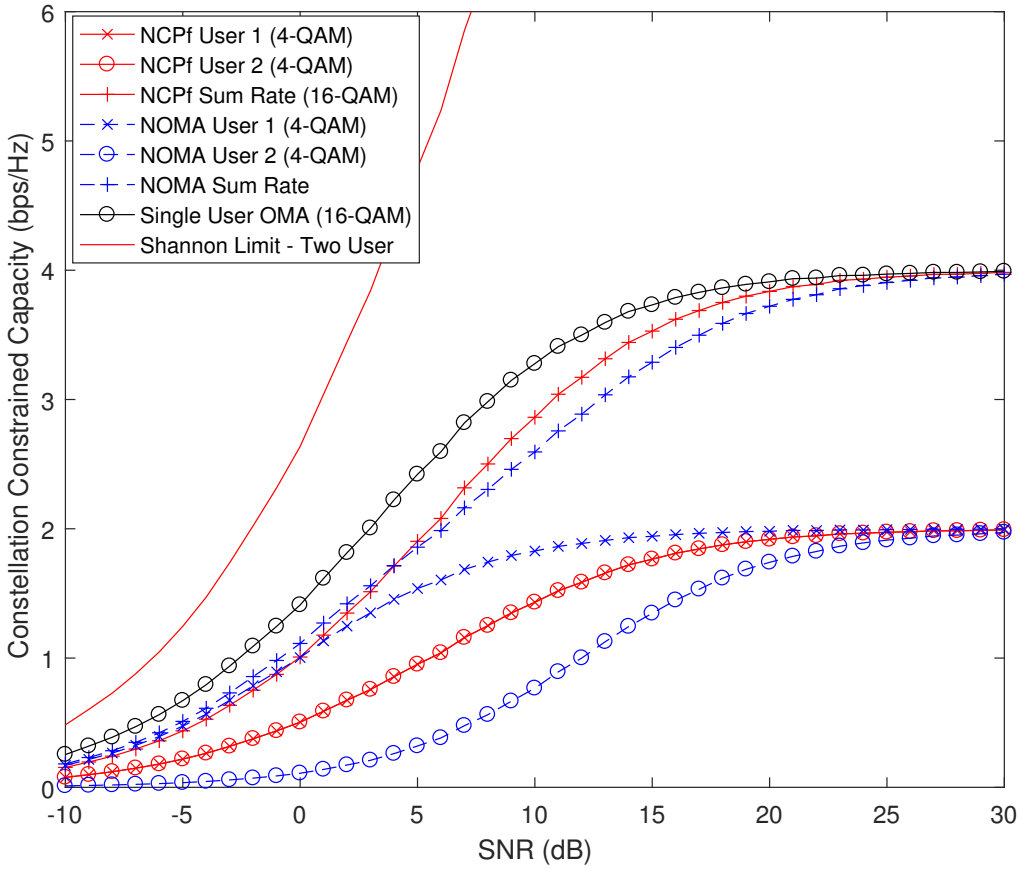

Figure 4.10: 2-user constellation constrained capacity performance for NCPf, compared to OMA and PD-NOMA with the users employing 4-QAM component constellations, respectively. Shannon bound is included for comparison.

Figure 4.11 shows the three-user CCC performance for NCPf, OMA and PD-NOMA with the users employing BPSK component constellations. It can be seen that we achieve 0.3 bps/Hz i.e 30% at 16 dB increase in sum-rate capacity compared to PD-NOMA. Furthermore, poor rates for the weak users can be seen for PD-NOMA which requires significant increase in SNR to achieve full user rate performance.

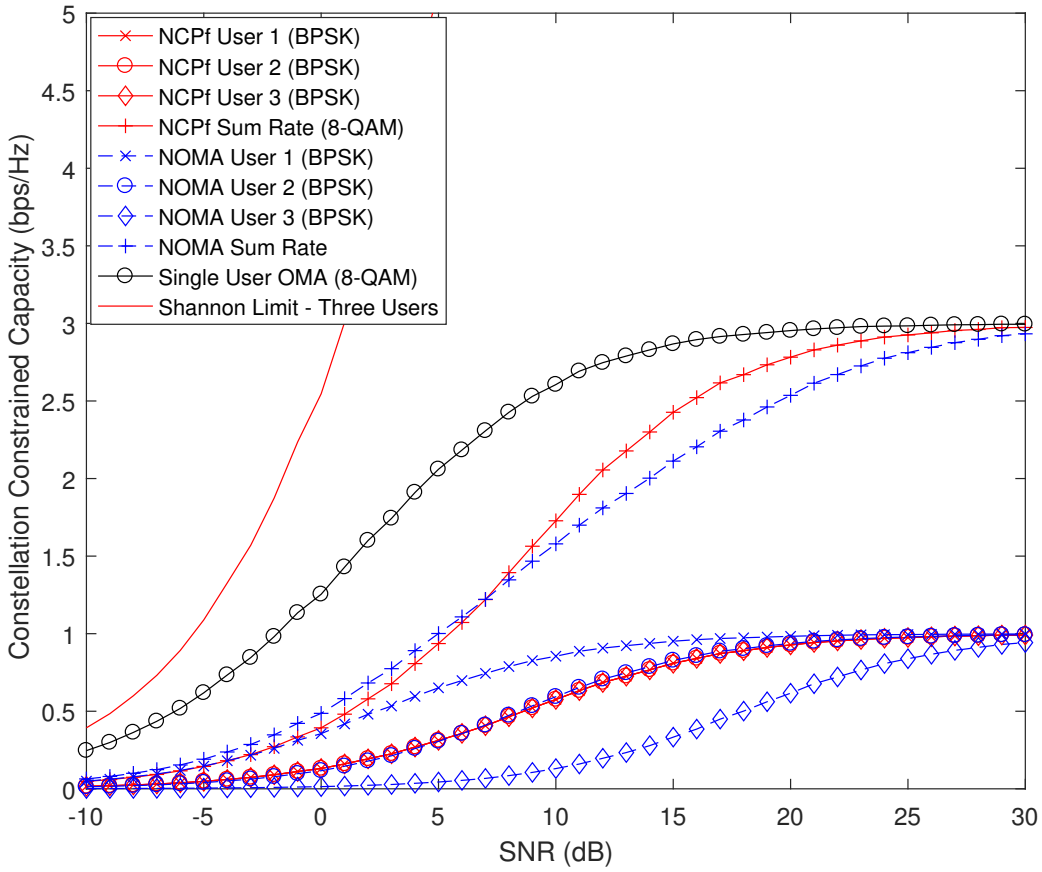

Figure 4.11: 3-user constellation constrained capacity performance for NCPf, compared to OMA and PD-NOMA with the users employing BPSK component constellations,respectively. Shannon bound is included for comparison.

4.5 Conclusion

In this chapter, we introduced a novel downlink NOMA scheme where a preformed multi-user broadcast constellation is designed at the eNB. In the scheme, called downlink NOMA with constellation preforming, the eNB preforms the users signal with power and phase weights prior to transmission. The preforming ensures multi-user interference is eliminated and the spectral efficiency maximized. The preformed composite constellation is broadcasted by the eNB which is received by all users. Subsequently, the users perform non-linear JML detection with the designed constellation to extract their indi-

vidual component signals.

By superposing in the power and phase domains, we achieve improved sum capacity and fairness compared to PD-NOMA employing SIC. This due to SIC large power separation requirements. Compared to the single OMA, we trade-off single user performance for system capacity. This is due to total average power constraint for all users in NCPf, compared to just the one user in OMA utilizing all available eNB power. However, we offset this loss by achieving significant increase in spectral efficiency.

Chapter 5

Downlink Multi-Antenna NOMA with Constellation Preforming

5.1 Introduction

In this chapter, we extend our novel downlink constellation preforming in spatial diversity and MIMO scenarios.

Although Multiple Antenna (MA) systems have been proven to increase system capacity, diversity/reliability and/or rate, it is still an active area of research, especially if the requirements of future generation mobile systems are to be met. Traditionally, the way to increase link capacity is by deploying some form of power control or more antennas (transmit L and/or receive K) where the number of streams that can be supported is $\min\{L, K\}$. This is due to the core principle of MA relying on the spatial channel properties. Furthermore, any excess $K-L$ or $L-K$ antennas can be utilized to achieve transmit and receive diversity gains, respectively . Intuitively, this means that in order to serve 100x spatial multiplexing streams, you need at least 100x transmit and receive an-

tennas, respectively. This however, increases system complexity such as the number of the costly RF chains, overheads, pilots, feedback, energy expenditure, ICI e.t.c. Thus, as our constellation preforming scheme in Chapter 4 combines multiple users into a single stream, we extend it to the MA systems and propose the following:

- First, we utilize additional transmit or receive antennas in Section 5.2 at both eNB or the users, to achieve transmit diversity or receive diversity, respectively. These improve the received signal reliability for our downlink preforming.

- Secondly, we extend the constellation preforming scheme to a MIMO spatial multiplexing with diversity scenario in Section 5.3. The objective is to increase system capacity with as few transmit antennas as possible. Traditionally, MIMO SM requires at least ML transmit antennas. However, for the proposed NCPf Spatial Multiplexing and Diversity scheme, we preform all the ML independent multi-user streams onto just L eNB transmit antennas i.e the l-th eNB antenna is composed of a subset of L independent streams of the M users.

- Finally, we propose a Group Layered MIMO scheme in Section 5.4, where several users are grouped to a particular antenna such that the total system capacity is maximized. Furthermore, the users are grouped according to their received SNR such that the group interferences are kept to a minimum. This is in comparison to the NCPf-SMD where the total antennas are utilized by the same users. This results in trade-off between user throughput in Section 5.3, and system capacity.

5.2 NOMA Constellation Preforming with Spatial Diversity

5.2.1 NOMA Constellation Preforming with Receive Diversity (NCPf-RD) Combining

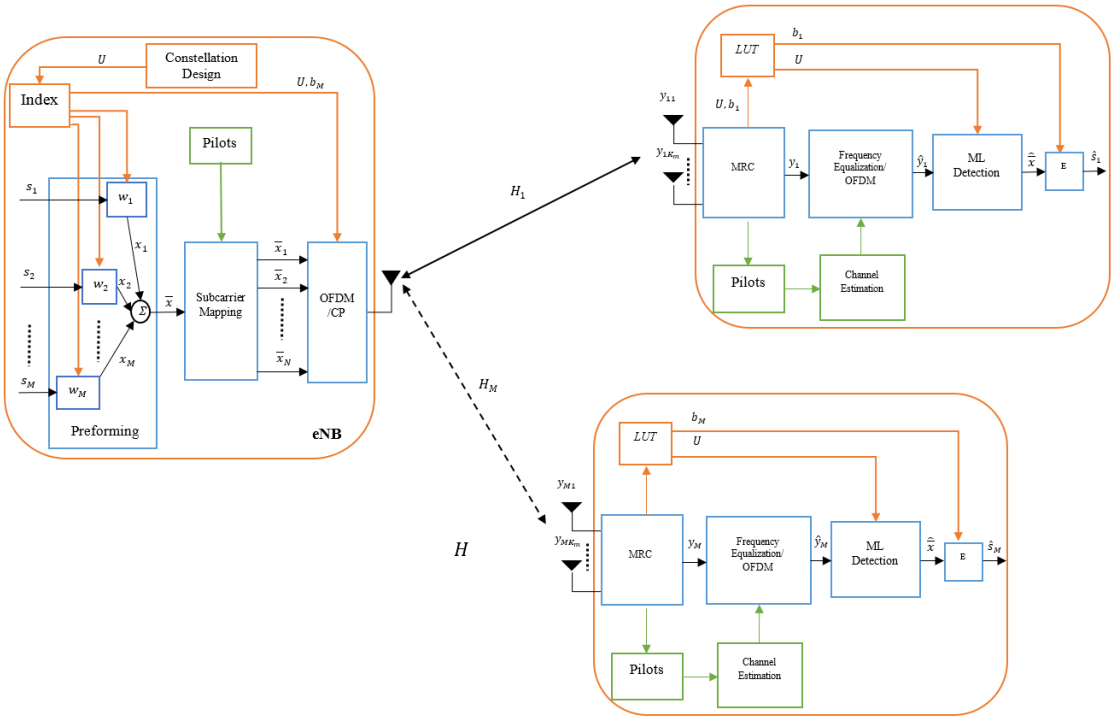

Figure 5.1: System Model of the proposed NOMA Constellation Preforming with Receive Diversity scheme. The figure shows the eNB with a single antenna broadcasting preformed superimposed data to multiple M users equipped with K_m antennas. The channel and noise are also illustrated. It is assummed the eNB transmits on N orthogonal subcarriers.

Consider the case where the eNB employs a single active antenna, and the users equipped with K_m receive antennas, as illustrated in Figure 5.1. The channel from the eNB antenna to each of the receive antennas at the users are assumed to be independent and uncorrelated. The eNB broadcasts the preformed composite constellation which is

received at each of the users receive antennas, expressed as

$$\mathbf{y}_m = \sum_{k=1}^{K_m} \mathbf{h}_{mk} \bar{\mathbf{x}} + \mathbf{z}_{mk} \tag{5.1}$$

where $\mathbf{h}_{mk}$ is the channel from the eNB antenna to the m-th user receive antenna $k \in K_m$, $\bar{\mathbf{x}}$ is the preformed composite signal containing the independent streams of the M users. $\mathbf{z}_{mk}$ is the additive white Gaussian noise at the m-th user antenna k with variance σ^2_{mk}. The users obtain the CSI, perform Maximum Ratio Combing (MRC) and JML detection with the pre-designed constellation $\mathbf{U}$ to recover their respective component signals which can be expressed as

$$\hat{\mathbf{x}} = \arg\left[\min_{\mathbf{U}}(\|\mathbf{y}_m - \mathbf{u}_i \sum_k \mathbf{h}_{mk}\mathbf{h}^*_{mk}\|^2)\right] \quad \forall i \tag{5.2}$$

where $\|\mathbf{y}_m - \mathbf{u}_i \sum_k \mathbf{h}_{mk}\mathbf{h}^*_{mk}\|^2$ is the Euclidean distance between the MRC received signal $\mathbf{y}_m$ and the pre-know composite constellation, normalized by the channel gains $\sum_k |\mathbf{h}_{mk}|^2$. This results in receive diversity gain where the users extract a more reliable received signal $\hat{\mathbf{s}}_m$ from the detected symbol $\hat{\mathbf{x}}$.

5.2.2 NOMA Constellation Preforming with Distributed Transmit Antenna Diversity (NCPf-DTAD)

This section considers the case where the eNB equipped with L geographically distributed transmit antennas, and each user equipped with a single antenna as illustrated in Figure 5.2. The channel from the l-th eNB antenna to the m-th user are assumed to be independent and uncorrelated. By utilizing the channel spectral signatures, we are able to provide improved reliability at the receiver in the form of transmit diversity gain.

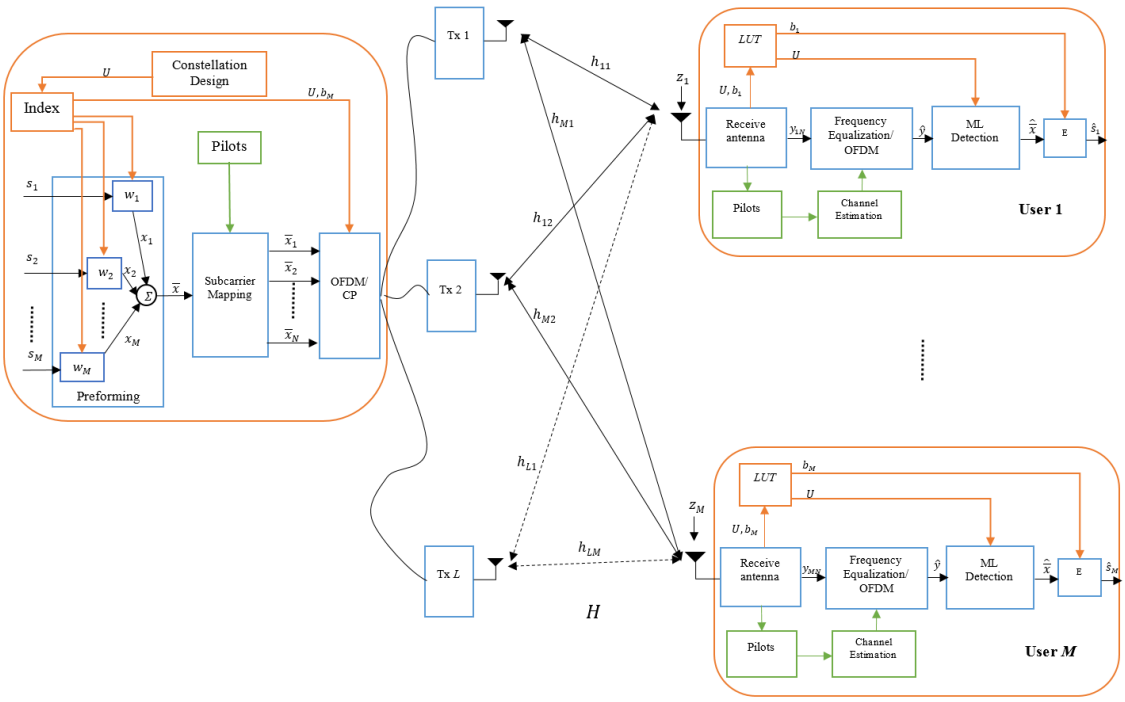

Figure 5.2: System Model of the proposed Constellation Preforming with Distributed Transmit Antenna Diversity. The figure shows the eNB with L antennas broadcasting preformed superimposed data to multiple M users equipped with a single antenna. The channel and noise are also illustrated. It is assummed the eNB transmits on N orthogonal subcarriers.

This is achieved by transmitting the same preformed composite signal on all the L eNB antennas. Thus, the received signal at the user is expressed as

$$\mathbf{y}_m = \sum_{l=1}^{L} \mathbf{h}_{ml} \bar{\mathbf{x}}_l + \mathbf{z}_m \tag{5.3}$$

where $\mathbf{h}_{ml}$ is the channel from the l-th eNB antenna to the m-th user, $\bar{\mathbf{x}}_l$ is the preformed composite signal transmitted from the l-th eNB antenna containing the independent streams of the M users. $\mathbf{z}_m$ is the additive white Gaussian noise at the m-th user with variance σ_m^2. The users estimate the CSI and perform JML detection with the pre-known designed constellation to recover their respective component signals which

can be expressed as

$$\hat{\mathbf{x}} = \arg\left[\min_{\mathbf{U}}(\|\mathbf{y}_m - \mathbf{u}_i \sum_l \mathbf{h}_{ml}\mathbf{h}_{ml}^*\|^2)\right] \quad \forall i \tag{5.4}$$

where $\|\mathbf{y}_m - \mathbf{u}_i \sum_l \mathbf{h}_{ml}\mathbf{h}_{ml}^*\|^2$ is the Euclidean distance between the received signal $\mathbf{y}_m$ and the pre-know composite constellation $\mathbf{U}$, normalized by the respective transmit channels gain $\sum_l |\mathbf{h}_{ml}|^2$. The users then extract their signal $\hat{\mathbf{s}}_m$ from the detected symbol $\hat{\mathbf{x}}$

5.3 MIMO NOMA Constellation Preforming with Spatial Multiplexing and Diversity (NCPf-SMD)

In this section, we consider our novel downlink constellation preforming scheme and apply it in a MIMO scenario. The aim of our MIMO preforming is to enable the multiplexing of multiple users' signals where the number of available transmit antennas is less than the number of component user streams.

5.3.1 Introduction

The key design principle for MIMO NOMA Constellation Preforming with Spatial Multiplexing and Diversity (NCPf-SMD) is to enable spatial multiplexing ML independent multi-user signals on to just L transmit antennas, compared to the required ML transmit antennas in traditional MIMO SM. This is achieved by preforming the users' component streams according to the transmit antennas. The component signals, each with modulation set $\mathbf{Q}_m$, are preformed with the objective that the d_{min} of the superposed composite constellation points are maximized and fully decodable.

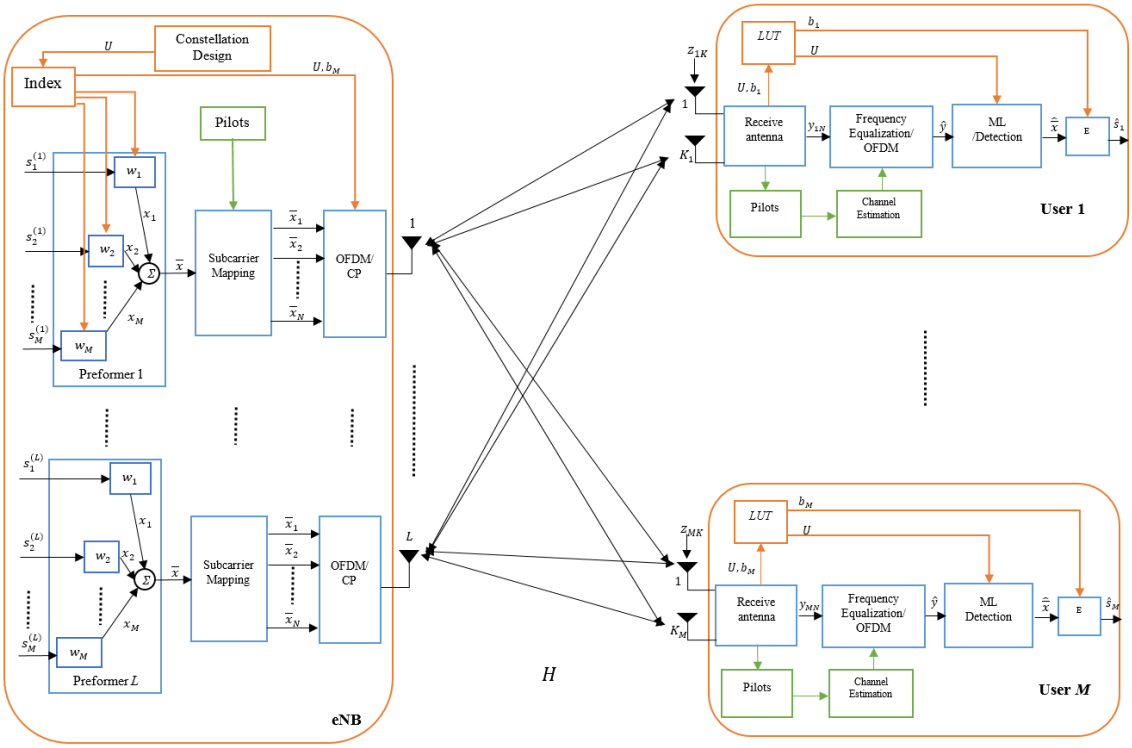

Figure 5.3: System Model of the proposed MIMO NOMA constellation preforming with spatial multiplexing and diversity scheme. The figure shows the eNB with L antennas broadcasting preformed superimposed data to multiple M users equipped with K_m antennas. The channel and noise are also illustrated. It is assumed the eNB transmits on N orthogonal subcarriers.

5.3.2 System Model

Consider a multi-antenna system of M active users each with K_m antennas communicating simultaneously with a eNB equipped with L antennas on N orthogonal subcarriers as illustrated in Figure 5.3. The signal transmitted from each eNB antenna, subject to eNB total power constraint, is a composite signal composed of a set of independent streams from each of the M users. The users employ non-linear JML detection for signal recovery and extraction. The received signal at the users as

$$\mathbf{y}_m = \mathbf{H}_m \bar{\mathbf{x}} + \mathbf{z}_m \tag{5.5}$$

where $\mathbf{y}_m$ is the received signal at the m-th user, $\mathbf{H}_m \in \mathbb{C}^{K_m \times L}$ is the m-th user channel matrix whose entries are assumed to be independent and uncorrelated zero mean unit

variance complex fading coefficients, $\bar{\mathbf{x}} \in \mathbb{C}^{L\times 1}$ is the transmitted signal vector from the L eNB antennas. $\mathbf{z}_m \in {}^{K_m\times 1}$ is zero mean, variance σ_m^2, independent and identically distributed (i.i.d) complex AWGN noise vector of the m-th user. The overall MIMO channel is expressed is thus

$$\mathbf{H} = [\mathbf{H}_1, \ldots, \mathbf{H}_m, \ldots, \mathbf{H}_M]^T \tag{5.6}$$

where $\mathbf{H} \in \mathbb{C}^{K\times L}$ is the channel matrix, with $K = \sum_m K_m$ as the number of total receive antennas.

We employ spatial multiplexing to our MA preforming scheme where M users have L independent streams to transmit on L eNB antennas. Traditionally, this requires at least ML transmit antennas. However, for the proposed NCPf-SMD, we preform all the multi-user streams onto just L eNB transmit antennas i.e the l-th eNB antenna is composed of a subset of L independent streams of the M users.

Let $\mathbf{s}_m = [\mathbf{s}_m^{(1)}, \ldots \mathbf{s}_m^{(l)}, \ldots, \mathbf{s}_m^{(L)}]^T; s_m^{(l)} \in \mathbf{Q}_m$ denote the L input streams of the m-th user, each from modulation set $\mathbf{Q}_m$. Furthermore, let $\mathbf{s}^{(l)} = [\mathbf{s}_1^{(l)}, \ldots, \mathbf{s}_m^{(l)}, \ldots, \mathbf{s}_M^{(l)}]^T$ denote the l-th stream of M users to be preformed for transmission on the l-th eNB antenna, the preformed composite signal at the l-th antenna can then be expressed as

$$\bar{\mathbf{x}}^{(l)} = \sum_{m=1}^{M} \mathbf{w}_m^{(l)} \mathbf{s}_m^{(l)} \qquad \mathbf{s}_m^{(l)} \in \mathbf{s}^{(l)} \tag{5.7}$$

where $\bar{\mathbf{x}}^{(l)}$ is the composite signal of the l-th stream of the M users, $\mathbf{w}_m^{(l)}$ is the preforming weight that maximizes the d_{min} between the constellation points of $\bar{\mathbf{x}}^{(l)}$. Therefore, each symbol $\bar{\mathbf{x}}^{(l)}$ belongs to one of $\mathbf{U}^{(l)}$ possible composite constellation points. The received

signal at the k-th antenna of the m-th user is then defined as

$$\mathbf{y}_{mk} = \sum_{l}^{L} \mathbf{h}_{mk}^{(l)} \bar{\mathbf{x}}^{(l)} + \mathbf{z}_{mk} \qquad k \in K_m \tag{5.8}$$

where $\mathbf{h}_{mk}^{(l)}$ is the channel from the l-th eNB antenna to the k-th receive antenna of the m-th user and $\mathbf{z}_{mk}$ is the additive white Gaussian noise at the m-th user antenna k with variance σ_{mk}^2.

As our MIMO preforming is as any MIMO SM system but with each stream a composite of component signals, we can employ any linear or non-linear detection scheme so long as channel state information and the designed composite constellation $\mathbf{U} = [\mathbf{U}^{(1)} \dots \mathbf{U}^{(l)} \dots \mathbf{U}^{(L)}]^T$ are known at the receiver.

5.3.2.1 Maximum Likelihood Joint Detection and recovery

The nonlinear JML detection for the combined received signals is employed at users. It is optimal in minimizing the error probability by searching for the most likely transmitted signals when compared with the pre-known designed constellation. We define

$$\dot{\mathbf{U}} = \mathbf{U}\mathbf{H}_m \tag{5.9}$$

as the reference composite constellation normalized by the channel. Employing the minimum distance criterion, the estimated signal at the users can be expressed as

$$\hat{\mathbf{x}} = \arg\left[\min_{\mathbf{U}}(\|\mathbf{y}_m - \dot{\mathbf{U}}\|^2)\right] \tag{5.10}$$

where $\|\mathbf{y}_m - \dot{\mathbf{U}}\|^2$ is the distance between the received signal and the possible transmitted vector $\bar{\mathbf{x}}$

5.3.2.2 Zero Forcing ML Detection

The suboptimal linear ZF receiver with ML decoding can be employed at the users to null-out the subsequent interfering composite streams by employing the Moore-Penrose pseudo-inverse of the channel matrix $\mathbf{G}_m = \mathbf{H}_m^{\dagger}$ where $\mathbf{H}_m^{\dagger} = (\mathbf{H}_m^* \mathbf{H}_m)^{-1} \mathbf{H}_m^*$. When $\mathbf{H}_m$ is square and invertible, then the output of a ZF receiver with perfect CSIR is thus given by

$$\begin{aligned} \hat{\mathbf{x}} &= \arg\left[\min_{\mathbf{U}}\left(\left\|\mathbf{G}_m \mathbf{y}_m - \mathbf{U}\right\|^2\right)\right] \\ &= \arg\left[\min_{\mathbf{U}}\left(\left\|\frac{\mathbf{H}_m^* \mathbf{H}_m \bar{\mathbf{x}}}{\mathbf{H}_m^* \mathbf{H}_m} + \frac{\mathbf{H}_m^* \mathbf{H}_m \mathbf{z}_m}{\mathbf{H}_m^* \mathbf{H}_m} - \mathbf{U}\right\|^2\right)\right] \end{aligned} \tag{5.11}$$

where $\hat{\mathbf{x}} \in \mathbb{C}^{L \times 1}$ is the detected signal vector. The joint decoding is decomposes the received signal into L streams which eliminates the MUI. However, this comes at the cost of noise enhancement as the noise term is also inverted in the detection process i.e. $\mathbf{z}_m \mathbf{G}_m$

5.4 MIMO with Group Layered NOMA Constellation Preforming (GL-NCPf)

5.4.1 System Model

Consider the case where the eNB is equipped with L antennas and each user with a single receive antennas. The channels from the l-th eNB antenna to each of the m users are assumed to be independent and uncorrelated. We group the users according to their

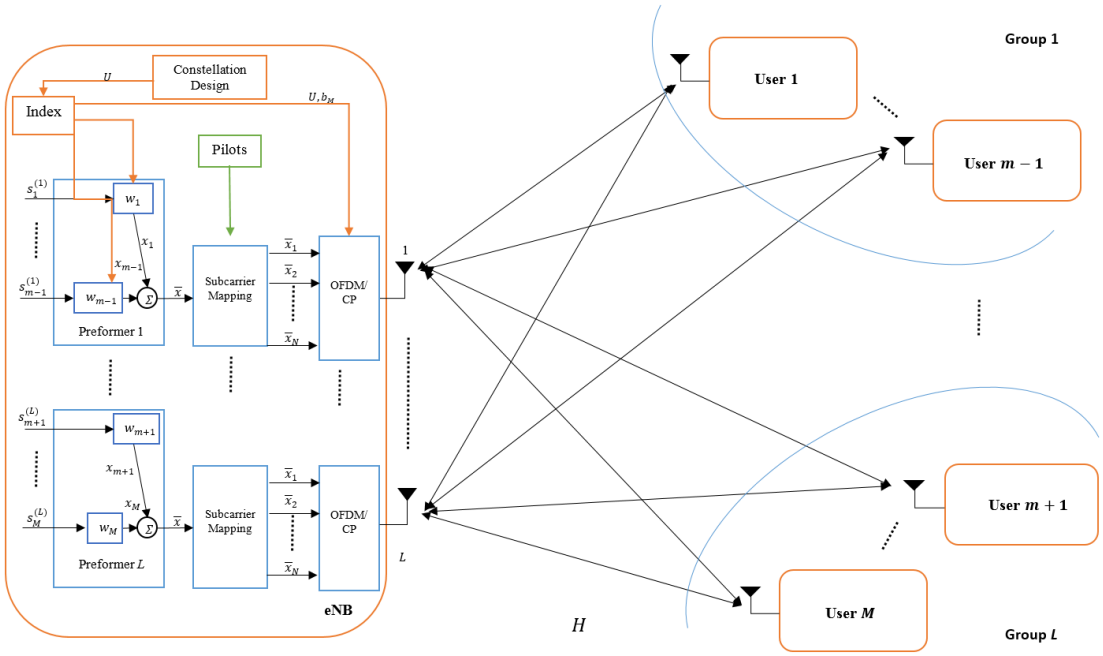

Figure 5.4: System Model of the proposed MIMO with group layered NOMA constellation preforming scheme. The figure shows the eNB with L antennas broadcasting grouped and preformed superimposed data to multiple M users. The channels are also illustrated. It is assumed the eNB transmits on N orthogonal subcarriers.

received SNRs which are assumed to be estimated from the users uplink transmissions.

This is illustrated in Figure 5.4.

Let $\mathbf{s}_m = [\mathbf{s}_1, \ldots \mathbf{s}_m, \ldots, \mathbf{s}_M]^T; s_m \in \mathbf{Q}_m$ denote the user input symbols and $\mathbf{y}_m = [\mathbf{y}_1 \geq \ldots \geq \mathbf{y}_m \geq \ldots \geq \mathbf{y}_M]^T$ the sorted average received SNR, we can then group the users according to L transmit antennas as

$$\begin{aligned} \mathbf{s}_{(l)} &= [\mathbf{s}_1^{(l)}, \ldots, \mathbf{s}_m^{(l)}]^T \\ &\vdots \\ \mathbf{s}_{(L)} &= [\mathbf{s}_{m+1}^{(L)}, \ldots, \mathbf{s}_M^{(L)}]^T \end{aligned} \tag{5.12}$$

where $\mathbf{s}_l$ denotes the l-th stream of the m-th user. The preformed composite signals is

then

$$\begin{aligned} \bar{\mathbf{x}}_{(l)} &= \textstyle\sum_{a=1}^{m} \mathbf{w}_a \mathbf{s}_a \\ &\vdots \\ \bar{\mathbf{x}}_{(L)} &= \textstyle\sum_{b=m+1}^{M} \mathbf{w}_b \mathbf{s}_b \end{aligned} \tag{5.13}$$

where $\bar{\mathbf{x}}_{(l)}$ is the composite signal of the l-th eNB antenna, $\mathbf{w}_{(\bullet)}$ are the preforming weights that maximizes the d_{min} between the constellation points of $\bar{\mathbf{x}}_{(l)}$. Thus, the received signal at the m-th user can be expressed as

$$\mathbf{y}_m = \mathbf{h}_{ml}\bar{\mathbf{x}}_{(l)} + \sum_{g \neq l}^{L} \mathbf{h}_{mg}\bar{\mathbf{x}}_{(g)} + \mathbf{z}_m \tag{5.14}$$

where $\mathbf{h}_{ml}$ is the channel from the l-th eNB antenna to the m-th user and $\sum_{g\neq l}^{L} \mathbf{h}_{mg}$ is interference from other antennas. $\mathbf{z}_m$ is the additive white Gaussian noise at the m-th user with variance σ_m^2. Similar to NCPf-SMD, we can employ any linear or non-linear detection scheme so long as channel state information and the respective designed composite constellations $\mathbf{U}$ are known at the receiver.

5.4.2 Maximum Likelihood Joint Detection with Interference Suppression

At the receiver, the users not only receive the desired signals, but also receive the interfering signal meant for other user groups. However, so long as the transmission to other user groups employ the same modulation sets, the users can employ the same reference constellation to solve the JML problem, suppressing the interference. This requires CSI knowledge of the the relevant channels at the receiver which are assumed to be estimated from orthogonal uplink pilots. We define the reference constellation with respect

to the channels as

$$\dot{\mathbf{U}}^{(l)} = \mathbf{U}^{(l)}\mathbf{h}_{ml} + \sum_{g\neq l}^{L} \mathbf{h}_{mg} \tag{5.15}$$

where the first term in Equation (5.15) is the desired composite signal, the second term the interfering composite signal, and $\dot{\mathbf{U}}^{(l)}$ as the reference constellation vector. Employing the minimum distance criterion, the estimated signal at the users can be expressed as

$$\hat{\mathbf{x}}_{(l)} = \arg\left[\min_{\dot{\mathbf{U}}}(\|\mathbf{y}_m - \mathbf{u}_i^{(l)}\|^2)\right]; \quad \forall \mathbf{u}_i^{(l)}, \forall l \tag{5.16}$$

where $\|\mathbf{y}_m - \mathbf{u}_i^{(l)}\|^2$ is the distance between the received signal $\mathbf{y}_m$ and the i-th possible composite constellation point $\mathbf{u}_i^{(l)} \in \dot{\mathbf{U}}^{(l)}$.

5.5 Performance Analysis

5.5.1 NOMA Constellation Preforming with Spatial Diversity

5.5.1.1 NCPf-RD

Consider the case where the user is equipped with K antennas, and the eNB transmitting on a single antenna. The users perform maximum ratio combination from all K_m antennas which maximizes the output SNR by performing the sum of SNR at each receive antenna. Thus, the expected value of the SNR is K_m times the average SNR at each antenna given by

$$\mathbb{E}(\gamma_m) = K_m \lambda_m \tag{5.17}$$

where γ_m is the instantaneous SNR, defined as

$$\gamma_m = \frac{\lambda_m}{2}\Gamma; \quad \Gamma = 2\sum_{k=1}^{K_m} |h_{mk}|^2 \bar{\mathbf{x}}_k \tag{5.18}$$

Thus, the system capacity for can be expressed as

$$C_{|\text{NCPf-RD}} = \mathbb{E}\left[\sum_{m=1}^{M} \log_2\left(1 + \frac{\lambda_m}{2} 2 \sum_{k}^{K_m} |h_{mk}|^2 \bar{\mathbf{x}}_k\right)\right] \tag{5.19}$$

It is well known that the sum of X independent random variables is the convolution of individual Probability Density Function (PDF) and the convolution of two functions is equivalent to multiplying the functions in frequency (Laplace) domain. Furthermore, the characteristic function of X is the Laplace transform of the PDF given by $\mathbb{E}[e^{-sX}]$. Thus, we can determine the PDF of the output SNR as

$$F_{\lambda_k}(s) = \mathbb{E}[e^{-s\gamma_k}] = \frac{1}{1+s\lambda} \tag{5.20}$$

$$F_{\lambda}(s) = \left[\frac{1}{1+s\lambda}\right]^{K_m} \tag{5.21}$$

$$\text{PDF}(\gamma) = f_{\lambda}(\gamma) = \ell^{-1} F_{\lambda}(s) = \frac{1}{2\pi j} \int_{c-j\infty}^{c+j\infty} \frac{e^{s\gamma}}{(1+s\lambda)^{K_m}} d\gamma \tag{5.22}$$

$$= \frac{1}{(K_m-1)!} \frac{\gamma^{K_m-1}}{\lambda^{K_m}} e^{-\gamma/\lambda} \tag{5.23}$$

where ℓ^{-1} denotes the inverse Laplace transform. We can then derive the BER from Equation (5.23) and Equation (4.6) as

$$P_{e|\text{NCPf-RD}} \approx \int_0^{\infty} (P_e^{DL}/\gamma) f_{\lambda}(\gamma) d\gamma = \int_0^{\infty} P_e^{DL} \frac{1}{(K_m-1)!} \frac{\gamma^{K_m-1}}{\lambda^{K_m}} e^{-\gamma/\lambda} d\gamma \tag{5.24}$$

$$\simeq \begin{bmatrix} 2K_m - 1 \\ K_m \end{bmatrix} (P_e^{DL})^{K_m} \tag{5.25}$$

5.5.1.2 NCPf-DTAD

For NCPf-DTAD, where the eNB is equipped with L distributed antennas, and a single antenna at each of the M users. The instantaneous SNR γ_m can be defined as

$$\gamma_m = \frac{\lambda_m}{2L}\Gamma; \quad \Gamma = 2\sum_{l}^{L} |h_{ml}|^2 \bar{\mathbf{x}}^{(l)} \tag{5.26}$$

The average SNR, $\mathbb{E}[\gamma_m] = \lambda_m$, is as a point-to-point system with a single transmit antenna. However, due to the independent channels from each of the transmitters, the PDF of the signal is different for different number of antennas. Furthermore, as the fading on each channel is independent, Γ, has a chi-squared distribution χ^2_{2L}. Thus, the diversity is related to PDF of γ. Diversity gain is then achieved as the PDF of γ_m tends towards its average value as the order $2L$ of the chi-distribution increases, increasing signal reliability at the receiver. Consequently, the capacity of the system can be defined as

$$C_{|\text{NCPf-DTAD}} = \mathbb{E}\left[\sum_{m=1}^{M} \log_2\left(1 + \frac{\lambda_m}{2L} 2\sum_{l}^{L} |h_{ml}|^2 \bar{\mathbf{x}}^{(l)}\right)\right] \tag{5.27}$$

5.5.2 NCPf-SMD

The sum rate capacity for each user in MIMO NCPf-SMD can be derived as the maximum possible mutual information between the input $\mathbf{X}$ and output $\mathbf{Y}$ given as

$$\mathrm{C} = \max_{f_{\mathbf{X}}(x)} I(\mathbf{X}|\mathbf{Y}) = \max_{f_{\mathbf{X}}(x)} [H(\mathbf{Y}) - H(\mathbf{Y}|\mathbf{X})] \tag{5.28}$$

where $H(\mathbf{Y}|\mathbf{X})$ is the entropy in $\mathbf{X}$ with PDF $f_{\mathbf{X}}(x)$. Thus, assuming the channel $\mathbf{H}$ is known at the receiver, the entropy in $\mathbf{Y}$ with respect to input $\mathbf{X}$ is wholly determined by

the additive noise $\mathbf{Z}$ with variance σ^2, expressed as

$$H(\mathbf{Y}|\mathbf{X}) = K_m \log_2(\pi e \sigma^2) = \log_2(\pi e \sigma^2)^{K_m} \tag{5.29}$$

Given the channel, the entropy in $\mathbf{Y}$ is determined by the distribution of $\mathbf{X}$, where $\mathbf{X} \sim \aleph(0, \sum_{\mathbf{x}})$ is Gaussian distributed and $\sum_{\mathbf{x}}$ is the covariance matrix of $\mathbf{X}$. Consequently, $\mathbf{Y}$ is also Gaussian distributed with $\mathbf{Y} \sim \aleph(0, \sum_{\mathbf{y}})$ where $\sum_{\mathbf{y}} = \sigma^2 \mathrm{I}_{K_m} + \mathbf{H} \sum_{\mathbf{y}} \mathbf{H}^*$ and I_{K_m} is the $K_m \times K_m$ identity matrix. Employing the entropy for Gaussian PDF

$$H(\mathbf{Y}) = \log_2 \left[(\pi e)^{K_m} \det \sum\nolimits_{\mathbf{y}} \right] \tag{5.30}$$

we can derive the user capacity as

$$C_m = \max_{f_{\mathbf{X}}(x)} I(\mathbf{X}|\mathbf{Y}) = \log_2 \left[(\pi e)^{K_m} \det(\sigma^2 \mathrm{I}_{K_m} + \mathbf{H} \sum\nolimits_{\mathbf{x}} \mathbf{H}^*) - \log_2(\pi e \sigma^2)^{K_m} \right] \tag{5.31}$$

$$= \log_2 \det \left(\mathrm{I}_{K_m} + \frac{1}{\sigma^2} \mathbf{H} \sum\nolimits_{\mathbf{x}} \mathbf{H}^* \right) \tag{5.32}$$

By eigen-decomposition of the input covariance matrix $\sum_{\mathrm{x}} = (\mathbf{P}/K_m)\mathrm{I}_{K_m}$, where $\mathbf{P} = \sum_l |\bar{\mathbf{x}}^{(l)}|^2$, the optimal covariance matrix can be shown as $\sum_{\mathrm{x}} = \mathbf{P}/K_m \sigma^2 \mathbf{H}\mathbf{H}^*$. Thus, we can derive the sum rate capacity as

$$C_{|\text{NCPf-SMD}} = \sum_{m=1}^{M} \log_2 \det \left(\mathrm{I}_{K_m} + \frac{\mathbf{P}}{\sigma^2} \mathbf{H}_m \mathbf{H}_m^* \right) \tag{5.33}$$

5.5.3 GL-NCPf

In GL-NCPf, as the user groups are served with a single respective antenna, the channel decomposes to a MISO system with co-channel interference; No interference from users

in the same group, but from other groups.

Let $\mathbf{R}_I = \mathbb{E}[\bar{\mathbf{x}}_{(g)}\bar{\mathbf{x}}^*_{(g)}]$ denote the interference covariance matrix, the optimal weight is then $\mathbf{w} = \mathbf{R}_I^{-1}\mathbf{h}_{ml}$. Accounting for additive white noise, the interference covariance matrix can be rewritten as

$$\mathbf{R}_I = \sum_{g \neq l}^{L} \mathbf{h}_{mg}\mathbf{h}^*_{mg} + \sigma_m \tag{5.34}$$

where σ_m is the noise variance at the user. Thus, the instantaneous signal-to-interference-plus-noise ratio is then defined by

$$\gamma_m = \frac{|\mathbf{w}^*\mathbf{h}_{ml}|^2}{\mathbb{E}[\mathbf{w}^*\bar{\mathbf{x}}_{(g)}\bar{\mathbf{x}}^*_{(g)}\mathbf{w}]} = \frac{|\mathbf{w}^*\mathbf{h}_{ml}|^2}{\mathbf{w}^*\mathbf{R}_I\mathbf{w}} = \frac{|\mathbf{h}^*_{ml}\mathbf{R}_I^{-1}\mathbf{h}_{ml}|^2}{\mathbf{h}^*_{ml}\mathbf{R}_I^{-1}\mathbf{R}_I\mathbf{R}_I^{-1}\mathbf{h}_{ml}} = \mathbf{h}^*_{ml}\mathbf{R}_I^{-1}\mathbf{h}_{ml} \tag{5.35}$$

Defining the covariance matrix of the desired signal as $\mathbb{Q}_{ml} = \mathbf{h}^*_{ml}\mathbf{h}_{ml}$, the characteristic function $\Psi(s) = \mathbb{E}[e^{-s\gamma}]$ of γ_m can be defined as

$$\mathbb{E}[e^{-s\gamma}] = \frac{1}{\pi\mathbb{Q}_{ml}} \int_{\mathbf{h}_m l} \exp[-\mathbf{h}^*_{ml}\mathbb{Q}^{-1}_{ml}\mathbf{h}_{ml} - s\gamma_m]\delta\mathbf{h}_{ml} \tag{5.36}$$

Accounting for the interference, Equation (5.36) can be rewritten as

$$\mathbb{E}[e^{-s\gamma}] = \frac{1}{\pi\mathbb{Q}_{ml}} \int_{\mathbf{h}_{ml}} \exp[-\mathbf{h}^*_{ml}(\mathbb{Q}^{-1}_{ml} + s\mathbf{R}_I^{-1})\mathbf{h}_{ml}]\delta\mathbf{h}_{ml} \tag{5.37}$$

Thus, the final integral can be solved as

$$\int_{\mathbf{h}_m l} \exp[-\mathbf{h}^*_{ml}(\mathbb{Q}^{-1}_{ml} + s\mathbf{R}_I^{-1})\mathbf{h}_{ml}]\delta\mathbf{h}_{ml} = \pi(\mathbb{Q}^{-1}_{ml} + s\mathbf{R}_I^{-1})^{-1} \Rightarrow \mathbb{E}\left[\frac{1}{1 + s\mathbb{Q}_{ml}\mathbf{R}_I^{-1}}\right] \tag{5.38}$$

Using the expectation in Equation (5.38), we can express the system capacity as

$$C_{|\text{GL-NCPf}} = \sum_{m=1}^{M} \log_2 \left(1 + \frac{\mathbf{P}}{\sigma^2} \mathbb{Q}_{ml} \mathbf{R}_I^{-1}\right) \tag{5.39}$$

5.6 Simulation Modelling and Results

5.6.1 Simulation Models

5.6.1.1 NCPf-RD and NCPf-DTAD

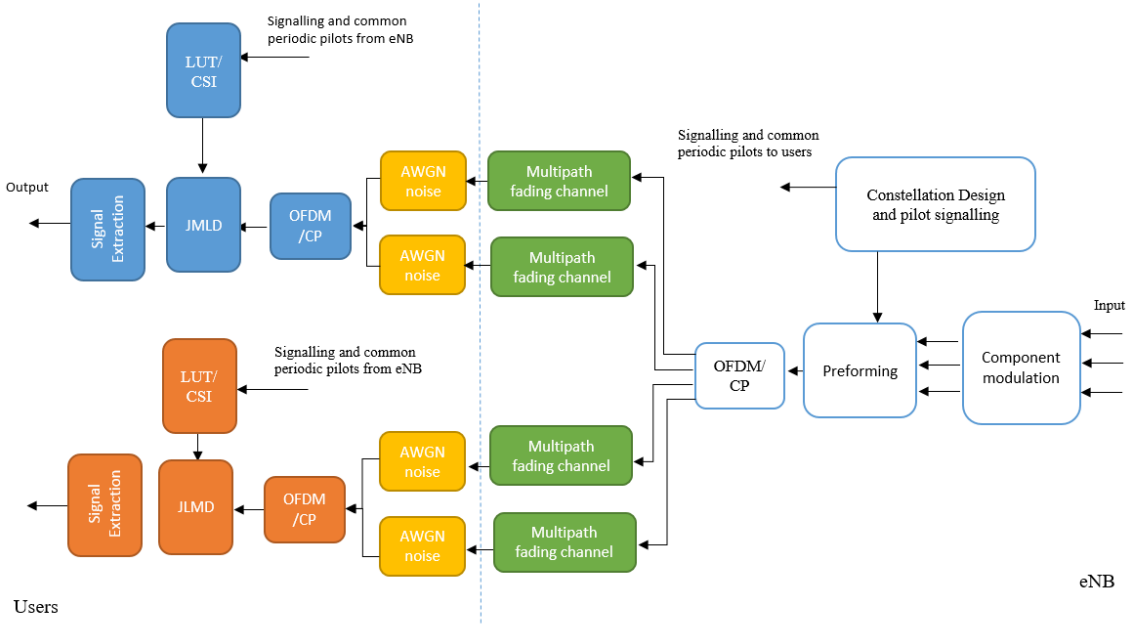

Figure 5.5: NCPf-RD simulation Model

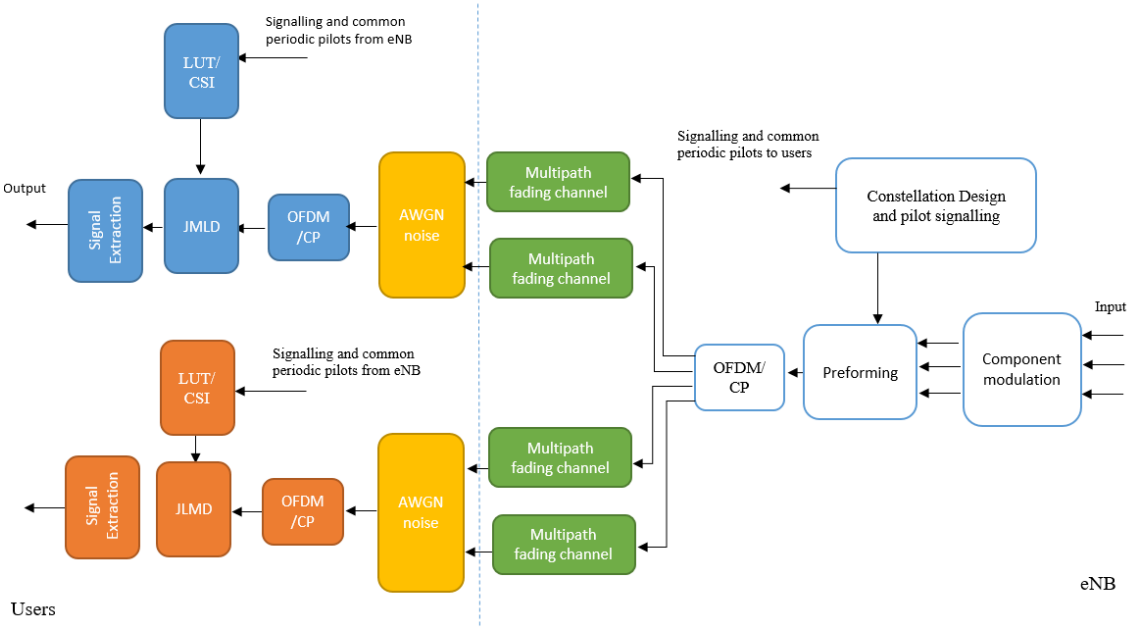

Figure 5.6: NCPf-DTAD simulation Model

A Monte-Carlo simulation is carried out in MATLAB to compare the performance of our proposed schemes. For simplicity, two users are considered. For NCPf-RD as illustrated in Figure 5.5, the user input streams are first modulated with the component modulation to be simulated. The symbols for each user are then mapped to N RE. The users signal on the n-th RE are then preformed, such that each subcarrier is composed of the M user signals. Next IFFT and CP are employed. The signals are then transmitted in to a multipath fading channel. The signals are received by the users, each equipped with K_m antennas. The users perform receive diversity combining and ML detection with the designed constellation as reference. It is assumed that the users have full channel state information. For NCPf-DTAD, the all the steps in NCPf-RD before transmission are employed. However as illustrated in Figure 5.6, the same OFDM signal is transmitted on L eNB antenna. Furthermore, the users are equipped with a single antenna, where they perform CSI and employ ML detection with the reference constellation. For the two schemes, AWGN noise is applied at the respective receivers.

The system performance is evaluated in terms of BER and capacity bounds over thousands of symbols. We compare our proposed scheme with conventional OMA and PD-NOMA schemes.

5.6.1.2 NCPf-SMD

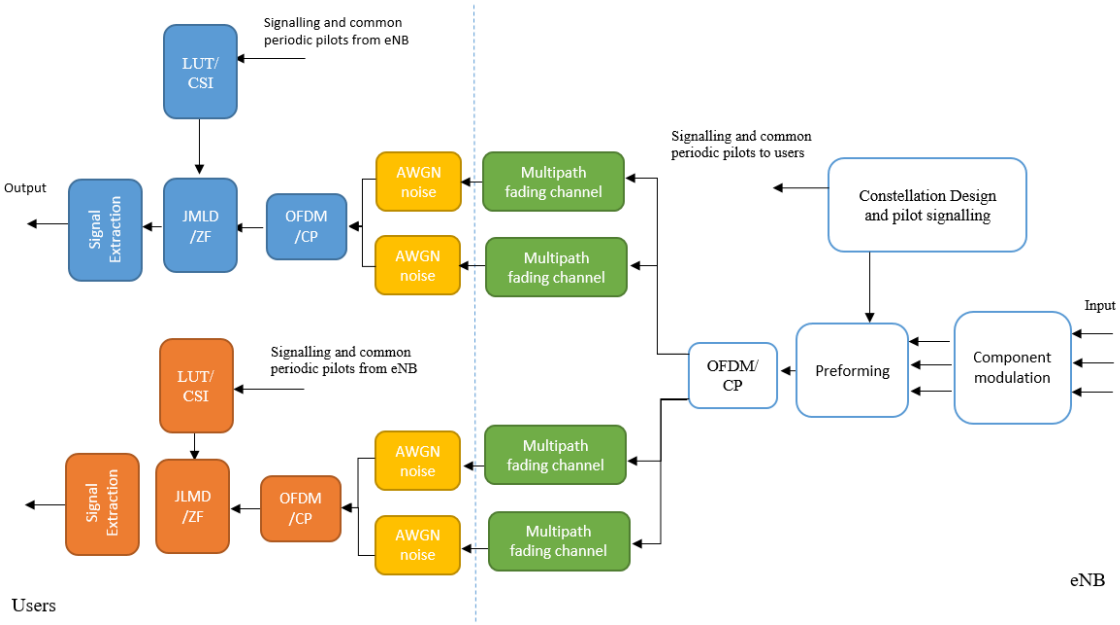

Figure 5.7: NCPf-SMD simulation Model

A Monte-Carlo simulation is carried out in MATLAB to compare the performance of our proposed scheme. For simplicity, a two user system is considered as illustrated in Figure 5.7. It is assumed that each of the user has two streams to transmit. The first stream of the two users are modulated with the component modulation to be simulated, and assigned to the first transmit antenna chain. The second streams are also modulated with the component modulation to be investigated, and applied to the second transmit antenna chain. The symbols for each chain are then mapped to N RE. The users signal on the n-th RE are then preformed, such that each subcarrier is composed of the M user signals. Next we employ IFFT and CP. The signals are then transmitted in to a 2x4 MIMO multipath fading channel, with AWGN noise applied at each receiver. The signals are

received by the users who user perform ML detection with the designed constellation as reference to receiver their two independent streams. It is assumed that the users have full channel state information. The system performance is evaluated in terms of capacity bounds over thousands of symbols. We compare our proposed scheme with conventional OMA, 2x2 MIMO SM and PD-NOMA schemes.

5.6.1.3 GL-NCPf

A Monte-Carlo simulation is carried out in MATLAB to compare the performance of our proposed scheme. For simplicity, a 4 user system is considered. Two users are grouped to transmit on the first transmit antenna, the other two on the second. The symbols to be transmitted on each chain are then mapped to N RE. The users signal on the n-th RE are then preformed, such that each subcarrier is composed of the user signals. Next we employ IFFT and CP on each chain. The signals are then transmitted in to a 2x4 MIMO multipath fading channel, with AWGN noise applied at each receiver. The signals are received by the users who user perform ML detection with the designed constellation as reference to receiver their two independent streams. It is assumed that the users have full channel state information. The system performance is evaluated in terms of capacity bounds over thousands of symbols. We compare our proposed scheme with conventional OMA, 4x4 MIMO SM and PD-NOMA schemes.

5.6.2 Results

5.6.2.1 NCPf-RD and NCPf-DTAD

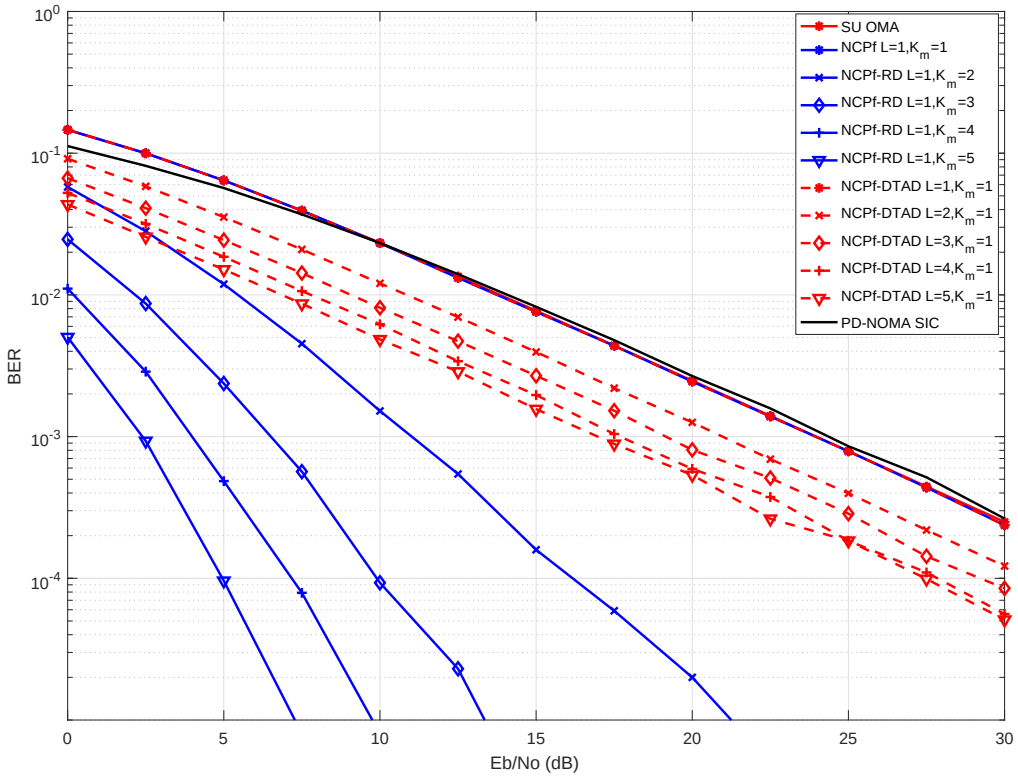

Figure 5.8: Average BER vs Eb/No performance of 2-user NCPf-RD and NCPf-DTAD scheme compared to single user OMA and 2-user PD-NOMA employing SIC.

By utilizing the available transmit and/or receive antennas, we could improve performance and achieve transmit and/or receive diversity gain. It can be seen in Figure 5.8 that we achieve transmit diversity gain for NCPf-DTAD of 3 dB, 5 dB, 6.32 dB and 7.04 dB for $K_m = 1$ and $L = 2, 3, 4$ and 5, respectively. When the eNB is transmitting on a single antenna, to a user equipped with multiple receive antennas in NCPf-RD, we achieve 13 dB, 17.5 dB, 20 dB and 21.5 dB receive diversity gain for $K_m = 2, 3, 4$ and 5, respectively.

Figure 5.9 shows 2-user shannon channel capacity performance for NCPf-RD. It can be seen that the capacity, as a function of K_m, is higher for the strong user compared

to the weak user. Furthermore, the capacities of the strong and weaker users are higher and lower, respectively, than the capacities if NOMA channel-dependent ordering is not employed. As an example, at SNR 10 db, we achieve about 0.3 bps/Hz gain and 0.4 loss in capacity for $K_m = 2, 3, 4, 5$ at 10 dB compared to non-ordered channels.

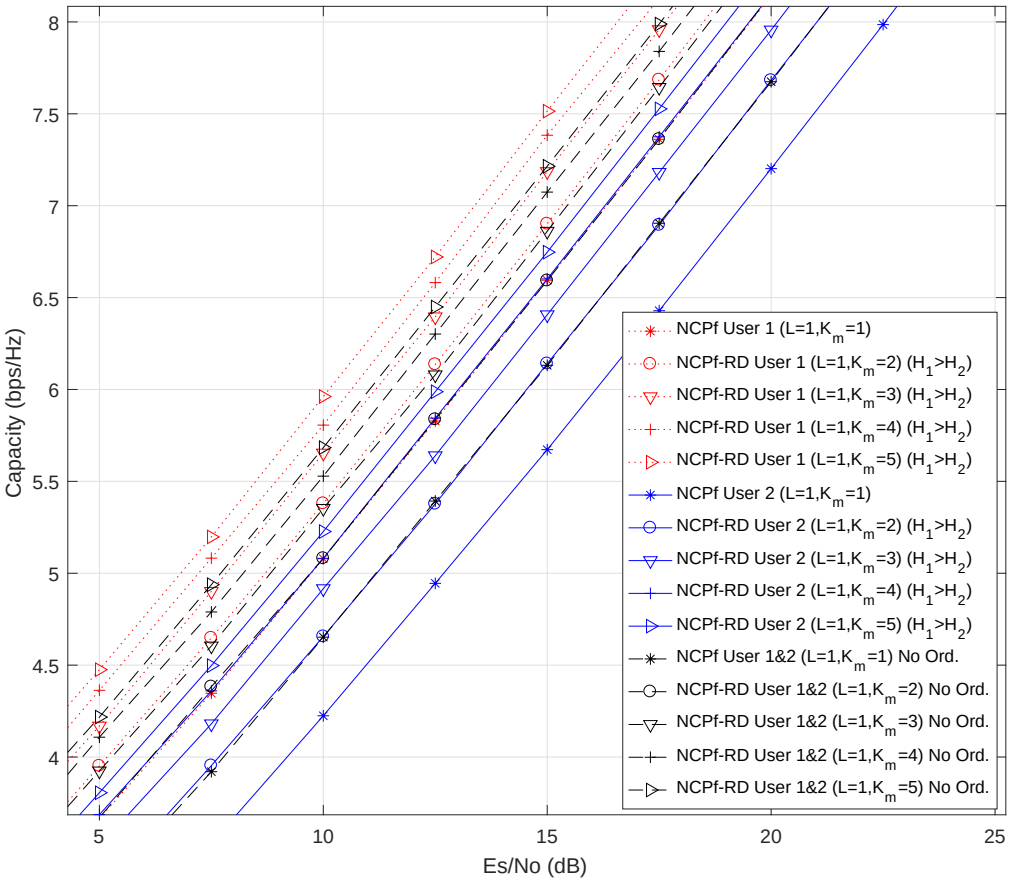

Figure 5.9: 2-user Shannon capacity performance for NCPf-RD.

Similarly, Figure 5.10 shows 2-user capacity performance for NCPf-DTAD. It can be seen that the capacity as a function of L is higher for the strong user compared to the weak user. As an example, at SNR 10 db, we achieve about 0.28 bps/Hz gain and 0.42 loss in capacity for $L = 2, 3, 4, 5$ at 10 dB compared to non-ordered channels. However, we achieve higher capacities for NCPf-RD compared to NCPf-DTAD. This is due to MRC employed in NCPf-RD.

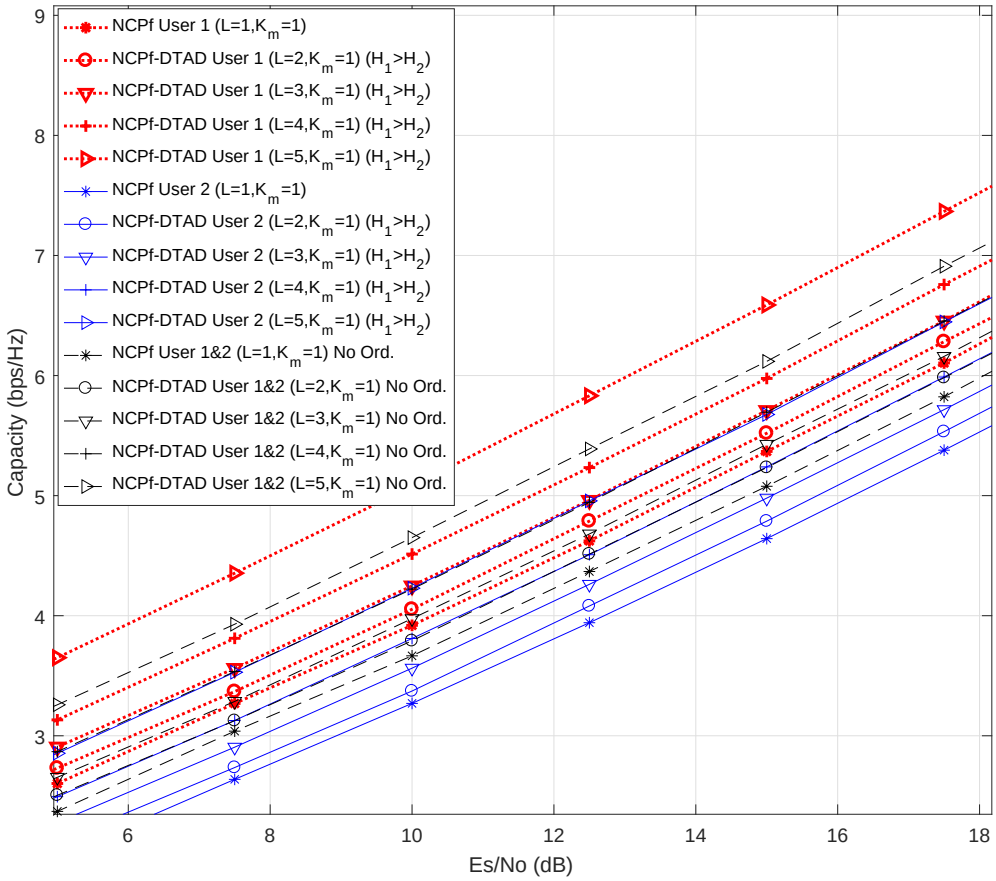

Figure 5.10: 2-user Shannon capacity performance for NCPf-DTAD.

5.6.2.2 NCPf-SMD and GL-NCPf

Due to 2x4 MIMO NCPf-SMD being a 2x2 MIMO from the users perspective, we achieve the BER performance as a 2x2 MIMO SM with ML detection at the receiver. However, as we preform each the two users streams to a single transmit antenna, we achieve twice the spectral efficiency with only 2 transmit antennas, compared to the 2x2 MIMO SM scheme. To achieve roughly the same rate with NCPf-SMD with all users employing the same component modulations, a MIMO SM scheme needs a 4x4 array with CSIT&R.

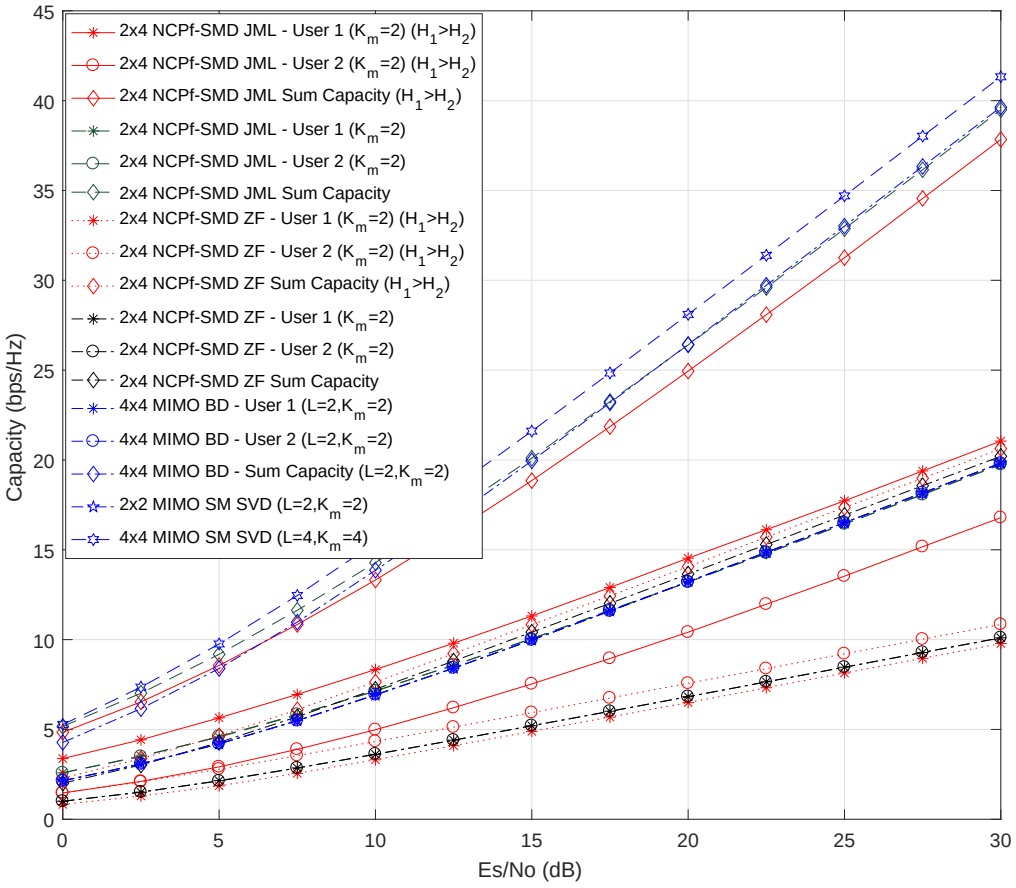

Figure 5.11: 2-user Shannon capacity performance for NCPf-SMD, compared to MIMO SM employing SVD and BD.

Figure 5.11 shows the shannon channel capacity performance for NCPf-SMD with ML and ZF detections, compared to 2x2 MIMO SM SVD, 4x4 MIMO SM SVD and 4x4 MIMO SM BD precoding, respectively. The comparisons are assumed to have perfect CSIT&R. It can be seen at 20 dB, we get 7.7 bps/Hz and 2.8 bps/Hz increase in capacity, and 10.9 bps/Hz in sum capacity, for the strong user NCPf-SMD user employing JML, compared with the user employing ZF. For the weak user employing JML, we achieve 12.8 bps/Hz increase compared to ZF detection. This is due to the loss in diversity gain and noise enhancement for ZF. However there is a slight decrease in capacity of 1.4 bps/Hz compared to non-channel ordered NCPf-SMD and MIMO SM with BD precoding.

The 4x4 MIMO SM SVD bound is illustrated for comparison.

For GL-NCPf, we trade-off diversity for spectral efficiency as illustrated in Figure 5.12. This allows more users to be accommodated with the same number transmit antennas in NCPf-SMD. It can be seen that at low SNR, we achieve almost the same performance with the 4x4 MIMO upper bound. Furthermore, by grouping the users according to their channel gains, we minimize the inter-group interference with only a small loss in spectral efficiency. This can be seen at SNR of 30 dB were we loose only 1.9 bps/Hz in spectral efficiency. However, this is well compensated with the fact that only two transmit antennas are employed compared to 4x4 array.

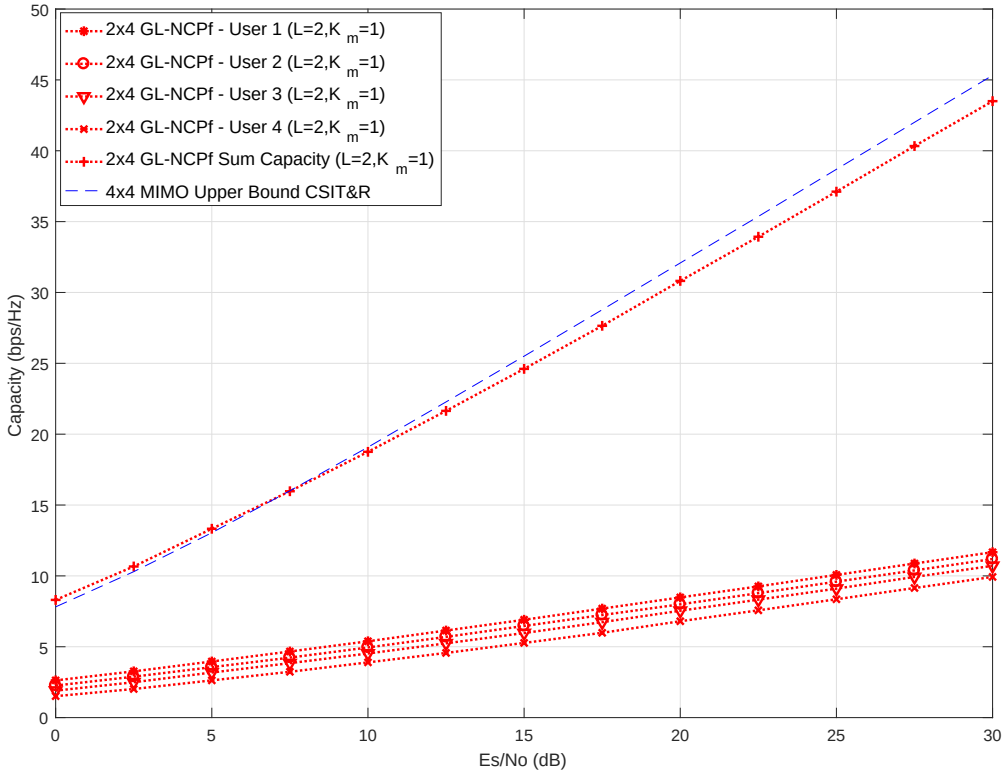

Figure 5.12: 4-user Shannon capacity performance for GL-NCPf, compared to 4x4 MIMO with CSIT&R upper bound

5.7 Conclusion

In this chapter, we apply our novel downlink constellation preforming in two spatial diversity and MIMO scenarios. In the first spatial diversity scheme, we utilize the available antennas at the users to achieve receive diversity gain. Furthermore, we employ our signal preforming in a distribute transmit antenna scenario were we also utilize the independent channel signatures to achieve transmit diversity.

We extended the constellation preforming to two MIMO scenarios. The first MIMO scheme, each eNB antenna transmits a preformed composite signal composed of a set of multiple users streams. This achieves spatial multiplexing with diversity with less transmit antennas, reducing the number of transmit antennas needed for spatial multiplexing, while still maximizing the sum rate. In the second MIMO scheme, a highly spectrally efficient MIMO preforming scheme was proposed where the eNB preforms to a specific group of users on each transmit antenna. This trades-off diversity for maximum system capacity. In all the schemes, the users perform JML detection to recover their signals. Furthermore, by grouping the users according to their received signal-to-noise ratios, we minimize inter-group interference.

Chapter 6

Coordinated Multipoint (CoMP) NOMA with Joint Constellation Processing (CoMP-JCP)

6.1 Introduction

The core principle of our constellation design proposed in chapters 3 and 4 enables simultaneous channel access, achieved by combining multiple users' component signals into a single and uniquely decodable composite constellation. Consequently, the multiple access interference is eliminated; Specifically, the Co-Channel Interference (CCI) since the users are typically located in the same cell coordinated by a central eNB. However, users located near the cell-edge of the primary eNB typically suffer from inter-cell-interference, degrading performance.

Coordinated Multipoint (CoMP) was introduced in LTE Rel.9 to solve the interference problem. This was achieved by either coordinating the primary and interfering cell

to improve the received signal power, or scheduling and/or beamforming to minimize the interference, respectively. However, increasing capacity for a SU-MIMO in CoMP requires not only additional receive antennas at the user, but also at all coordinating eNBs. This results in degraded system performance where the other antennas could have been employed to serve other users.

This chapter introduces a novel NOMA precoding scheme in CoMP which aims to exploit the extra degrees of freedom provided by CoMP systems. The objective is to utilize the CCI to not only eliminate the CCI, but increase cell-edge user capacity. This is achieved by employing our signal design principles such that the independent streams for the user are simultaneously transmitted from multiple Coordinating eNB (CeNB) and received on a single antenna at the user, significantly reducing the number of required antennas for SM.

The proposed scheme is particularly useful in ultra-dense small cell deployments where the close cell proximities result in high CCI; inter-cell distances are insufficient for power law to have any big effect, which results in high power cell-edge interferences. Because of this, we evaluate our scheme in a Femto-cell deployment. Although we employ our constellation design in CoMP and femto-cells, it can be employed in any MISO system.

The contributions of this chapter are as follows:

- The robustness of the constellation design is shown in CoMP, where performance of SU-MIMO spatial multiplexing is a problem. The scheme, called CoMP with Joint Constellation Processing (CoMP-JCP), the additional degrees of freedom, in form of interfering eNBs, are utilized to enable spatial multiplexing to a user with a single receive antenna. This is achieved by precoding each stream from the CeNB

with designed weights signalled by a central eNB. Consequently, the inter-cell interference is eliminated as well as the number of antennas required. Furthermore, due to the power gain achieved by the composite constellation, the sum-rate is maximized compared to single user point-to-point and MIMO schemes employing the same component constellations.

- An active cell selection scheme, called CoMP-JCP-ACS is proposed where the precoding is employed on the highest interferers to the user. This technique reduces the total power spent on precoding.

- To minimize the interference to the macrocell layer, we employ our signal design principle where the transmission power is adapted to the average channel gain.

6.2 Motivation and Related Work

Cell edge users typically suffer from high Co-Channel Interference (CCI) from adjacent eNB and low signal to SINR from serving BS. With the use of OFDM to cancel out intra-cell interference, CoMP has been shown to significantly improve cell-edge user performance as the interference from the adjacent cells is treated as useful interference [**?**].

CoMP is divided into two categories; Joint processing and Coordinated scheduling and/or beamforming [8]. In JP, backhaul data and channel information intended for a user is shared among coordinating eNB. In this method CCI is reduced as the interference from the CeNB is used to assist the transmission whereas in (CS/CB), data is only transmitted from one CeNB, however scheduling and beamforming are coordinated to reduce the effect of CCI.

In CoMP systems, it is assumed that a cluster of CeNB are connected to a central

processing unit/central scheduler via backhaul links [132]. In each cluster, channel state information for each user can be estimated at each CeNB based on uplink channel measurements or alternatively each user estimates/predicts the CSI and feeds it back to the eNB via uplink signalling [8]. In both cases the CSI can then be forwarded to the central scheduler.

The performance of CoMP systems however depends on accurate CSI, the type of precoding employed, feedback and backhaul limitations. The amount of data to be shared by CBS can introduce overheard and latency issues as well.

An improved architecture in [133] is discussed which shows CoMP is most suited to macro cells as they are connected to more powerful X2 interfaces and thus communication between cells takes place between the backplane links of eNB instead of the traditional X2 interface.

In JP, which are normally MISO broadcast transmissions, beamforming with channel inversion/Truncated Channel Inversion (TCI) has been shown to provide array gain on the order of the number of transmit antennas and also maximize the sum rate [134].

Performance of Spatial Multiplexing implementation in CoMP also depends on the type of precoding employed. Dirty Paper Precoding has been shown to achieve capacity region over Gaussian broadcasting channels [135], however its complex to implement in practice. Linear precoding techniques such as zero-forcing and minimum mean-square error precoders have been shown to provide sub-optimal sum rates [136]. Furthermore, their performance is limited by the number of antennas available for transmission.

Therefore, to minimize interference and at same time reduce the cost of RF chains, we employ our signal preforming such that we utilize the interferences to enable spatial multiplexing to a user with a single receive antenna.

6.3 Principles of Joint Constellation Processing

The key design principle CoMP-JCP is to enable the efficient utilization of antennas as well as inter-cell interference. This is possible so long as the cells have the necessary information to coordinate themselves, or are connected to a central processing unit, which coordinate the cells.

By employing our constellation design principles in Chapter 3, we precode both the primary and the interfering cell signals, such that the interference is mitigated. Furthermore, we provide spatial multiplexing from the coordinating cells such that their signals are received by a single receive antenna at the user. This is in contrast with SU-MIMO spatial multiplexing were the number of streams is a direct function with the number of transmit/receive antennas. The signals transmitted from the CeNB are designed such that they form a unique constellation pattern, known at the receiver. We employ our search algorithm to compute power and phase precoding values for each eNB that maximizes the joint receive signal constellations. More specifically, the signals from J CeNBs are superposed to form a composite signal that belongs to a QAM constellation $\mathbf{U}$ of size Ω, which can be expressed as

$$\mathbf{U} = \mathbf{V} \times \mathbf{W} \tag{6.1}$$

where $\mathbf{V} \in \mathbb{C}^{\Omega \times J}$ is a matrix whose rows represent the possible combinations of J signals and $\mathbf{W} \in \mathbb{C}^{J \times 1}$ is a complex matrix whose entries represent the power and phase precoding weights. The composite constellation is expressed as $\mathbf{U} = [\mathbf{u}_1, \ldots, \mathbf{u}_i, \ldots, \mathbf{u}_\Omega]^T$

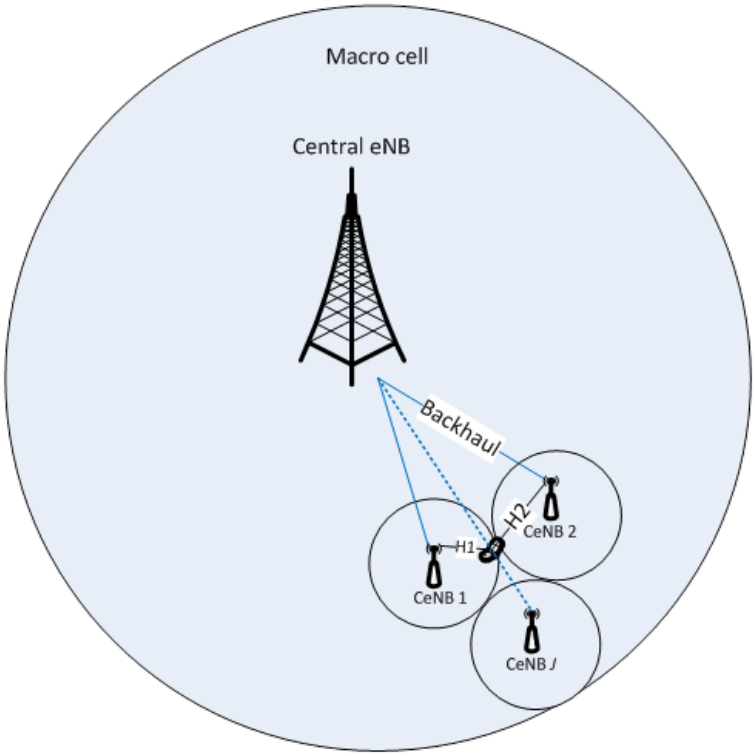

Figure 6.1: Example of coordinating femtocells

6.4 Joint Constellation Processing (CoMP-JCP)

6.4.1 System Model

Figure 6.1 shows an illustration of CoMP-JCP deployment where J CeNBs are connected to a central eNB and a UE located at the edge of primary CeNB. It is assumed that each CeNB is equipped with one or more antennas and the joint processing for the UE is carried out at the central eNB. Also, the UE is connected to its primary serving cell and $J-1$ adjacent cells. CSI is estimated at CeNB by means of pilot signals from uplink transmission, where uplink/downlink channel reciprocity is assumed. It is assumed that the transmitted symbols, each from a modulation set $\mathbf{Q}$, have unit energy per symbol, and that the transmitted vectors from the CeNB are synchronized so that they arrive at the UE at the same time. The modulated symbols are mapped onto N subcarriers assigned by the central eNB. Before N-point IFFT, in order to avoid interference to other

RB on the same OFDM symbol period, guard band zeros are split and padded to the edges to the spectrum. After IFFT, CP is appended to the transmission to avoid ISI. The CP is assumed to be larger than the delay spread, τ , of the channel with t paths

The received signal $\mathbf{y}_n$ and channel $\mathbf{h}_{jn}$ on the n-th subcarrier at the j-th CeNB expressed as

$$\mathbf{y}_n = \sum_{j=1}^{J} \mathbf{h}_{jn}\mathbf{x}_{jn} + \mathbf{z}_n \tag{6.2}$$

where $\mathbf{h}_{jn} = \alpha_{jn}e^{i\vartheta_{jn}} = \sum_{t=1}^{T} \alpha_{jnl}e^{i2\pi jn\tau_t/N}$ denotes the channel of the t-th path of the n-th subcarrier at the j-th CeNB; α and ϑ represents the channel gain and phase respectively, with the different paths assumed to be independent of each other. $\mathbf{z}_n$ is a white complex Gaussian noise with zero mean and variance σ_n^2

The multiple streams from J CeNB are precoded such that the combined signal is received by a single receive antenna at the UE. The precoding is designed at the central eNB to be fully decodable and to minimize interference.

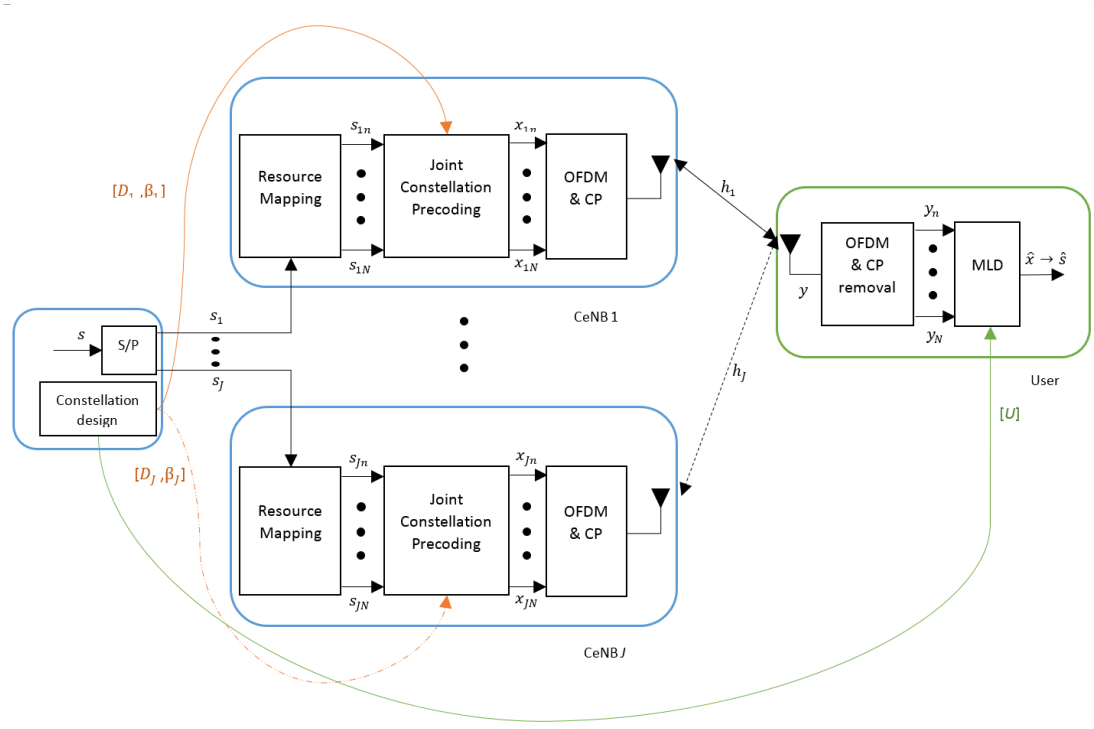

Figure 6.2: Example of J CoMP-JCP downlink processing

Figure 6.2 illustrates CoMP-JCP downlink processing where power and phase of the signals at each subcarrier at the jth-CeNB, before IFFT, are adjusted via CI such that they produce a unique interference pattern known at the receiver. The received composite signal at the receiver, after FFT, belongs to a higher Ω-QAM constellation with a rate equal to the sum rate of all CeNB and with a structure that aims to maximize the minimum Euclidean distance (d_{min}).

Let $\mathbf{s}_{jn}$ denote the modulated symbols at n-th subcarrier of the jth-CeNB with average constellation power fixed to one. By applying the designed power and phase precoding weights, the transmitted symbol becomes

$$\mathbf{x}_{jn} = \mathbf{w}_{jn}\mathbf{s}_{jn} \tag{6.3}$$

where $\mathbf{w}_{jn} = \sqrt{\mathbf{P}}_{jn}e^{-j\theta_{jn}}$ represents the power, $\mathbf{P}_{jn}$, and phase, θ_{jn}, adjustments, respectively, at each CeNB to ensure the received signal matches to the precoding indexes $\mathbf{D}_j$ and β_j, assigned by the eNB. $\mathbf{P}_{jn}$ and θ_{jn}, are given as

$$\mathbf{P}_{jn} = \frac{\mathbf{D}_j}{|\mathbf{h}_{jn}|^2} \tag{6.4}$$

$$\theta_{jn} = \beta_j - \vartheta_{jn} \tag{6.5}$$

6.4.2 Maximum Likelihood Detection

At the receiver, the user performs ML detection using the designed constellation as reference. For a CoMP-JCP system with J CeNBs each with modulation set of $\mathbf{Q}$, the possible

signal vectors at the channel input and output, ignoring the additive noise, is given as

$$\mathbf{x}_n^{(q)} = [\mathbf{x}_{1n}^{(q)} \dots \mathbf{x}_{jn}^{(q)} \dots \mathbf{x}_{Jn}^{(q)}]^T; \qquad q \in \mathbf{Q} \tag{6.6}$$

$$\bar{\mathbf{x}}_n^{(\bar{q})} = \sum_{j=1}^{J} \mathbf{h}_j \mathbf{x}_j^{(q)}; \qquad \bar{q} \in \mathbf{U} \tag{6.7}$$

where $\mathbf{x}_n^{(q)}$ is the q-th possible transmitted symbol from the j-th CeNB at every subcarrier, and $\bar{\mathbf{x}}_n^{(\bar{q})}$ is the $\bar{q}$-th possible composite signal at the receiver. Therefore, the received signal from Equation (6.2) can be re-written as

$$\mathbf{y}_n = \bar{\mathbf{x}}_n^{(\bar{q})} + \mathbf{z}_n \tag{6.8}$$

By employing the minimum distance criterion, the estimated signal at the user is given as

$$\hat{\mathbf{x}} = \arg[\min_{\mathbf{U}}(\|\mathbf{y}_n - \bar{\mathbf{x}}_n^{(\bar{q})}\|^2)]; \qquad \bar{q} = 1, \dots, \mathbf{U} \tag{6.9}$$

where $\|\mathbf{y}_n - \bar{\mathbf{x}}_n^{(\bar{q})}\|^2$ is the distance between the received signal an the possible receive signal $\bar{\mathbf{x}}_n^{(\bar{q})}$

6.4.3 Joint Constellation Processing Procedures

The procedure for CoMP-JCP are summarized as follows:

1. The central eNB designs the constellations which are assumed are assumed to be known by the CeNBs, as well as the user. Each power and phase weight combinations are assumed to correspond with an index, such that only the index is signalled.

2. The central eNB splits and forwards packets meant for a user to the corresponding

CeNB. In addition, the central eNB signals the precoding indexes $\mathbf{w}_j$ to the CeNBs, and reference constellation index $\mathbf{U}$ to the user.

3. Each CeNB estimates and tracks the effective channel of the user $\mathbf{h}_{jn}$ based on uplink channel measurements, assuming uplink/downlink channel reciprocity, reported by the user.

4. The CeNBs look up the precoding weights $\mathbf{D}_j$ and β_j based on precoding index, and precodes the symbols with the channel measurements in (3) to produce $\mathbf{x}_{jn}$.

5. The CeNBs determine and employ any timing and synchronization requirements before transmitting the precoded signal. This is carried out such that the signals form all CeNBs are received at the same time by the user.

6. If the channel changes between (3) and (5) due to excessive timing and synchronization delays in (5), the CeNBs notify the central eNB and loop back to (4). Otherwise the CeNB skip (7).

7. The user performs maximum likelihood detection between the composite received signal y_n and the reference constellation $\mathbf{U}$ from (2).

6.5 Joint Constellation Processing with Active Cell Selection (CoMP-JCP-ACS)

In this section, we employ Active Cell Selection (ASC) to our CoMP-JCP scheme, with the aim of reducing the total power spent on precoding. This is achieved by selecting and transmitting from the CeNBs with the strongest interference to a user. As the channels from the high SINR CeNB are stronger, by employing ACS, the power needed to maintain

a fixed average SNR is reduced. Consequently, the higher the number of CeNB available, the higher the reduced power selection gain achieved.

In CoMP-JCP-ACS, the central eNB actively tracks, sorts and indexes all the channels in a group of J-CeNB and, according to the number of L independent streams, selects the $K = L$ CeNBs with the strongest interference to the user for transmission, with the UE completely blind to the selection.

6.5.1 System Model

Consider a CoMP system with the strongest K interfering CeNBs out of J total CeNBs. The CeNBs are assumed to be connected to a central eNB and the user located at the edge of active primary CeNB 1. It is also assumed that each CeNB is equipped with one or more antennas, and the joint processing for the user is carried out at the central eNB. The Full CSI are assumed to be estimated at the CeNB by means of pilot signals from uplink transmission. The transmitted symbols are assumed to have unit energy per symbol and that the transmitted vectors from the selected CeNB are synchronized so that they arrive at the UE at the same time.

Let $|\mathbf{h}_1|^2 > \ldots > |\mathbf{h}_j|^2 > \ldots > |\mathbf{h}_J|^2$ denote the channels from the j-th CeNB to the user ordered in decreasing channel power. Furthermore, let L denote the number of streams, such that $L = K$, we can then express the total channel vector as

$$\mathbf{H} = [\mathbf{h}_1, \ldots, \mathbf{h}_k, \ldots, \mathbf{h}_K, \mathbf{h}_{j=K+1}, \ldots, \mathbf{h}_J]^T \tag{6.10}$$

where $\mathbf{h}_k$ denotes the channels of the active selected strong interferers and $\mathbf{h}_j$ denotes the non-selected CeNBs.

Let $\mathbf{s}_{kn}; k \in K$ denote the modulated symbols at n-th subcarrier of the k-th active

CeNB, by applying power and phase adjustment to ensure transmission power is adapted to the allocated power D_k and phase β_k values, the transmitted symbol becomes

$$\mathbf{x}_{kn} = \mathbf{w}_{kn}\mathbf{s}_{kn} \tag{6.11}$$

where $\mathbf{w}_{kn} = \sqrt{\mathbf{P}}_{kn}e^{-j\theta_{kn}}$ represents the power, $\mathbf{P}_{kn}$, and phase, θ_{kn} adjustments, respectively, given as

$$\mathbf{P}_{kn} = \frac{\mathbf{D}_k}{|\mathbf{h}_{kn}|^2} \tag{6.12}$$

$$\theta_{kn} = \beta_k - \vartheta_{kn} \tag{6.13}$$

Thus, the sum total average transmit power on N subcarriers from the K selected CeNBs can be defined as

$$\mathbf{P}_{tot} = \sum_{k=1}^{K}\frac{1}{N}\sum_{n=0}^{N-1}\mathbf{x}_{kn} = \sum_{k=1}^{K}\frac{1}{N}\sum_{n=0}^{N-1}\mathbf{w}_{kn}\mathbf{s}_{kn} \tag{6.14}$$

and the received signal at user

$$\mathbf{y}_n = \sum_{k=1}^{K}\mathbf{h}_{kn}\mathbf{x}_{kn} + \mathbf{z}_n \tag{6.15}$$

6.5.2 Active Cell Selection and Transmission Procedures

The procedures for CoMP-JCP-ACS are carried out as follows:

1. The central eNB designs the constellations to be employed by the CeNBs. It is assumed that the designed constellations are known at the CeNBs, as well as the user. Each power and phase weight combinations are assumed to correspond with an index, such that only the index is signalled.

2. Each CeNB estimates and tracks the effective channel of the user $\mathbf{h}_{jn}$ based on uplink channel measurements. The CeNBs then report the channel information to the central eNB.

3. The central eNB sorts the reported channels $|\mathbf{h}_1|^2 > \ldots > |\mathbf{h}_j|^2 > \ldots > |\mathbf{h}_J|^2$ in decreasing SINR order, to determine the strongest interfering CeNBs to the user.

4. Based on the number of streams $L = K$ to be multiplexed, the central eNB actively selects K out of J CeNBs for transmission.

5. The central eNB splits and forwards packets meant for a user to the selected K CeNB. In addition, the central eNB signals the precoding indexes $\mathbf{w}_k$ to the CeNBs, and reference constellation index $\mathbf{U}$ to the user.

6. The CeNBs look up the precoding weights $\mathbf{D}_k$ and β_k based on precoding index, and precodes the symbols with the channel $\mathbf{h}_{kn}$ to produce $\mathbf{x}_{kn}$.

7. The CeNBs also determine and employ any timing and synchronization requirements before transmitting the precoded signal. This is carried out such that the signals form the active CeNBs are received at the same time by the user.

8. If the channel changes between (2) and (7) due to excessive timing and synchronization delays, the CeNBs notify the central eNB and loop back to (2)

9. The user performs maximum likelihood detection between the composite received signal y_n and the reference constellation $\mathbf{U}$ from (2).

6.6 CoMP Joint Constellation Processing with Mean Channel Adaptation (CoMP-JCP-MCA)

In this section, we propose a power control scheme called CoMP Joint Constellation Processing with Mean Channel Adaptation (CoMP-JCP-MCA). As the CeNBs are located within a central eNB cell area, we employ power control such that the interferences to the macrocell/cross-tier layers are minimized. This is achieved by adapting the transmission power according to the Mean Channel Gain (MCG) across multiple resource blocks in both time (T OFDM symbols) and frequency (N subcarriers), which we assume stays constant for the duration of transmission; and/or transmission within coherence time of the channels. This ensures the interference is kept to a minimum, and a constant SNR is maintained at the receiver. i.e.

$$\overline{\lambda}_j = \sum_{t=1}^{T} \sqrt{\frac{1}{N} \sum_{n=1}^{N} |\alpha_{jn}(t)|^2} \tag{6.16}$$

Let $\mathbf{s}_j(t) = [\mathbf{s}_{j1}(t), \mathbf{s}_{j2}(t), \ldots, \mathbf{s}_{jN}(t)]^T$ denote the modulated symbols at n-th subcarrier of the jth-CeNB with average constellation power fixed to one. Employing the designed power D_j and phase β_j precoding weights, the transmission power is adapted to the MCG, which is expressed as

$$\mathbf{x}_n(t) = \mathbf{w}_{jn}(t)\mathbf{s}_{jn}(t) \tag{6.17}$$

where $\mathbf{w}_{jn}(t) = \sqrt{\mathrm{P}_{jn}(t)}e^{-j\theta_{jn}(t)}$ represents the power, $\mathrm{P}_{jn}(t)$, and phase, $\theta_{jn}(t)$, adjustments, respectively, at OFDM symbol period t, determined by TCI as

$$\mathrm{P}_{jn}(t) = \begin{cases} [\frac{\mathrm{D}_j}{\alpha_{jn}(t)}]^2 & |\alpha_{jn}(t)|^2 > \mu \\ 0 & |\alpha_{jn}(t)|^2 \leq \mu \end{cases} \tag{6.18}$$

$$\theta_{jn}(k) = \beta_j - \vartheta_{jn}(k) \tag{6.19}$$

where μ is the cut-off i.e. compensate fading only above a certain fade depth determined by the CeNBs antennas peak power. D_j is chosen not to be greater than the inverse of the mean channel gain from Equation (6.16), i.e.

$$\mathrm{D}_j \leq \frac{1}{\overline{\lambda}_j} \tag{6.20}$$

Due to the MCG variation at each CeNB, the eNB designs the constellations by performing an exhaustive search to find the precoding weights that maximizes the minimum distance of the combined received constellation points.

6.6.1 CoMP-JCP-MCA Transmission Procedures

The procedures for CoMP-JCP-MCA are carried out as follows:

1. Each CeNB estimates and tracks the effective channel of the user $\mathbf{h}_{jn}$ based on uplink channel measurements.

2. Based on the number of streams to be multiplexed, the central eNB designs the constellations by averaging the channel estimates in (1) to find the MCG for computing the precoding weights that maximize the d_{min} of the composite constella-

tion points.

3. The central eNB splits and forwards packets meant for a user to the CeNB. In addition, the central eNB forwards the MCA precoding weights to the respective CeNBs, and the designed reference constellation **U** to the user.

4. The CeNBs precode the symbols with the signalled weights to produce $\mathbf{x}_{jn}$.

5. The CeNBs also determine and employ any timing and synchronization requirements before transmitting the precoded signal. This is carried out such that the signals form the active CeNBs are received at the same time by the user.

6. If the average channel changes between step 2 and step 5, the CeNBs notify the central eNB and loop back to step 1.

7. The user performs maximum likelihood detection between the composite received signal y_n and the reference constellation **U** from step 3.

6.7 Simulation Modelling and Results

6.7.1 Simulation Modelling

6.7.1.1 CoMP-JCP and CoMP-JCP-ACS

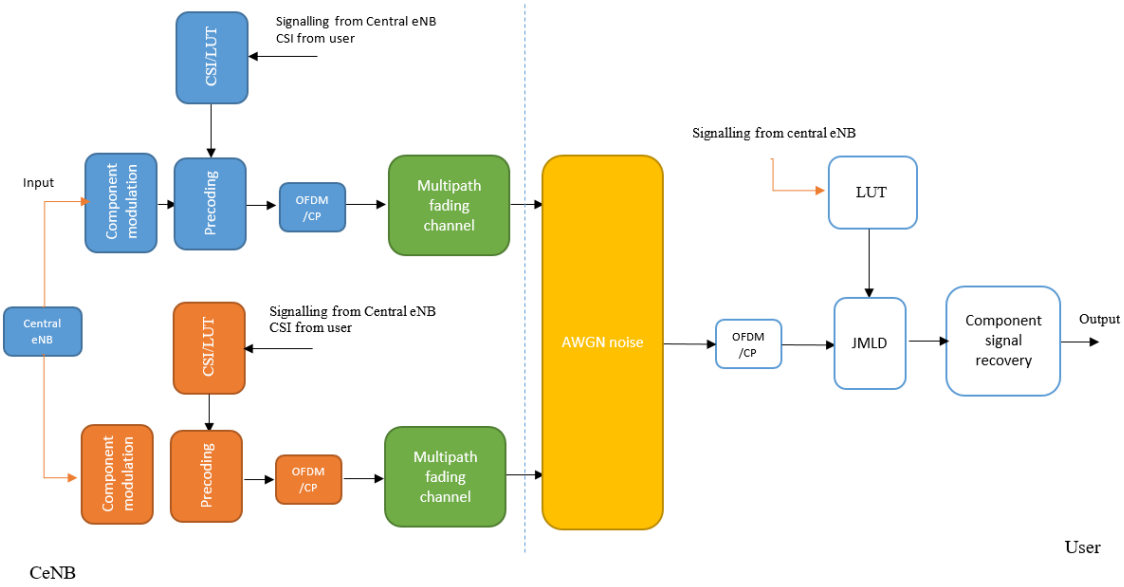

Figure 6.3: CoMP-JCP simulation Model

A Monte-Carlo type simulation is carried out in MATLAB environment to compare the performance of our CoMP-JCP scheme. The simulation model is illustrated in Figure 6.3. The central eNB is assumed to forward packets as well as precoding weights to the CeNBs. All the CeNBs are assumed to be equipped with a single antenna. Component modulation and precoding is employed on each subcarrier at each CeNB. Perfect CSI is assumed at each CeNB estimated from uplink pilots from the user. The system performance is evaluated in terms of BER and capacity bounds in a multipath channel response with 10 paths over thousands of OFDM symbol periods. It is assumed that the user is connected to and receiving synchronized data from the CeNBs and that the reference constellation is known at the user. We compare our proposed scheme with a single user MIMO scheme employing SVD and single user employing the composite

constellation in a point-to-point in additive white noise scheme. Perfect CSI is assumed for the comparison schemes and is available at both the transmitters and receivers. Furthermore, we extend our simulation to CoMP-JCP-ACS scheme where the precoding is only employed on the highest K out of J interferers to the user. The total average power spent on precoding for selected K CeNBs is plotted as a function of J total single antenna CeNBs.

6.7.1.2 CoMP-JCP-MCA

A Monte-Carlo type simulation is carried out in MATLAB environment to compare the performance of our CoMP-JCP-MCA scheme. All the CeNBs are assumed to be equipped with a single antenna. The CeNB forwards the MCG estimated from uplink pilots to the central eNB. Perfect CSI is assumed at each CeNB estimated from uplink pilots from the user. The central eNB then performs a search to find the power and phase weights that maximize the d_{min} of the composite constellation. Subsequently, the central eNB forwards the packets are precoding weights to be employed by the CeNBs. Component modulation and precoding is employed on each subcarrier at each CeNB based on MCG precoding weights signalled by the central eNB. The user performs ML detection between the received signal and the designed constellation signalled by the central eNB. The system performance is evaluated in terms of BER and capacity bounds in a multipath channel response with 10 paths over thousands of OFDM symbol periods. It is assumed that the user is connected to and receiving synchronized data from the CeNBs and that the reference constellation is known at the user. We compare our proposed scheme with a single user MIMO scheme employing SVD and single user employing the composite constellation in a point-to-point in additive white noise scheme with the same power control. Perfect CSI is assumed for the comparison schemes and is available at both the

transmitters and receivers

6.7.2 Results

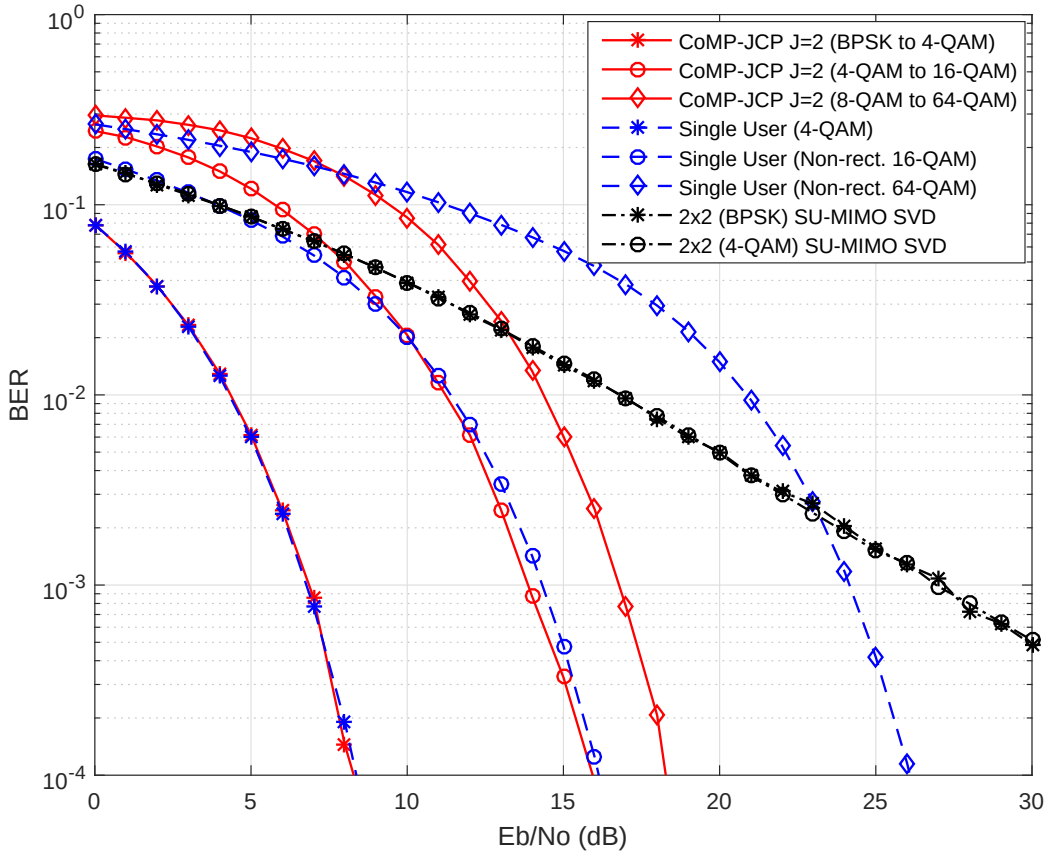

Figure 6.4: BER vs Eb/No performance of $J = 2$ CoMP-JCP compared with a 2x2 single user MIMO scheme employing SVD and single user employing the composite constellation in a point-to-point in additive white noise scheme.

Figure 6.4 illustrates BER performance of CoMP-JCP with $J = 2$ CeNBs. BPSK, 4-QAM and 8-QAM component modulations are employed at each CeNB to produce non-rectangular 4-QAM, 16-QAM and 64-QAM composite constellation, respectively, at the user. We compare the performance with that of a single user employing the respective composite constellation, and a 2x2 single user MIMO spatial multiplexing employing SVD precoding. For BPSK component modulations, it can be seen that we achieve the same BER as that of a single user employing 4-QAM. For 4-QAM and 8-QAM component modula-

tions, we achieve a 0.3 dB and 7.7 dB gain at BER 10^{-4}, respectively compared to the single user. This is as a result of the power gain achieved by the sum of CeNBs powers, compared to the constellation average power of $|\mathbf{x}|^2 = 1$. The performance of 2x2 is given as upper bounds in fading environment.

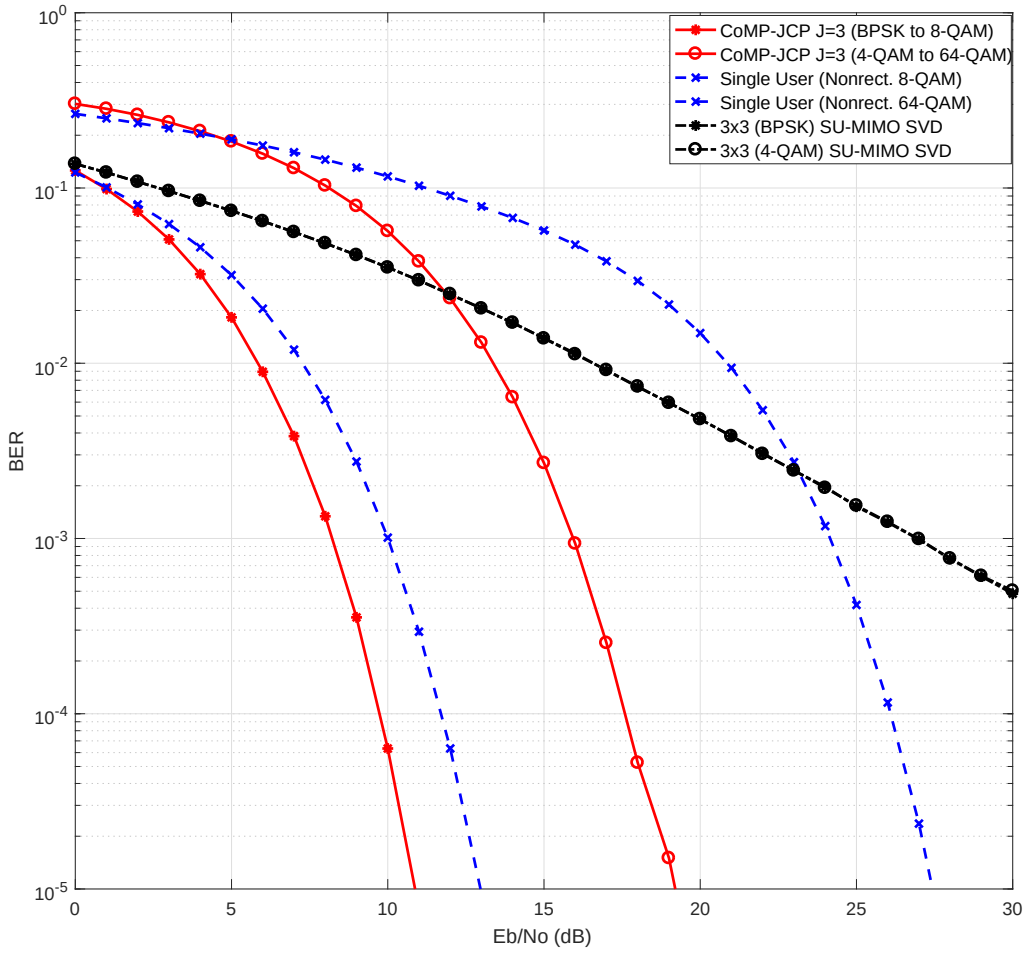

Figure 6.5: BER vs Eb/No performance of $J = 3$ CoMP-JCP compared with a 3x3 single user MIMO scheme employing SVD and single user employing the composite constellation in a point-to-point in additive white noise scheme.

Similarly, Figure 6.5 illustrates BER performance of CoMP-JCP with $J = 3$ CeNBs. BPSK and 4-QAM component modulations are employed at each CeNB to produce non-rectangular 8-QAM and 64-QAM composite constellation, respectively, at the user. The performance is also compared with that of a single user employing the respective com-

posite constellation, and a 3x3 single user MIMO spatial multiplexing employing SVD precoding. For the BPSK and 4-QAM component modulations, we achieve a 2.1 dB and 8.2 dB gain at BER 10^{-4}, respectively compared to the single user case. The 3x3 SU MIMO are also shown as upper bounds.

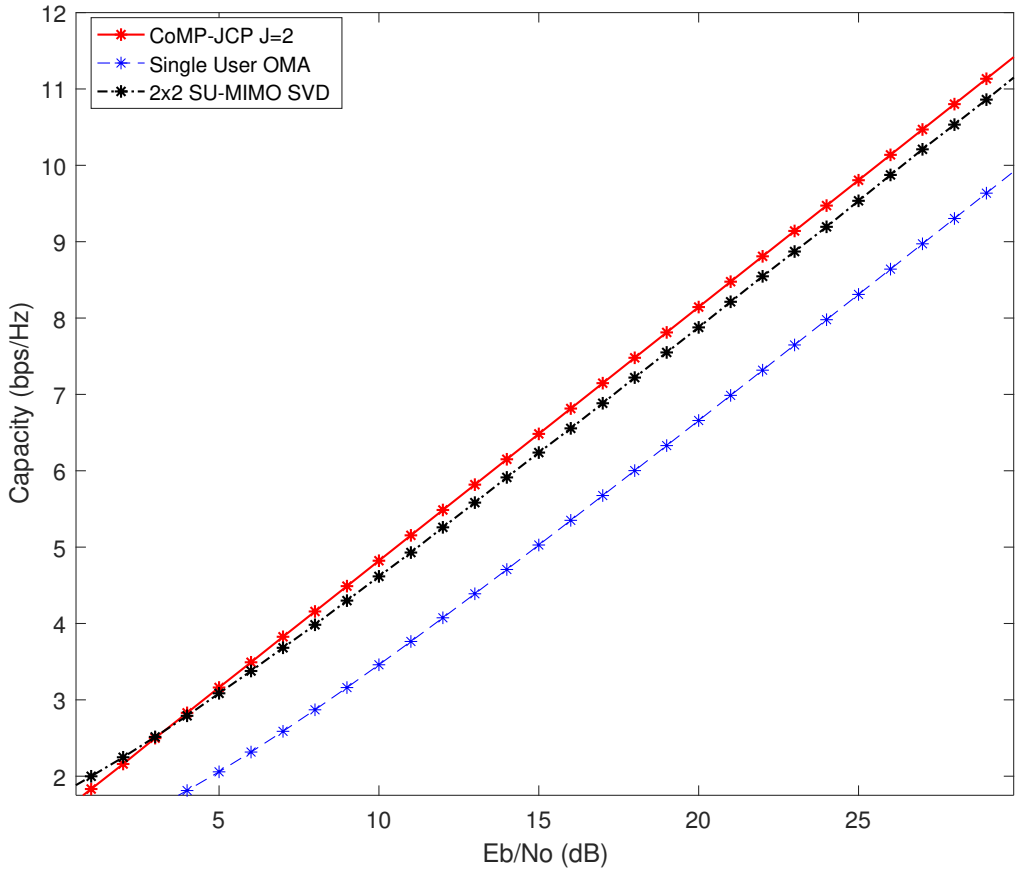

Figure 6.6: Shannon capacity performance of $J = 2$ CoMP-JCP compared with a 2x2 single user MIMO scheme employing SVD, and single user in a point-to-point in additive white noise scheme.

Figure 6.6 illustrates the channel capacity of CoMP-JCP with $J = 2$ CeNBs. It can be seen that we achieve increase in capacity of 0.25 bps/Hz at 15 dB compared to a SU-MIMO system employing SVD precoding. Furthermore, we achieve 1.4 bps/Hz increase in channel capacity compared to single user in OMA.

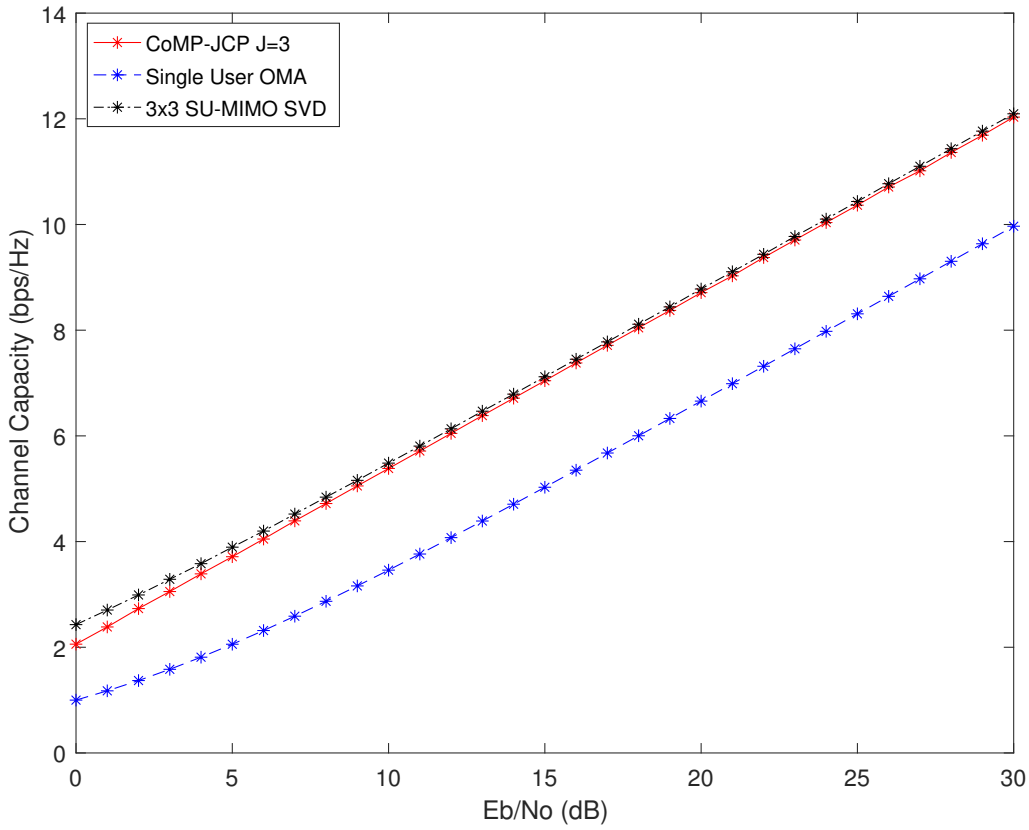

Figure 6.7: Shannon capacity performance of $J = 3$ CoMP-JCP compared with a 3x3 single user MIMO scheme employing SVD, and single user in a point-to-point in additive white noise scheme.

For CoMP-JCP with $J = 3$ CeNBs as shown in fig. 6.7, we get a very slight decrease in capacity compared to 3x3 SU MIMO with SVD precoding of 0.075 bps/Hz. However, this is well compensated in throughput performance as CoMP-JCP is noise limited, while the performance in SU-MIMO with SVD is limited by the channel dependent eigenvalues.

For CoMP-JCP-ACS, figs. 6.8 and 6.9 illustrate the total average transmit power of $K = 2$ and $K = 3$ selected highest interferers, as a function of total $J = 50$ CeNBs. We assume Es/No where $E_s = \rho E_b$ is the symbol energy, $\rho = \log_2(\Omega)$ the number of bits per symbol, E_b the energy per-bit, and N_o the AWGN noise where we set the variance as $\sigma^2 = 1$. We evaluate for $4, 8, 16$ and 64-respectively. It can be seen that as the number of available CeNBs increase, the total transmit power density decreases. This is evident

in Figures 6.10(a) to 6.10(f) where the PDF of the K highest interfering CeNB are plotted as a function of total J CeNBs.

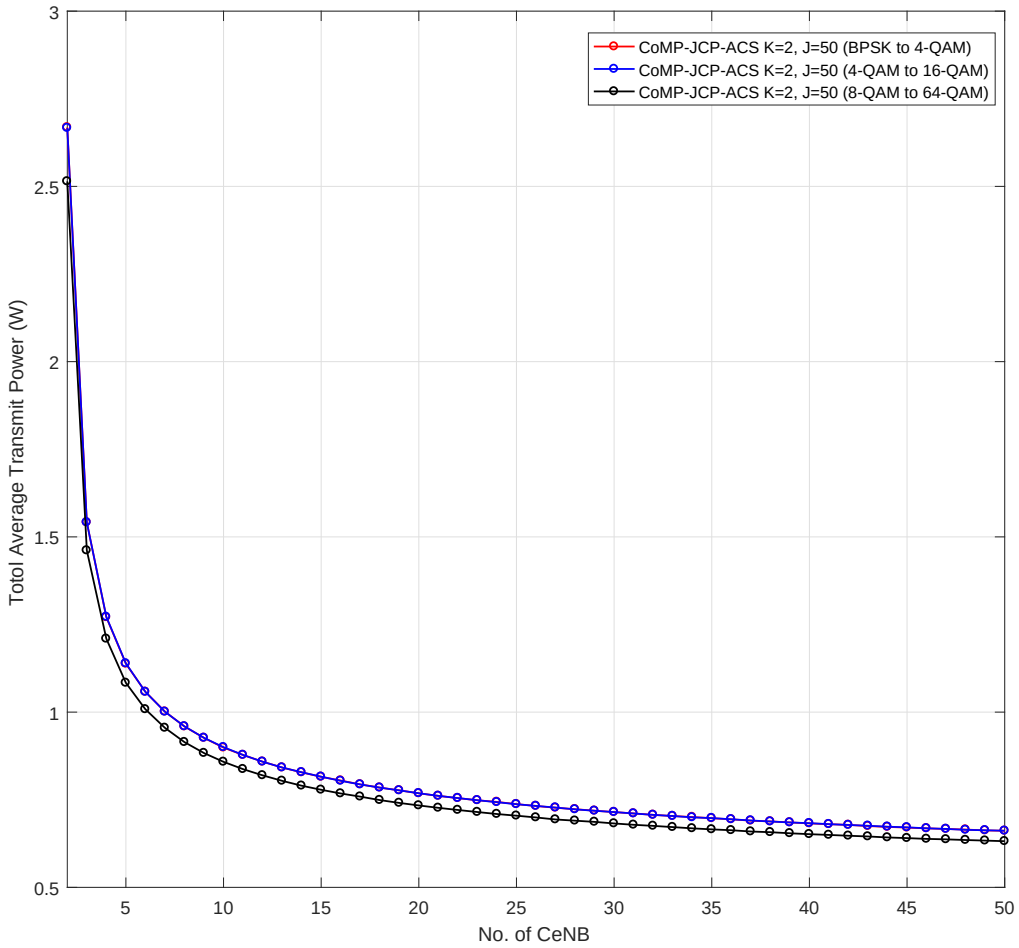

Figure 6.8: Total power spent on precoding for 4, 16 and 64-QAM CoMP-JCP-ACS with K=2 and J=50. We assume Es/No where $E_s = \rho E_b$ is the symbol energy, ρ the number of bits-per-symbol, E_b the energy per-bit, and N_o the AWGN noise with the variance defined as $\sigma^2 = 1$. We evaluate for $\rho = 2, 4$ and 6 for 4, 16 and 64-QAM, respectively.

It is shown that assuming the channels are ordered from the highest interferers to the lowest, selecting the K strongest interferers results in higher channel power density, which requires less transmit power to maintain a specific SNR. However, as J increases, ACS advantage decreases exponentially.

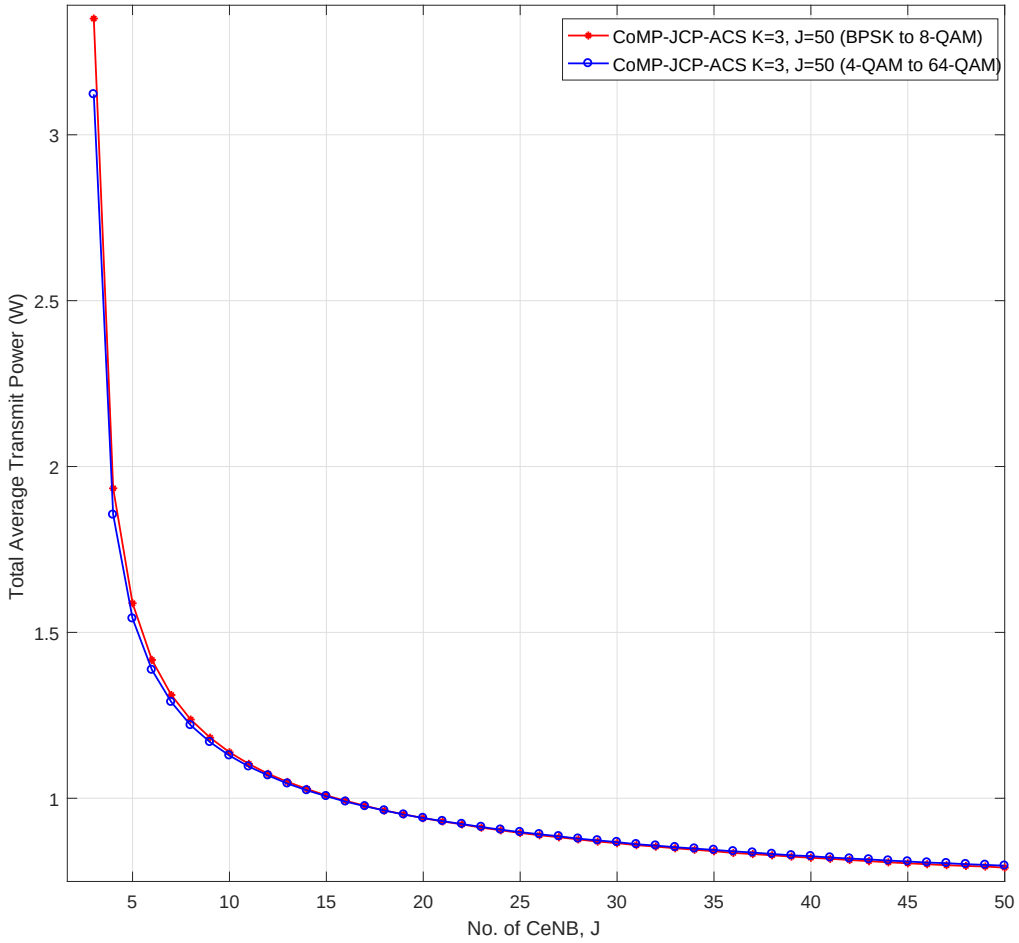

Figure 6.9: Total power spent on precoding for 8 and 64-QAM CoMP-JCP-ACS with K=3 and J=50. We assume Es/No where $E_s = \rho E_b$ is the symbol energy, ρ the number of bits-per-symbol, E_b the energy per-bit, and N_o the AWGN noise with the variance defined as $\sigma^2 = 1$. We evaluate for $\rho = 3$ and 6 for 8 and 64-QAM, respectively.

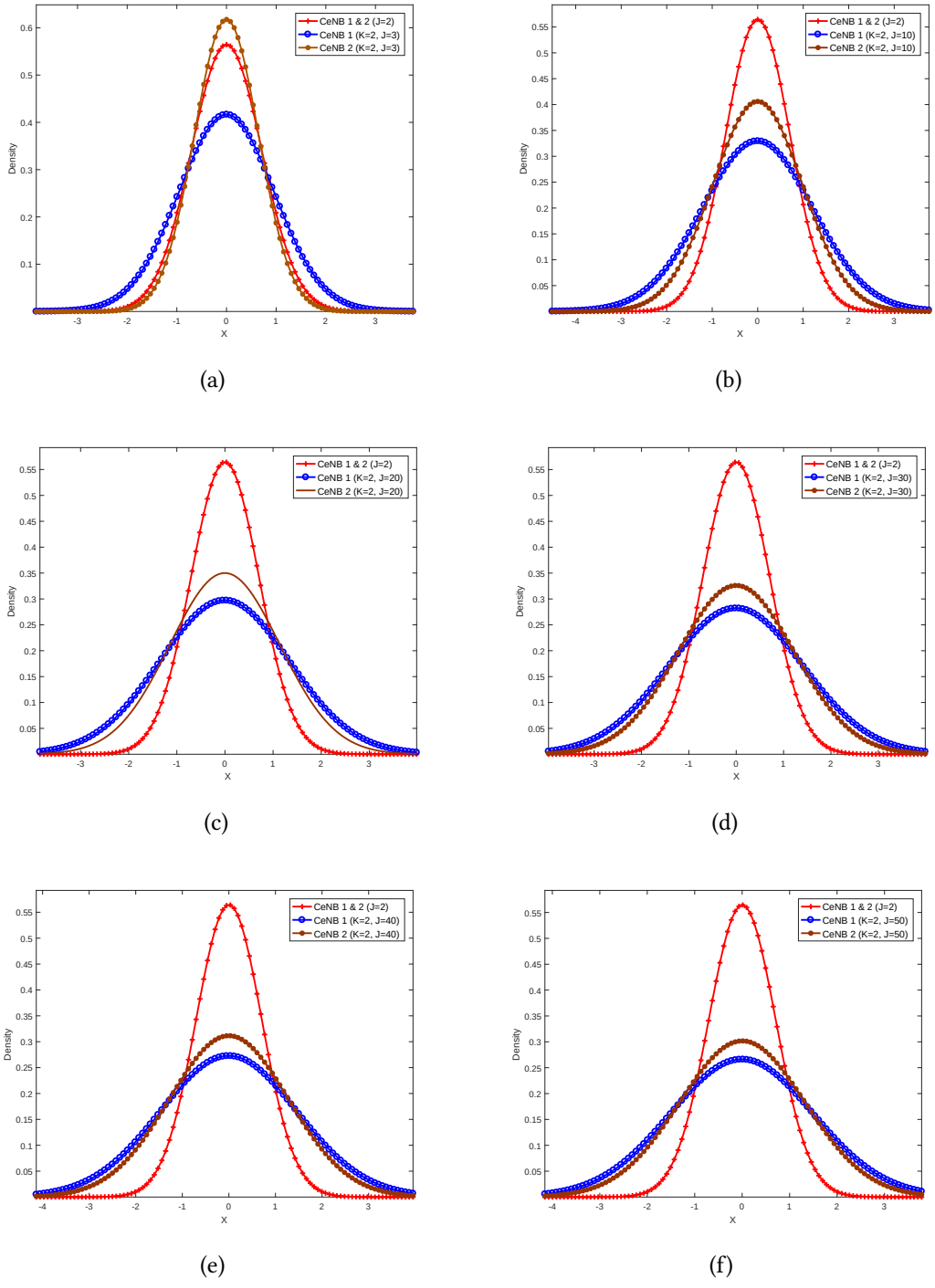

Figure 6.10: Probability density function plot of the highest $K = 2$ interfering CeNB channels as a function of total available J CeNBs. A Rayleigh fading channel with $\aleph(0, 1)$ is given as reference. (a) $K = 2$ selected CeNBs out of $J = 3$. (b) $K = 2$ selected CeNBs out of $J = 10$. (c) $K = 2$ selected CeNBs out of $J = 20$. (d) $K = 2$ selected CeNBs out of $J = 30$. (e) $K = 2$ selected CeNBs out of $J = 40$. (f) $K = 2$ selected CeNBs out of $J = 50$. The plots assume the channels are ordered in decreasing order i.e. $|\mathbf{h}_1|^2 > \ldots > |\mathbf{h}_j|^2 > \ldots > |\mathbf{h}_J|^2$

For CoMP-JCP-MCA scheme, it can be seen in Figure 6.11 that by adapting our trans-

mission according to the MCG, we get a TCI power difference of around 21dB at BER of 10^{-4} compared to single user employing 4-QAM with ML detection and CSIR. For the same user employing 4-QAM with MCA power control, we achieve the same BER performance. However, due to the inter-cell interference, the user suffers rate degradation. The performance of a 2x2 MIMO with CSIT&R is shown for comparison. Due to mean channel adaptation, we trade-off BER performance for reduced interference to the macro cell layer, as can be seen if the full TCI is employed.

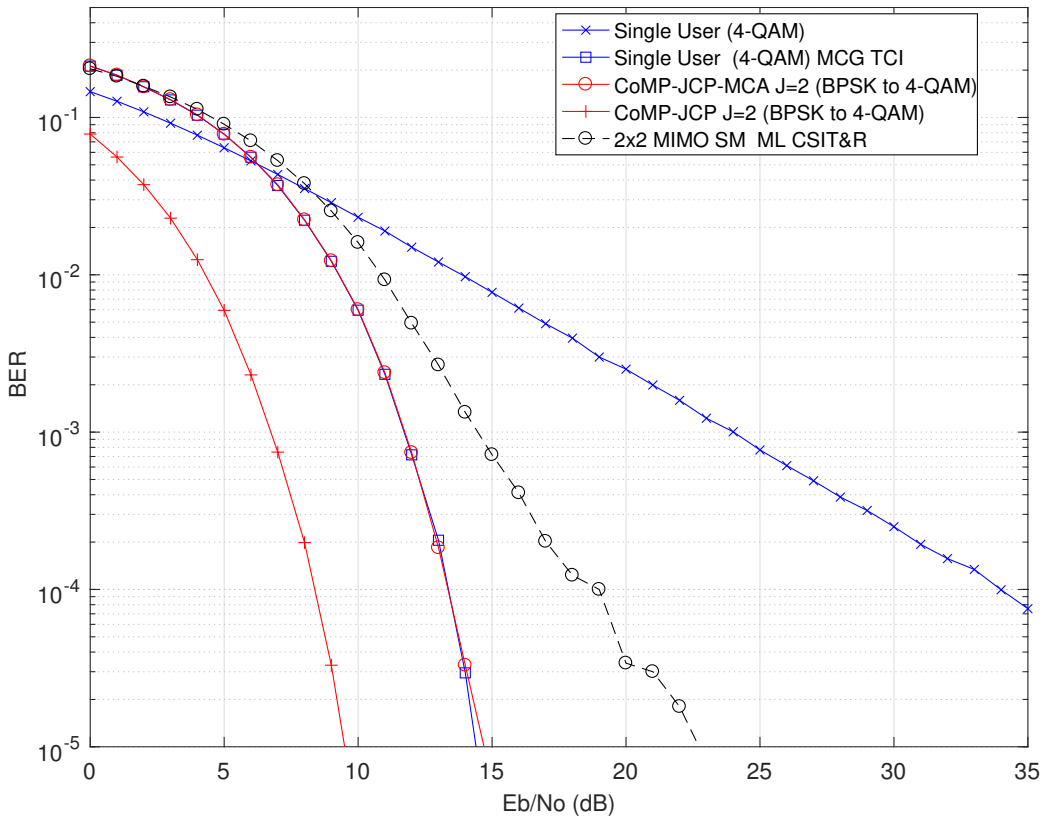

Figure 6.11: BER vs Eb/No performance of CoMP-JCP-MCA with each CeNB employing BPSK, compared with a single user employing 4-QAM and 2x2 MIMO SM.

These results show that we can mitigate the interference from the neighbouring cell, and at the same time, utilize the extra DoF to provide SM to a user equipped with a single antenna, while still maintaining decodability without the need for CSIR, compared to

traditional SM schemes.

6.8 Conclusion

In this chapter, a novel CoMP joint constellation processing was proposed. The scheme aims to exploit the extra degrees of freedom provided by CoMP to mitigate ICI, and at the same time, achieve spatial multiplexing to a user equipped with a single receive antenna.

The independent streams from multiple CeNB are precoded with weights such that the composite received signal is uniquely decodable, with the distance between the composite constellation points maximized. As a result, inter-cell interference is eliminated and the rate maximized. To reduce the total power spent on precoding, the precoding is employed on the highest interferes to the user. Furthermore, we applied mean channel gain power control scheme in order to reduce interference to the central eNB layer.

Chapter 7

Conclusion and Future Work

7.1 Conclusions

In this thesis, we introduced a spectrally efficient non-orthogonal multiple access (NOMA) signal design that utilizes the signal superposition principle. The goal of the proposed schemes is to allow simultaneous utilization of the same time/frequency network resources without the consequence of signal interferences. This is achieved by designing component signals in both power and phase domain such that as many users are precoded or preformed to form a single and uniquely decodable composite signal. The design criteria are based on maximizing either the sum rate or spectral efficiency, minimizing multi-user interference and detection ambiguity, and maximizing the minimum Euclidean distance between the designed signal composite constellation points. We employ the signal design in uplink, downlink and coordinated multipoint scenarios. By superposing in the power and phase domain, we relax the large power separation requirement in power domain NOMA (PD-NOMA) employing successive interference cancellation (SIC), which is detrimental to weak user rates, and maximize the sum rate. We showed

that these gains in multiple access and spectral efficiency can be achieved utilizing only a small feedback and independent of the number of receive antennas.

To fulfil these design objectives, a new non-orthogonal multiple access scheme called uplink NOMA with constellation precoding (UL-NCPr) was proposed in chapter 3. The main design principle for UL-NCPr is to allow multiple users share a common channel without the consequence of multi-user interference. This is possible so long as a weighted (power and phase) combination of their signals over the common channel produces a single and uniquely decodable composite signal that is known at the receiver. Furthermore, to eliminate detection ambiguity and improve performance, the minimum euclidean distance between the composite signal constellation points are fully maximized. The eNB designs the user precoding weights by employing an exhaustive search algorithm, in-line with the defined search criteria. It was shown that a non-ambiguous composite constellations can be formed for any practical combination of users component constellations. Furthermore, the search considers the QoS requirements of the users by adjusting the search component constellations according to the respective users. At the eNB, joint maximum likelihood (JML) is employed to recover the component signals.

Through simulation and analysis, it was shown that UL-NCPr can achieve a significant increase in link spectral efficiency compared to tradition multiple access schemes. Furthermore, as the composite constellation is as that of a single user transmitting that same constellation, multiple access interference can be viewed as absent, which allows multiple users to transmit at their full rates. The designs also enables fairness for weak users'rate, compared to Power Domain NOMA (PD-NOMA), where large power separation is required.

Since increasing the number of users or the size of their component constellation

leads to an exponential increase in constellation size, we limit the number of users or their component modulation size such that the size of the composite signal does not exceed LTE specification standards.

In Chapter 4, we extended our constellation design principle to the downlink in the scheme called NOMA with constellation preforming (NCPf). The key difference is that the users are superposed prior to transmission. Throughout this thesis, we refer to this downlink superposition as Constellation Preforming. As the users are subject to eNB power constraints, we employ the search algorithm to find the combinations of power fractions and phase rotations that maximize the minimum distance of the preformed composite constellation points. Thus, we improve the distance-dependent PD-NOMA by utilizing the phase domain as an additional degree of freedom to improve fairness and sum spectral efficiency. As the performance of NCPf is distance-dependent, when the channels are ordered from the strongest to the weakest, we offset the loss in BER with higher BER performance for the strongest user, while the weak users have a slightly lower BER performance.

We further extend our constellation preforming to multi-antenna scenarios in Chapter 5. In order to improve signal reliability at the users, we utilize side-multi antenna to achieve spatial diversity gain in Section 5.2. When the users are equipped with multiple receive antennas, we prosed the scheme called NOMA constellation preforming with receive diversity (NCPf-RD), where we employ maximum ratio combining (MRC) of the pre-formed signals from all the user receive antennas. This is especially beneficial to the weak/far user as the signal reliably is improved. In Section 5.2.2, we propose the constellation preforming scheme in a distributed transmit antenna scenario. The scheme, called NOMA constellation preforming with distribute transmit antenna diversity, we

utilize the independent channel spectral signatures to achieve transmit diversity gain. Similar to NCPf-RD, we increase signal reliability at the users, however, we loose the MRC gain.

In the second part of Chapter 5, we employ our signal design in two MIMO scenarios. The first scenario, we employ the constellation preforming scheme to a MIMO spatial multiplexing with diversity scheme (Section 5.3). The scheme, called NOMA constellation with spatial multiplexing and diversity (NCPf-SMD). The key principle is to achieve spatial multiplexing to our constellation preforming design to a scenario where the number of transmit antennas is less than the number of users stream. This is achieved by preforming each eNB antenna with a set of multiple users streams. This allows increased diversity and capacity with less transmit antennas compared to traditional MIMO SM.

To increase the number of users accommodated in our MIMO preforming scheme, we propose group layered scheme in Section 5.4. In the scheme, called group-layer NOMA with constellation preforming, we group a set of users to a particular transmit antenna. To minimize inter-group interference, we sort the users according to their received signal-to-interference-plus-noise ratios. Thus we trade-off sum rate for spectral efficiency compared to NCPf-SMD.

Finally, we show the adaptability to our constellation design by achieving spatial multiplexing to a user with a single receive antenna in Chapter 6. Specifically, we employ the design in a coordinated multi-point scenario where performance is affected by inter-cell interference. The fist scheme, called CoMP with joint constellation processing (Section 6.3), the additional degrees of freedom, in form of interfering eNBs, are utilized to enable spatial multiplexing to a user with a single receive antenna. This is achieved by precoding each stream from the coordinating eNB with weights designed

in Chapter 3. Consequently, the inter-cell interference is eliminated and the sum-rate maximized. Secondly, to reduce the total power spent on precoding, an active cell selection scheme is proposed where the precoding is employed on the highest interferers to the user (Section 6.5). Furthermore, the design principle is extended to low power eNB in Section 6.6, where the objective is to reduce cross-layer interference by adapting the transmission power to the mean channel gain.

7.2 Future Work

With all the benefits of our constellation design schemes above, the key drawbacks and future works are as follows

- Throughout this thesis, we assume an ideal system i.e. perfect channel conditions, estimation, synchronization, linearity e.t.c. Thus, the performance serve as an upper-bound for any future work on non-ideal conditions e.g. imperfect channel state information and estimation, mobility, time/frequency synchronization errors, outage e.t.c.

- Increased complexity in terms of the proposed search algorithms. However, as the algorithms are assumed to be carried out just once, the benefits might potentially outweigh the complexity. However, it is worth investigating an optimized algorithm that reduces the number of calculations while still maximizing the d_{min} of the composite constellation points. Recent advances in computational mathematics and/or operations can be utilized to offset the cost of the complexity.

- Although ML detection is optimal in terms of BER, as the size of users or their component constellation increases, the search complexity increases. For example,

employing sphere based search detection can significantly reduce the number of search iteration.

- It will be worth investigating the performance of our proposed scheme in massive MIMO scenarios. For example, in array of 100 transmit antennas, assuming each element is preformed with 2 users, the system can serve at least 200 users without significant drop in performance or increase in overheads.

References

[1] Linglong Dai, Bichai Wang, Yifei Yuan, Shuangfeng Han, Chih-lin I, and Zhaocheng Wang. Non-orthogonal multiple access for 5G: solutions, challenges, opportunities, and future research trends. *IEEE Communications Magazine*, 53(9):74–81, sep 2015. 3, 24, 42, 49, 50, 75

[2] Yuya Saito, Yoshihisa Kishiyama, Anass Benjebbour, Takehiro Nakamura, Anxin Li, and Kenichi Higuchi. Non-Orthogonal Multiple Access (NOMA) for Cellular Future Radio Access. In *2013 IEEE 77th Vehicular Technology Conference (VTC Spring)*, pages 1–5. IEEE, jun 2013. 3, 24, 49

[3] Fahimeh Rezaei, Michael Hempel, and Hamid Sharif. LTE PHY performance analysis under 3GPP standards parameters. *Computer Aided Modeling and Design of Communication Links and Networks CAMAD 2011 IEEE 16th International Workshop on*, pages 102–106, 2011. 9, 21

[4] Arunabha Ghosh, Jun Zhang, Rias Muhamed, and Jeffrey G Andrews. *Fundamentals of LTE.* Number March. Prentice Hall PTR, 2010. 9, 20

[5] Dahlman Erik, Parkvall Stefan, and Skold Johan. *4G LTE/LTE-Advanced for Mobile Broadband.* Elsevier Ltd, Oxford, 2006. 9

[6] 3GPP. UTRA-UTRAN Long Term Evolution (LTE) and 3GPP System Architecture Evolution (SAE) Long Term Evolution of the 3GPP radio technology. (March):2–3, 2006. 11, 12

[7] 3GPP. TS36.401; Evolved Universal Terrestrial Radio Access Network (E-UTRAN); Architecture description. *Technical Specification*, 2015. 11

[8] 3GPP. PTR 36.814 V9.0.0; Further advancements for E-UTRA physical layer aspects (Release 9). *Technical Specification*, 2010. 12, 139, 140

[9] 3GPP. TS 36.211 version 10.0.0 Release 10; Evolved Universal Terrestrial Radio Access (E-UTRA); Physical channels and modulation. *Technical Specification*, page 9, 2011. 12, 16

[10] 3GPP. TS 136 321 V9.0.0; Evolved Universal Terrestrial Radio Access (E-UTRA); Medium Access Control (MAC) protocol specification. *Technical Specification*, 2010. 14

[11] Narayan Prasad, Honghai Zhang, Hao Zhu, and Sampath Rangarajan. Multiuser scheduling in the 3GPP LTE cellular uplink. *IEEE Transactions on Mobile Computing*, 2014. 16, 22

[12] 3GPP. TS 136 212 - V9.2.0 - LTE; Evolved Universal Terrestrial Radio Access (E-UTRA); Multiplexing and channel coding (3GPP TS 36.212 version 9.2.0 Release 9). *Technical Report*, 0:0–62, 2010. 16, 49

[13] 3GPP. TR 36.871 V11.0.0; Evolved Universal Terrestrial Radio Access (E-UTRA); Downlink Multiple Input Multiple Output (MIMO) enhancement for LTE-AdvancedNo Title. *Technical Report*, 2012. 16

[14] Andrei Vasile Iordache and Ion Marghescu. LTE downlink performance. pages 179–182. Ieee, nov 2012. 17

[15] Pooja S Suratia and Satish.K. Shah. Performance analysis of Open and Closed Loop Spatial Multiplexing in LTE Downlink Physical Layer. pages 60–63. Ieee, jul 2012. 17

[16] Tan Shuang, Tommi Koivisto, Helka-Liina Maattanen, Kari Pietikainen, Timo Roman, and Mihai Enescu. Design and Evaluation of LTE-Advanced Double Codebook. *2011 IEEE 73rd Vehicular Technology Conference (VTC Spring)*, pages 1–5, may 2011. 17

[17] Ralf Irmer, Patrick Marsch, Michael Grieger, Gerhard Fettweis, Technische Universität Dresden, Hans-Peter Mayer, Alcatel-lucent Bell Labs, Heinz Droste, Patrick Marsch, Michael Grieger, Gerhard Fettweis, Stefan Brueck, Hans-Peter Mayer, Lars Thiele, and Volker Jungnickel. Coordinated Multipoint : Concepts, Performance and Field Trial Results. *IEEE Communications Magazine*, 49(February), 2011. 18

[18] V. Jungnickel, K. Manolakis, W. Zirwas, B. Panzner, V. Braun, M. Lossow, M. Sternad, R. Apelfrojd, and T. Svensson. The role of small cells, coordinated multipoint, and massive MIMO in 5G. *IEEE Communications Magazine*, 52(5):44–51, may 2014. 18, 44

[19] Amitava Ghosh, Rapeepat Ratasuk, Bishwarup Mondal, Nitin Mangalvedhe, and Tim Thomas. LTE-advanced: next-generation wireless broadband technology. *IEEE Wireless Communications*, 17(3):10–22, jun 2010. 18

[20] Atsushi Nagate, Sho Nabatame, Daigo Ogata, Kenji Hoshino, and Teruya Fujii. Field Experiment of CoMP Joint Transmission over X2 Interface for LTE-Advanced. In *2013 IEEE 77th Vehicular Technology Conference (VTC Spring)*, pages 1–5. IEEE, jun 2013. 18

[21] Hidetoshi Kayama and Huiling Jiang. Evolution of LTE and new Radio Access technologies for FRA (Future Radio Access). In *2014 48th Asilomar Conference on Signals, Systems and Computers*, pages 1944–1948. IEEE, nov 2014. 19

[22] Lei Lei. *From Orthogonal to Non-orthogonal Multiple Access : Energy- and Spectrum-Efficient Resource Allocation.* Number 1752. 2016. 19

[23] J. Harshan and B. Sundar Rajan. Orthogonal vs Non-Orthogonal Multiple Access with Finite Input Alphabet and Finite Bandwidth. *arXiv*, page 7, jan 2010. 19

[24] Guowang Miao, Jens Zander, KW Sung, and SB Slimane. *Fundamentals of Mobile Data Networks.* 2016. 19, 20

[25] Marwan Aldroubi. *Collaborative Modulation Multiple Access for Single Hop and Multihop Networks.* PhD thesis, University of Sussex, 2012. 21

[26] IEEE. *IEEE Standard for Air Interface for Broadband Wireless Access Systems*, volume 2012. 2012. 21

[27] L. Cimini. Analysis and Simulation of a Digital Mobile Channel Using Orthogonal Frequency Division Multiplexing. *IEEE Transactions on Communications*, 33(7):665–675, jul 1985. 21

[28] Michele Morelli, C.-C. Jay Kuo, and Man-On Pun. Synchronization Techniques for Orthogonal Frequency Division Multiple Access (OFDMA): A Tutorial Review. *Proceedings of the IEEE*, 95(7):1394–1427, jul 2007. 21

[29] H. Sari, Y. Levy, and G. Karam. An analysis of orthogonal frequency-division multiple access. *GLOBECOM 97. IEEE Global Telecommunications Conference. Conference Record*, 3(l):1635–1639, 1997. 21

[30] Guocong Song and Y. Li. Adaptive subcarrier and power allocation in OFDM based on maximizing utility. In *The 57th IEEE Semiannual Vehicular Technology Conference, 2003. VTC 2003-Spring.*, volume 2, pages 905–909. IEEE. 21

[31] S. E. Elayoubi, O. Ben Haddada, and B. Fourestié. Performance evaluation of frequency planning schemes in OFDMA-based networks. *IEEE Transactions on Wireless Communications*, 7(5):1623–1633, 2008. 21, 22

[32] C. Wengerter, J. Ohlhorst, and A. Golitschek Edler von Elbwart. Fairness and Throughput Analysis for Generalized Proportional Fair Frequency Scheduling in OFDMA. In *2005 IEEE 61st Vehicular Technology Conference*, volume 3, pages 1903–1907. IEEE. 21

[33] Hoon Kim, Youngnam Han, and Jayong Koo. Optimal subchannel allocation scheme in multicell OFDMA systems. In *2004 IEEE 59th Vehicular Technology Conference. VTC 2004-Spring (IEEE Cat. No.04CH37514)*, volume 3, pages 1821–1825. IEEE. 21

[34] Taneli Riihonen, Risto Wichman, Jyri Hamalainen, and Ari Hottinen. Analysis of subcarrier pairing in a cellular OFDMA relay link. In *2008 International ITG Workshop on Smart Antennas*, pages 104–111. IEEE, feb 2008. 21

[35] S. Pietrzyk and G.J.M. Janssen. Multiuser subcarrier allocation for QoS provision in the OFDMA systems. In *Proceedings IEEE 56th Vehicular Technology Conference*, volume 2, pages 1077–1081. IEEE. 21

[36] M. Ismail, Ridza Fauzi, Jamil Sultan, N. Misran, H. Mohamad, and Waheb A. Jabbar. Performance evaluation of PAPR in OFDM for UMTS-LTE system. In *2012 IEEE 23rd International Symposium on Personal, Indoor and Mobile Radio Communications - (PIMRC)*, pages 1342–1347. IEEE, sep 2012. 22

[37] Harsha S. Eshwaraiah and A. Chockalingam. SC-FDMA for multiuser communication on the downlink. In *2013 Fifth International Conference on Communication Systems and Networks (COMSNETS)*, pages 1–7. IEEE, jan 2013. 23

[38] Michael A. Ruder, Uyen Ly Dang, and Wolfgang H. Gerstacker. User Pairing for Multiuser SC-FDMA Transmission over Virtual MIMO ISI Channels. In *GLOBECOM 2009 - 2009 IEEE Global Telecommunications Conference*, pages 1–7. IEEE, nov 2009. 23

[39] Najah Abu-Ali, Abd-Elhamid M. Taha, Mohamed Salah, and Hossam Hassanein. Uplink Scheduling in LTE and LTE-Advanced: Tutorial, Survey and Evaluation Framework. *IEEE Communications Surveys & Tutorials*, 16(3):1239–1265, 2014. 23, 49

[40] Dionysia Triantafyllopoulou, Konstantinos Kollias, and Klaus Moessner. QoS and Energy Efficient Resource Allocation in Uplink SC-FDMA Systems. *IEEE Transactions on Wireless Communications*, 14(6):3033–3045, jun 2015. 23

[41] Daniel Castanheira, Adao Silva, Rui Dinis, and Atilio Gameiro. Efficient Transmitter and Receiver Designs for SC-FDMA Based Heterogeneous Networks. *IEEE Transactions on Communications*, 63(7):2500–2510, jul 2015. 23

[42] Jinwei Ji, Guangliang Ren, and Huining Zhang. PAPR Reduction of SC-FDMA Signals Via Probabilistic Pulse Shaping. *IEEE Transactions on Vehicular Technology*, 64(9):3999–4008, sep 2015. 23

[43] Kimia Shamaei and Maryam Sabbaghian. Analytical Performance Evaluation of SC-FDMA Systems in the Presence of Frequency and Time Offset. *IEEE Transactions on Wireless Communications*, 14(11):6230–6239, nov 2015. 23

[44] A. Ahmad. Power allocation for uplink SC-FDMA systems with arbitrary input distribution. *Electronics Letters*, 52(2):111–113, jan 2016. 23

[45] Bichai Wang, Kun Wang, Zhaohua Lu, Tian Xie, and Jinguo Quan. Comparison study of non-orthogonal multiple access schemes for 5G. In *2015 IEEE International Symposium on Broadband Multimedia Systems and Broadcasting*, pages 1–5. IEEE, jun 2015. 24, 44, 49

[46] Yunzheng Tao, Long Liu, Shang Liu, and Zhi Zhang. A survey: Several technologies of non-orthogonal transmission for 5G. *China Communications*, 12(10):1–15, oct 2015. 24, 44

[47] Wen Tong, Jianglei Ma, and Peiying Zhu Huawei. Enabling technologies for 5G air-interface with emphasis on spectral efficiency in the presence of very large number of links. In *2015 21st Asia-Pacific Conference on Communications (APCC)*, pages 184–187. IEEE, oct 2015. 24

[48] Fa-Long Luo and Charlie Zhang. *Signal processing for 5G : algorithms and implementations*. Wiley-IEEE Press, 2016. 24, 29

[49] Huseyin Haci. Non-orthogonal Multiple Access (NOMA) with Asynchronous Interference Cancellation, mar 2015. 24, 42

[50] Qi Sun, Shuangfeng Han, Chin-Lin I, and Zhengang Pan. On the Ergodic Capacity of MIMO NOMA Systems. *IEEE Wireless Communications Letters*, 4(4):405–408, aug 2015. 24, 49

[51] Zhiguo Ding, Mugen Peng, and H. Vincent Poor. Cooperative Non-Orthogonal Multiple Access in 5G Systems. *IEEE Communications Letters*, 19(8):1462–1465, aug 2015. 24, 50

[52] Stelios Timotheou and Ioannis Krikidis. Fairness for Non-Orthogonal Multiple Access in 5G Systems. *IEEE Signal Processing Letters*, 22(10):1647–1651, oct 2015. 24

[53] Peng Xu, Zhiguo Ding, Xuchu Dai, and H. Vincent Poor. A New Evaluation Criterion for Non-Orthogonal Multiple Access in 5G Software Defined Networks. *IEEE Access*, 3:1633–1639, 2015. 24, 49

[54] S. M. Riazul Islam, Nurilla Avazov, Octavia A. Dobre, and Kyung-Sup Kwak. Power-Domain Non-Orthogonal Multiple Access (NOMA) in 5G Systems: Potentials and Challenges. *IEEE Communications Surveys & Tutorials*, (c):1–1, 2016. 24

[55] J.J. Caffery and G.L. Stuber. Overview of radiolocation in CDMA cellular systems. *IEEE Communications Magazine*, 36(4):38–45, apr 1998. 26

[56] S. Hara and R. Prasad. Overview of multicarrier CDMA. *IEEE Communications Magazine*, 35(12):126–133, 1997. 26

[57] A. Baier, U.-C. Fiebig, W. Granzow, W. Koch, P. Teder, and J. Thielecke. Design study for a CDMA-based third-generation mobile radio system. *IEEE Journal on Selected Areas in Communications*, 12(4):733–743, may 1994. 26

[58] Ali F.H. Shakya I.L. and Stipidis E. High user capacity collaborative code-division multiple access. *IET Communications*, 5(3):307–319, feb 2011. 26, 49

[59] S. Bopping and J.M. Shea. Superposition coding in the downlink of CDMA cellular systems. *IEEE Wireless Communications and Networking Conference*, 4:1978–1983, 2006. 26, 49

[60] Marwan Aldroubi and Falah H. Ali. Hybrid multiple access coding with adaptive modulation. *2013 IEEE 24th Annual International Symposium on Personal, Indoor, and Mobile Radio Communications*, pages 476–480, sep 2013. 26

[61] R. Razavi, R. Hoshyar, M. A. Imran, and Y. Wang. Information Theoretic Analysis of LDS Scheme. *IEEE Communications Letters*, 15(8):798–800, aug 2011. 28

[62] Razieh Razavi, Mohammed AL-Imari, Muhammad Ali Imran, Reza Hoshyar, and Dageng Chen. On Receiver Design for Uplink Low Density Signature OFDM (LDS-OFDM). *IEEE Transactions on Communications*, 60(11):3499–3508, nov 2012. 28

[63] Jinho Choi. Low density spreading for multicarrier systems. In *Eighth IEEE International Symposium on Spread Spectrum Techniques and Applications - Programme and Book of Abstracts (IEEE Cat. No.04TH8738)*, pages 575–578. IEEE. 28

[64] Tao Huang, Jinhong Yuan, Xingqing Cheng, and Wan Lei. Design of degrees of distribution of LDS-OFDM. In *2015 9th International Conference on Signal Processing and Communication Systems (ICSPCS)*, pages 1–6. IEEE, dec 2015. 28

[65] Anahid R. Robert Safavi, Alberto Perotti, and Branislav M. Popovic. Ultra Low Density Spread Transmission. *IEEE Communications Letters*, pages 1–1, 2016. 28

[66] Hosein Nikopour and Hadi Baligh. Sparse code multiple access. In *2013 IEEE 24th Annual International Symposium on Personal, Indoor, and Mobile Radio Communications (PIMRC)*, pages 332–336. IEEE, sep 2013. 28

[67] Shunqing Zhang, Xiuqiang Xu, Lei Lu, Yiqun Wu, Gaoning He, and Yan Chen. Sparse code multiple access: An energy efficient uplink approach for 5G wireless systems. In *2014 IEEE Global Communications Conference*, pages 4782–4787. IEEE, dec 2014. 28

[68] Lei Lu, Yan Chen, Wenting Guo, Huilian Yang, Yiqun Wu, and Shuangshuang Xing. Prototype for 5G new air interface technology SCMA and performance evaluation. *China Communications*, 12(Supplement):38–48, dec 2015. 28

[69] Zhifeng Yuan, Guanghui Yu, Weimin Li, Yifei Yuan, Xinhui Wang, and Jun Xu. Multi-User Shared Access for Internet of Things. In *2016 IEEE 83rd Vehicular Technology Conference (VTC Spring)*, pages 1–5. IEEE, may 2016. 29

[70] Jie Zeng, Bing Li, Xin Su, Liping Rong, and Rongrong Xing. Pattern division multiple access (PDMA) for cellular future radio access. In *2015 International Conference on Wireless Communications & Signal Processing (WCSP)*, pages 1–5. IEEE, oct 2015. 29

[71] Shanzhi Chen, Bin Ren, Qiubin Gao, Shaoli Kang, Shaohui Sun, and Kai Niu. Pattern Division Multiple Access (PDMA) - A Novel Non-orthogonal Multiple Access for 5G Radio Networks. *IEEE Transactions on Vehicular Technology*, pages 1–1, 2016. 29

[72] Jie Zeng, Dan Kong, Xin Su, Liping Rong, and Xibin Xu. On the performance of pattern division multiple access in 5G systems. In *2016 8th International Conference on Wireless Communications & Signal Processing (WCSP)*, pages 1–5. IEEE, oct 2016. 29

[73] T. Riihonen, S. Werner, and R. Wichman. Comments on âĂŸSimple formulas for SIMO and MISO ergodic capacities'. *Electronics Letters*, 48(2):127, 2012. 30

[74] Jing Wang, Yifei Zhao, Limin Xiao, Xibin Xu, and Xianfeng Wang. Degrees of freedom of SIMO X channel. *IET Communications*, 7(11):1081–1088, jul 2013. 30

[75] M. Reza Khanzadi, Giuseppe Durisi, and Thomas Eriksson. Capacity of SIMO and MISO Phase-Noise Channels With Common/Separate Oscillators. *IEEE Transactions on Communications*, 63(9):3218–3231, sep 2015. 30

[76] A. Goldsmith, S.A. Jafar, N. Jindal, and S. Vishwanath. Capacity limits of MIMO channels. *IEEE Journal on Selected Areas in Communications*, 21(5):684–702, jun 2003. 31

[77] R.S. Blum. MIMO capacity with interference. *IEEE Journal on Selected Areas in Communications*, 21(5):793–801, jun 2003. 31

[78] S. Catreux, P.F. Driessen, and L.J. Greenstein. Data throughputs using multiple-input multiple-output (MIMO) techniques in a noise-limited cellular environment. *IEEE Transactions on Wireless Communications*, 1(2):226–235, apr 2002. 31

[79] Lingjia Liu, Runhua Chen, Stefan Geirhofer, Krishna Sayana, Zhihua Shi, and Yongxing Zhou. Downlink MIMO in LTE-advanced: SU-MIMO vs. MU-MIMO. *IEEE Communications Magazine*, 50(2):140–147, feb 2012. 31

[80] Chen-Nee Chuah, D.N.C. Tse, J.M. Kahn, and R.A. Valenzuela. Capacity scaling in MIMO wireless systems under correlated fading. *IEEE Transactions on Information Theory*, 48(3):637–650, mar 2002. 31

[81] Won-Yong Shin, Sae-Young Chung, and Yong H. Lee. DiversityâĂŞMultiplexing Tradeoff and Outage Performance for Rician MIMO Channels. *IEEE Transactions on Information Theory*, 54(3):1186–1196, mar 2008. 31

[82] V. Sreekanth Annapureddy and Venugopal V. Veeravalli. Sum Capacity of MIMO Interference Channels in the Low Interference Regime. *IEEE Transactions on Information Theory*, 57(5):2565–2581, may 2011. 31

[83] Yair Yona and Meir Feder. On the Diversity-Multiplexing Tradeoff of Unconstrained Multiple-Access Channels. *IEEE Transactions on Information Theory*, 61(9):4630–4662, sep 2015. 31

[84] B.R. Vojcic and Won Mee Jang. Transmitter precoding in synchronous multiuser communications. *IEEE Transactions on Communications*, 46(10):1346–1355, 1998. 35

[85] Yan Xin, Zhengdao Wang, and G.B. Giannakis. Space-time diversity systems based on linear constellation precoding. *IEEE Transactions on Wireless Communications*, 2(2):294–309, mar 2003. 35

[86] A. Stamoulis, L. Zhiqiang, and G.B. Giannakis. Space-time block-coded OFDMA with linear precoding for multirate services. *IEEE Transactions on Signal Processing*, 50(1):119–129, 2002. 35

[87] Luca Sanguinetti and Michele Morelli. Non-Linear Pre-Coding for Multiple-Antenna Multi-User Downlink Transmissions with Different QoS Requirements. *IEEE Transactions on Wireless Communications*, 6(3):852–856, mar 2007. 35

[88] A. Scaglione, P. Stoica, S. Barbarossa, G.B. Giannakis, and H. Sampath. Optimal designs for space-time linear precoders and decoders. *IEEE Transactions on Signal Processing*, 50(5):1051–1064, may 2002. 35

[89] H. Sampath and A. Paulraj. Linear precoding for space-time coded systems with known fading correlations. *IEEE Communications Letters*, 6(6):239–241, jun 2002. 35

[90] Q.H. Spencer, A.L. Swindlehurst, and M. Haardt. Zero-Forcing Methods for Downlink Spatial Multiplexing in Multiuser MIMO Channels. *IEEE Transactions on Signal Processing*, 52(2):461–471, feb 2004. 35

[91] R.D. Wesel and J.M. Cioffi. Achievable rates for Tomlinson-Harashima precoding. *IEEE Transactions on Information Theory*, 44(2):824–831, mar 1998. 36

[92] A.A. D'Amico and M. Morelli. Joint Tx-Rx MMSE Design for MIMO Multicarrier Systems with Tomlinson-Harashima Precoding. *IEEE Transactions on Wireless Communications*, 7(8):3118–3127, aug 2008. 36

[93] G. Lebrun, J. Gao, and M. Faulkner. MIMO transmission over a time-varying channel using SVD. *IEEE Transactions on Wireless Communications*, 4(2):757–764, mar 2005. 36

[94] Heunchul Lee, Seokhwan Park, and Inkyu Lee. A new two-step precoding strategy for closed-loop MIMO systems. *IEEE Transactions on Communications*, 57(3):861–870, mar 2009. 36

[95] Rahul Pupala, Larry Greenstein, and David Daut. Downlink throughput statistics in interference-limited cellular systems with multi-element antennas. *IEEE Transactions on Communications*, 58(1):311–317, jan 2010. 36

[96] Zukang Shen, Runhua Chen, Jeffrey Andrews, Robert Heath Jr., and Brian Evans. Sum Capacity of Multiuser MIMO Broadcast Channels with Block Diagonalization. *IEEE Transactions on Wireless Communications*, 6(6):2040–2045, jun 2007. 38

[97] Le-Nam Tran, Markku Juntti, and Een-Kee Hong. On the Precoder Design for Block Diagonalized MIMO Broadcast Channels. *IEEE Communications Letters*, 16(8):1165–1168, aug 2012. 38

[98] Carlos A. Viteri-Mera and Fernando L. Teixeira. Space-Time Block Diagonalization for Frequency-Selective MIMO Broadcast Channels. *IEEE Access*, 4:6602–6613, 2016. 38

[99] Weiheng Ni and Xiaodai Dong. Hybrid Block Diagonalization for Massive Multiuser MIMO Systems. *IEEE Transactions on Communications*, 64(1):201–211, jan 2016. 38

[100] S.H. Ting, K. Sakaguchi, and K. Araki. On the Practical Performance of VBLAST. *IEEE Communications Letters*, 8(9):564–566, sep 2004. 40

[101] W. Yan, S. Sun, and Z. Lei. A Low Complexity VBLAST OFDM Detection Algorithm for Wireless LAN Systems. *IEEE Communications Letters*, 8(6):374–376, jun 2004. 40

[102] M.O. Damen, H. El Gamal, and G. Caire. On maximum-likelihood detection and the search for the closest lattice point. *IEEE Transactions on Information Theory*, 49(10):2389–2402, oct 2003. 40

[103] S. Verdu. Minimum probability of error for asynchronous Gaussian multiple-access channels. *IEEE Transactions on Information Theory*, 32(1):85–96, jan 1986. 40

[104] Michail Matthaiou, Caijun Zhong, Matthew R. McKay, and Tharmalingam Ratnarajah. Sum Rate Analysis of ZF Receivers in Distributed MIMO Systems. *IEEE Journal on Selected Areas in Communications*, 31(2):180–191, feb 2013. 41

[105] X. Shao, J. Yuan, and Y. Shao. Error performance analysis of linear zero forcing and MMSE precoders for MIMO broadcast channels. *IET Communications*, 1(5):1067, 2007. 41

[106] R. Xu and F.C.M. Lau. Performance analysis for MIMO systems using zero forcing detector over fading channels. *IEE Proceedings - Communications*, 153(1):74, 2006. 41

[107] Tsung-Hsien Liu. Some results for the fast MMSE-SIC detection in spatially multiplexed MIMO systems. *IEEE Transactions on Wireless Communications*, 8(11):5443–5448, nov 2009. 41, 42

[108] Dimitrios D. Vergados and Nikolaos I. Miridakis. Efficient detection-switching based on successive interference cancellation for multiple-input multiple-output orthogonal frequency division multiplexing systems. *IET Signal Processing*, 7(5):436–443, jul 2013. 42

[109] Hugo Tullberg, Petar Popovski, Zexian Li, Mikko A. Uusitalo, Andreas Hoglund, Omer Bulakci, Mikael Fallgren, and Jose F. Monserrat. The METIS 5G System Concept: Meeting the 5G Requirements. *IEEE Communications Magazine*, 54(12):132–139, dec 2016. 43

[110] Gerhard Wunder, Peter Jung, Martin Kasparick, Thorsten Wild, Frank Schaich, Yejian Chen, Stephan Brink, Ivan Gaspar, Nicola Michailow, Andreas Festag, Luciano Mendes, Nicolas Cassiau, Dimitri Ktenas, Marcin Dryjanski, Slawomir Pietrzyk, Bertalan Eged, Peter Vago, and Frank Wiedmann. 5GNOW: non-orthogonal, asynchronous waveforms for future mobile applications. *IEEE Communications Magazine*, 52(2):97–105, feb 2014. 43

[111] Peter Hoeher and Tianbin Wo. Superposition modulation: myths and facts. *IEEE Communications Magazine*, 49(12):110–116, dec 2011. 49

[112] Hosein Nikopour, Eric Yi, Alireza Bayesteh, Kelvin Au, Mark Hawryluck, Hadi Baligh, and Jianglei Ma. SCMA for downlink multiple access of 5G wireless networks. In *2014 IEEE Global Communications Conference*, pages 3940–3945. IEEE, dec 2014. 49

[113] Md Shipon Ali, Hina Tabassum, and Ekram Hossain. Dynamic User Clustering and Power Allocation for Uplink and Downlink Non-Orthogonal Multiple Access (NOMA) Systems. 49, 65, 75, 98

[114] Mohammed Al-Imari, Pei Xiao, Muhammad Ali Imran, and Rahim Tafazolli. Uplink Non-Orthogonal Multiple Access for 5G Wireless Networks. *2014 11th International Symposium on Wireless Communications Systems (ISWCS)*, pages 781–785, aug 2014. 49, 50

[115] Zhiguo Ding, Fumiyuki Adachi, and H. Vincent Poor. The Application of MIMO to Non-Orthogonal Multiple Access. *IEEE Transactions on Wireless Communications*, 15(1):537–552, mar 2015. 49

[116] Joerg Schaepperle. Throughput of a wireless cell using superposition based multiple-access with optimized scheduling. In *21st Annual IEEE International Symposium on Personal, Indoor and Mobile Radio Communications*, pages 212–217. IEEE, sep 2010. 50

[117] Anxin Li, Anass Benjebbour, and Atsushi Harada. Performance Evaluation of Non-Orthogonal Multiple Access Combined with Opportunistic Beamforming. In *2014 IEEE 79th Vehicular Technology Conference (VTC Spring)*, pages 1–5. IEEE, may 2014. 50

[118] Jinho Choi. Minimum Power Multicast Beamforming With Superposition Coding for Multiresolution Broadcast and Application to NOMA Systems. *IEEE Transactions on Communications*, 63(3):791–800, mar 2015. 50

[119] Mehmet Bahadir Celebi and Huseyin Arslan. Theoretical Analysis of the Co-Existence of LTE-A Signals and Design of an ML-SIC Receiver. *IEEE Transactions on Wireless Communications*, 14(8):4626–4639, aug 2015. 50

[120] B. Suard and T. Kailath. Uplink channel capacity of space-division-multiple-access schemes. *IEEE Transactions on Information Theory*, 44(4):1468–1476, jul 1998. 50, 74, 84

[121] Walid Al-Hussaibi and Falah H. Ali. On the Capacity Region of Promising Multiple Access Techniques. In *PGNET 2011 The 12th Annual Postgraduate Symposium on the Convergence of Telecommunications, Networking and Broadcasting*. PGNET, 2011. 50, 76, 84

[122] Mohamed Oussama Damen, Hesham El Gamal, and Giuseppe Caire. On maximum-likelihood detection and the search for the closest lattice point. *IEEE Transactions on Information Theory*, 49(10):2389–2402, 2003. 51

[123] Mai Vu. MISO capacity with per-antenna power constraint. *IEEE Transactions on Communications*, 59(5):1268–1274, 2011. 57

[124] N. L. Biggs. The roots of combinatorics. *Historia Mathematica*, 6(2):109–136, 1979. 58

[125] N L Biggs. The roots of combinatorics. *Historia Mathematica*, 6(2):109–136, 1979. 58

[126] David Guichard. *An Introduction to Combinatorics and Graph Theory.* 2016. 58

[127] L. Brunel. Multiuser Detection Techniques Using Maximum Likelihood Sphere Decoding in Multicarrier CDMA Systems. *IEEE Transactions on Wireless Communications*, 3(3):949–957, may 2004. 71

[128] Babak Hassibi and Haris Vikalo. On the Sphere-Decoding Algorithm I. Expected Complexity. *IEEE Transactions on Signal Processing*, 53(8):2806–2818, aug 2005. 71

[129] Junqiang Li, K.B. Letaief, R.S. Cheng, and Zhigang Cao. Multi-stage low complexity maximum likelihood detection for OFDM/SDMA wireless LANs. In *ICC 2001. IEEE International Conference on Communications. Conference Record (Cat. No.01CH37240)*, volume 4, pages 1152–1156. IEEE. 71

[130] Ameneh Golnari, Mahdi Shabany, Alireza Nezamalhosseini, and Glenn Gulak. Design and Implementation of Time and Frequency Synchronization in LTE. *IEEE Transactions on Very Large Scale Integration (VLSI) Systems*, PP(99):1–1, 2015. 73

[131] Thomas M. Cover. Comments on broadcast channels. *IEEE Transactions on Information Theory*, 44(6):2524–2530, oct 1998. 74

[132] Jingya Li, Carmen Botella, and Tommy Svensson. Resource allocation for clustered network MIMO OFDMA systems. *EURASIP Journal on Wireless Communications and Networking*, 2012(1):175, may 2012. 140

[133] Stefan Brueck, Lu Zhao, Jochen Giese, and M. Awais Amin. Centralized scheduling for joint transmission coordinated multi-point in LTE-Advanced. *2010 International ITG Workshop on Smart Antennas (WSA)*, (Wsa):177–184, feb 2010. 140

[134] Jun Zhu and Hong-Chuan Yang. Low-Complexity Coordinated Beamforming Transmission for Multiuser MISO Systems and Its Performance Analysis. *2010 IEEE Global Telecommunications Conference*, pages 1–5, 2010. 140

[135] Le-Nam Tran, Markku Juntti, Mats Bengtsson, and Bjorn Ottersten. Beamformer Designs for MISO Broadcast Channels with Zero-Forcing Dirty Paper Coding. *IEEE Transactions on Wireless Communications*, 12(3):1173–1185, mar 2013. 140

[136] Zhikun Xu, Chenyang Yang, Geoffrey Ye Li, Yalin Liu, and Shugong Xu. Energy-Ef fi cient CoMP Precoding in Heterogeneous Networks. *IEEE Transactions on Signal Processing*, 62(4):1005–1017, 2014. 140